California AHMCT Center
University of California at Davis
California Department of Transportation

# A DIFFERENTIAL KINEMATIC METHOD
# FOR APPLICATION OF GPS IN ITS

**GPS (Global Positioning System)**
**ITS (Intelligent Transportation System)**

Hassan Abou Ghaida

AHMCT Research Report
UCD-ARR-99-10-14-01

Interim Report of Contract
RTA 65A0054

October 14, 1999

# A Differential Kinematic Method For Application of GPS in ITS

GPS (Global Positioning System)
ITS (Intelligent Transportation System)

by

**Hassan Abou Ghaida**

DISSERTATION

Submitted in partial satisfaction of the requirements for the degree of

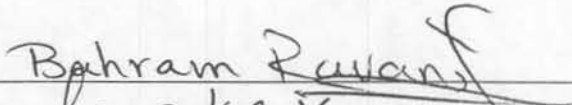DOCTOR OF PHILOSOPHY
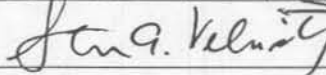
in

Mechanical Engineering

in the

OFFICE OF GRADUATE STUDIES

of the

UNIVERSITY of CALIFORNIA
DAVIS

Approved:

Committee in Charge

1999

i

Committee in Charge:

Pr. Bahram Ravani, Chair
Professor of Mechanical Engineering

Pr. Steve Velinsky
Professor of Mechanical Engineering

Pr. Khaled Abdel-Ghaffar
Professor of Electrical and Computer Engineering

# A Differential Kinematic Method For Application of GPS in ITS

GPS (Global Positioning System)
ITS (Intelligent Transportation System)

Copyright 1999

by

Hassan Abou Ghaida

iii

Hassan Abou Ghaida
June 1999
Mechanical Engineering

A Differential Kinematic Method For Application of GPS in ITS

## ABSTRACT

We introduce a new method that performs accurate sensing of a vehicle position within highway lanes. The method would serve as a part of a Driver Assistance System (DAS) on specialty highway maintenance vehicles, such as snowplows. DAS will provide the operator of the vehicle with precise absolute position and lane departure warnings. The method is also explored as the most appropriate method for the purpose of vehicle automatic lateral control on the Automated Highway System (AHS) lanes. Previously, proposed methods for lane sensing are based on pavement magnetic marker sensing, a vehicle vision system, or DGPS (Differential Global Positioning System). The criteria in choosing the prevailing method for DAS or AHS is based on accuracy, implementation cost in the highway and vehicle infrastructure, and reliability in all conditions. The new method, IS-DGPS (In-Situ DGPS), is based on the use of GPS along with discrete reference markers (e.g. magnetic nails) placed on the roadway with a spacing of three or more seconds of traveling time. With IS-DGPS, the vehicle's receiver generates the GPS differential corrections, needed for accurate positioning, using the road markers instead of relying on ground base stations and a wireless communication link, as in the case of DGPS. IS-DGPS positioning formulation is developed. Experimental

results show its accuracy in determining the vehicle's position. Robustness of the method is discussed. An improved approach of IS-DGPS, using a multi-antenna receiver and GPS relative positioning, is presented.

# Acknowledgements

First, I would like to thank my research advisor Professor Bahram Ravani for introducing me to the field of GPS, suggesting the topic of this dissertation, his help in the development of my dissertation and the invaluable financial support.

I would like to thank Professor Steven Velinsky for his great help, especially in editing this dissertation.

I would like to thank Professor Khaled Abdel-Ghaffar for his time and assistance.

I would like to thank Dr. Ahmed El-Mowafy, Dr. Ahmed Mohamed, Dr. Ahmed El-Rabbani, and Dr. Mohamed Mostapha for their valuable advise and comments on the work of this dissertation.

I would like to thank my AHMCT Center friends, Kin Yen, Stephen Donecker, Dr. Ty Lasky, Ron Kappesser, Colin Thorne, Jim Stiles, Mike Jenkinson and Pat Shepherd for their help and also, for creating a friendly environment in the office.

I would like to thank the California Department of Transportation (Caltrans) for supporting this research effort in equipment and finances, through the UCD AHMCT Center.

Very special thanks to my wife, Rahme who, really, put up with me all this time, and made it happen!

To my wife,

Who made it possible

# Contents

# List of Figures

x

# List of Tables

# List of Acronyms

| | |
|---|---|
| AHS | Automated Highway System |
| AVCSS | Advanced Vehicle Control and Safety Systems |
| BPSK | Binary Phase Shift Key |
| C/A-Code | Coarse/Acquisition Code |
| DAS | Driver Assistance System |
| DGPS | Differential GPS |
| DOP | Dilution Of Precision |
| GIS | Geographic Information System |
| GLONASS | Global Navigation Satellite System |
| GPS | Global Positioning System |
| HMI | Human Machine Interface |
| HUD | Heads Up Display |
| ITS | Intelligent Transportation System |
| P-Code | Precision Code |
| PDOP | Position Dilution Of Precision |
| RTK | Real-Time Kinematics |
| UERE | User Equivalent Range Error |

# Chapter 1

# Introduction

In the past decade, great advances in Intelligent Vehicle technologies have been made, striving toward the goal of establishing an Intelligent Transportation System (ITS). ITS integrates highways and vehicles in a coherent information network using computer, positioning, communications and control technologies. The ultimate goal of ITS is to relieve roadway congestion and meet the increasing demand of vehicle travel without building new highways or widening existing ones. When implemented, ITS will provide several services and functions such as advanced traffic management, advanced traveler information, advanced vehicle control, an advanced public transportation system, and an advanced rural transportation system. The contents of this dissertation contributes to the categories of advanced vehicle control and advanced rural transportation systems.

In recent years, the effort of various transportation research groups has been directed toward using the advances and experience gained in Intelligent Vehicle technologies to improve safety and efficiency with specialty highway maintenance vehicles, such as snow removal vehicles. One plan is to outfit these vehicles with a Driver Assistance

System (DAS). DAS integrates lane position indication and lane departure warning, a collision warning and avoidance system, and a drowsy driver detection system in a Human Machine Interface (HMI). A snow plow is an ideal example of a specialty highway maintenance vehicle that has to perform efficiently in harsh and hazardous conditions. In addition, it has to perform with good safety measures in order to protect the operator, the public and the vehicle. Figure 1.1 shows an instrumented snow plow, under development at UC-Davis, with the added sensing and displaying technologies that constitute the DAS. The work in this dissertation deals with sensing the position and heading of highway maintenance specialty vehicles, in any road and weather condition. The sensed position and attitude of the vehicle and the road map would be displayed on the head-up display (HUD) to assist the driver while operating the vehicle [Lim et al., '99].
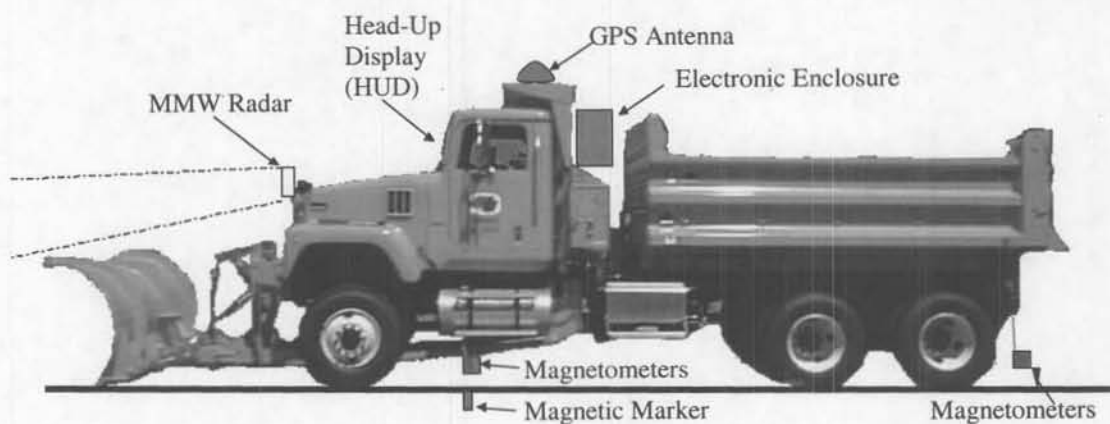


**Figure 1.1**: Instrumented Snow Plow

On another front, one of the goals of ITS is the implementation of an Automated Highway System (AHS) [Sinko and Galijan, '96]. AHS can be envisioned as a system of

instrumented vehicles and roadways that permits achieving hands-off and feet-off driving, where vehicles are fully and automatically controlled. A major area in the development of the AHS is the Advanced Vehicle Control and Safety Systems (AVCSS) [Shladover, '95]. AVCSS addresses the issues of vehicle automatic control, sensing of the vehicle's position, velocity and acceleration, and collision avoidance. Achieving the automated operation in AVCSS requires the ability to accurately sense the vehicle's position within the lane, in any weather condition. The sensing data would serve as an input to the automatic steering controller. This dissertation addresses the issue of lateral sensing of the vehicle's position within the AHS lanes.

Several methods have been proposed and demonstrated to perform highway lane sensing/lane following for use in vehicle lateral control. The most promising methods are the use of roadway discrete magnetic markers [Zhang and Parsons, '90], a vision based system [Crisman and Thorpe, '90], and GPS (Global Positioning System) [Boder et al., '96], [Sinko and Galijan, '96]. The basis for choosing the prevailing method, that will be used in DAS or AHS, is its reliability and the cost involved to implement it. In looking at these methods, we find that each method has some advantages and disadvantages. The method of using discrete magnetic markers has the problem of high cost of highway infrastructure. The vision system method has the high cost problem along with its ill performance in bad lighting conditions and in bad weather. The GPS method has reliability and technical problems due to the radio communication link between the vehicle and the differential ground base stations, that makes it complicated to do real-time kinematics (RTK) of the vehicle [Lapucha et al., '95].

The proposed lane sensing method in this dissertation, In-Situ Differential GPS (IS-DGPS), is based on the use of the Global Positioning System (GPS) along with a set of discrete reference markers embedded in the road (Figure 1.2). GPS could provide absolute position, velocity and 3-D orientation of the vehicle. The discrete markers are used to generate the differential correction signals needed to cancel the errors inherent in the GPS measurements in order to provide suitable accuracies.
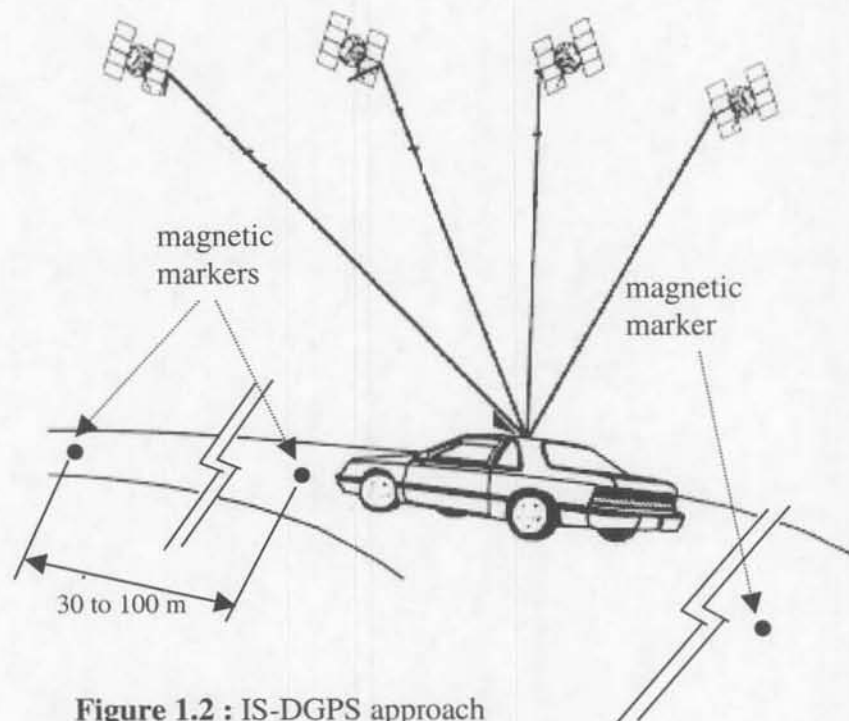


**Figure 1.2 :** IS-DGPS approach

# 1.1 Motivation

The deciding factors in adopting a method that performs highway lane sensing are the cost of the vehicle and highway infrastructure and the reliability of the method. The

motivation for this work was the possibility of providing a new method that takes into consideration the issues of reducing highway implementation and vehicle infrastructural cost, and guaranteeing acceptable accuracy and reliability.

The new method IS-DGPS (In Situ-DGPS) would require only minor and low cost changes to the highway infrastructure. It does not require costly GPS differential ground base stations that are needed in DGPS. It would only need sparsely placed roadway markers as compared to closely placed markers used for lateral control.

An important achievement of IS-DGPS is the elimination of the problematic data communication link associated with DGPS ground base stations. The data link imposes time delays on the positioning process, requires continuous heavy computation for accurate positioning and requires a continuous line of sight between the vehicle and the base. All these factors make real-time kinematic (RTK) updating with DGPS a problematic task.

The robustness of the GPS system is increasing with time through the launch of upgraded satellites, the addition of a new civilian signal, and the elimination of the accuracy degrading Selective Availability by year 2006. Moreover, GPS equipment is getting more sophisticated, computationally more powerful and less expensive.

IS-DGPS benefits from GPS's unique ability in providing both absolute and relative positioning data to simultaneously keep the vehicle within the lane boundaries and separated from other vehicles, night and day, and under all weather conditions. GPS could provide absolute position, velocity and orientation of the vehicle and relative position and velocity to other vehicles.

## 1.2 Overview of the Dissertation

The second chapter reviews the existing literature in two major areas, namely, highway lane sensing and GPS. The chapter reviews the already proposed approaches for lateral sensing of the vehicle's position within the highway lane (lane sensing) and also, cites literature on the GPS system, GPS error analysis, real-time kinematics (RTK) with GPS and vehicle attitude determination with GPS.

The third chapter introduces GPS and its techniques, such as, the various measurement errors that degrades the GPS positioning accuracy, Differential GPS, relative positioning, RTK, and vehicle attitude determination.

The fourth chapter presents the new method of highway lane sensing, In-Situ-Differential GPS (IS-DGPS), using a single antenna carrier phase receiver.

The fifth chapter introduces an improved IS-DGPS approach, by using a multi-antenna GPS receiver, which provides better positioning accuracy, a more robust method and full knowledge of the attitude of the vehicle (roll, pitch and yaw).

The sixth chapter presents the conclusions of the research and new research topics that can be explored in order to engineer a more robust highway vehicle guidance system.

Appendix A presents the algorithm used to transform the GPS ephemeris satellite orbital Keplerian elements to positions in an Earth Centered Earth Fixed coordinate system.

# Chapter 2

# Existing Literature

Sensing of the vehicle's position within the highway lane (or simply lane sensing) could be achieved in a variety of ways using broadly different technologies. Lane sensing would serve as a part of the Driver Assistance System (DAS) or the vehicle's automatic steering system on the Automated Highway System (AHS). This literature review will discuss the existing lane sensing approaches that were proposed by different research institutions. Furthermore, since the new approach presented in this dissertation uses GPS for lane sensing, the review will also cite literature on the GPS system, GPS positioning measurements and its measurement errors. It also describes the methods and techniques used in GPS to do accurate positioning, vehicle orientation and compute real-time kinematics for moving vehicles.

# 2.1 Promising Approaches for Lane Sensing

Three main approaches have been presented by different institutions and proved to have the potential for accurate lane sensing on the highway. These approaches use discrete road magnetic marker based system, a vehicle vision based system, and GPS.

## 2.1.1 Pavement Discrete Magnetic Marker Approach

The California PATH group at UC Berkeley developed a vehicle lateral control system using discrete magnetic markers [Shladover et al., '91] (Figure 2.1). This approach requires the insertion of closely spaced magnets, 1.2 meters apart, for the entire length of each lane of the highways. The accuracy in detecting the magnets at a high speed is better than ±1.5 cm laterally and ±3 cm longitudinally. The approach has been implemented and demonstrated on a strip of highway I-15 near San Diego. The demonstration showed a robust lateral control of the vehicle.

The problem with this approach is that it requires major changes in the highway infrastructure at a high cost.
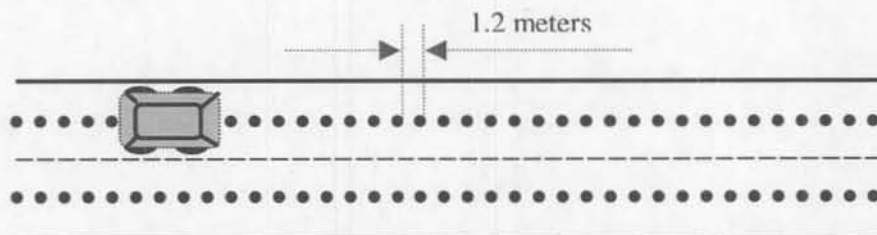


**Figure 2.1**: Use of pavement embedded magnetic markers

## 2.1.2 Vision System Approach

Carnegie Mellon University [Crisman and Thorpe, '90], [Pomerleau, '92] and other institutions adopted a different approach, using an image-based vision system. Roadway features such as high quality paint stripes, road edges and oil slicks are used in the lane sensing process.

This approach was demonstrated with good success except that it requires extensive vehicle and roadway infrastructure and maintenance. It also gives poor performance in poor weather and in poor lighting conditions, which makes using it on some highway maintenance vehicles, such as snow removal vehicles, impractical.

## 2.1.3 DGPS Approach

Several institutions and companies have looked at the possibility of using GPS for guidance and control of land vehicles on the highways. Sinko and Galijan '96 presented a concept of AHS based on Differential GPS (Figure 2.2). They proposed using GPS as the sensing method that provides absolute positioning of the vehicle with respect to a global coordinate frame. The proposed method requires placing differential ground base stations along the highway, one about every 40 kilometers (Figure 2.3). The base station would provide the differential corrections to the vehicle's GPS receiver. A base station consists of a high quality GPS receiver and a powerful radio signal transmitter placed on a high tower in order to establish a line of sight link between the differential correction signal transmitter and the vehicles on the highway. In [Sinko and Galijan, '96], the method was

demonstrated using a ¼ scale model car going in a circular trajectory, with a base station placed 200 m from the experiment area. The results showed a maximum error of 2 cm and an RMS deviation of 0.5 cm.

Bodor et al., '96 at the University of Minnesota, used a DGPS system coupled with an IMU (Inertial Measurement Unit) to perform highway lane sensing in order to prevent vehicle road departure in case the driver becomes incapable of handling the vehicle, e.g. in a case in which the driver falls asleep. They used DGPS to sense the position of the vehicle, so it can be automatically steered to safety if it begins to run off the road. They used a single frequency carrier phase receiver in their experiments. The dynamic error perpendicular to the direction of motion was 4.57 cm with a standard deviation of 39.6 cm.

The need for differential ground base stations has limited the application of GPS technology for use in automatic guidance and control of vehicles on the nation's highways. There are two major problems with using the differential ground base stations on the highways. Firstly, establishing the base stations amounts to a major roadway infrastructure change at a high cost (one station every about 40 km). Secondly, it has the inherent problem with the communication link between the GPS receivers of the base station and the vehicle, which prevents acquiring accurate and continuous real-time kinematics data on the vehicle. Some of the problems with the communication link are: a requirement of a continuous line of sight [Hofmann et al., '97] and restrictions on vehicle-base distance due to GPS atmospheric and orbital error decorrelation [Parkinson and Enge, '96].

[Lapucha and Baker, '95] stated the operational limitations of doing RTK with DGPS, due to data link latency and time matching delays. They suggested giving up time matching at the base station and vehicle, and rely on using a second order extrapolation model to extrapolate the differential corrections to the current user's time.
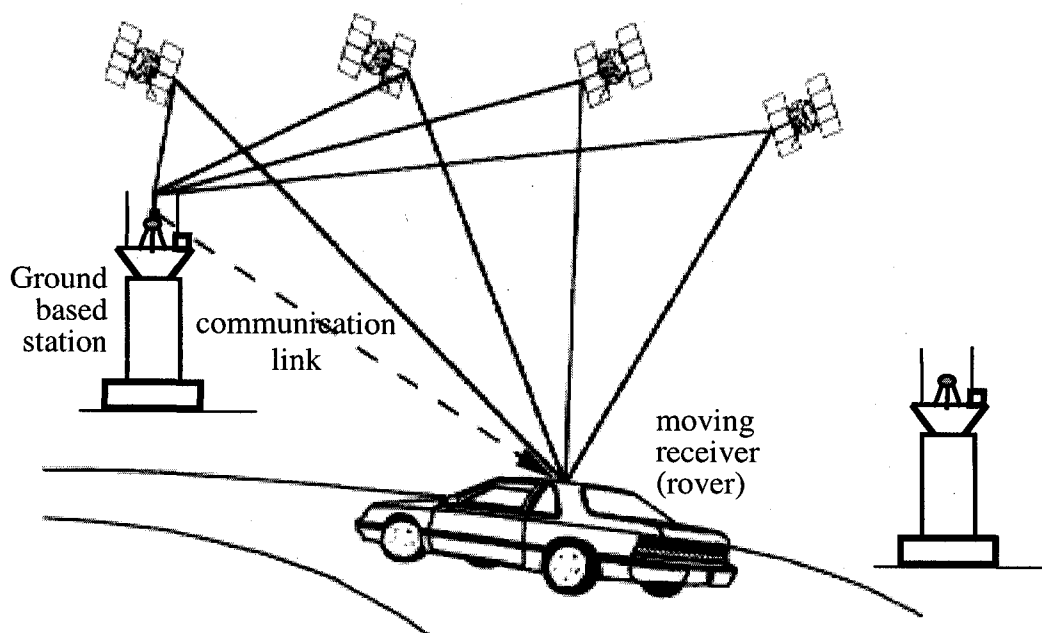
**Figure 2.2:** DGPS Approach



12 mi

110 miles
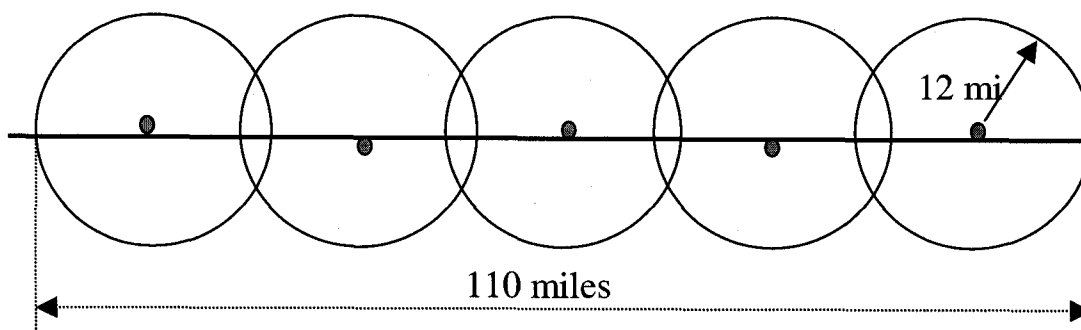
**Figure 2.3:** Frequency of Ground based stations

# 2.2 The Global Positioning System (GPS)

In the past decade, GPS has evolved to be an area of high interest for various applications in many disciplines. A lot of research has been conducted and a high volume of publications have been written on the subject. This part of the literature review addresses the GPS system and GPS related topics.

## 2.2.1 GPS, GPS Observables and GPS Error Analysis

[Hoffman et al., '97] [Kaplan '96] and [Strang and Borre '96] presented a detailed introduction to all GPS concepts from an engineering point of view. They described the various GPS measurement observables and their applications to the positioning problem. [Parkinson, '96] presented an explicit formulation of the GPS observable equations that accounted for all GPS errors, along with a characterization of these errors. The official description of the GPS signal is given in the GPS Interface Control Document ICD-GPS-200, cf. Airnc Research Corporation 1992.

## 2.2.2 DGPS, Relative Positioning and RTK

DGPS and relative positioning principles are discussed in most GPS books, for instance, [Parkinson and Enge, '96] presented analytically and quantifiably how DGPS eliminates, reduces or leaves behind errors.

Relative positioning is a technique that applies differencing without any latency. Relative positioning in moving vehicles becomes a real-time kinematic problem (RTK)

that has a lot of challenges and limitations. [Lapucha and Baker, '95], argued against carrier phase relative positioning RTK because of the operational limitations that still exist in the real-time environment. These limitations are due to time-matching delays that add a few seconds to the data link delay. Lapucha and Baker suggested using the carrier phase DGPS method without direct differencing (without relative positioning). The result is an uninterrupted and more robust DGPS positioning with slightly degraded accuracy. To make up for some of the accuracy degradation, they included the correction accelerations by using a second order extrapolation model.

## 2.2.3 Ambiguity Resolution with RTK

In RTK applications, it is necessary to be able to resolve the cycle ambiguities associated with carrier phase measurements while the vehicle is in motion. This process is known as on-the-fly (OTF) ambiguity resolution. Several methods and algorithms have been presented and used to deal with the OTF problem. These methods include the least square ambiguity search technique [Hatch, '90], the ambiguity function method (AFM) [Counselman and Gourevitch, '81], the fast ambiguity resolution approach (FARA) [Frei and Beutler, '90] and the fast ambiguity search filter (FASF) [Chen and Lachapelle '94].

## 2.2.4 Vehicle Attitude Determination with DGPS

Multi-antenna GPS receivers are usually used for attitude determination of the vehicle along with its absolute position. A carrier phase dual-antenna receiver gives the

absolute position of the vehicle and its azimuth (heading). A three-antenna or more receiver gives the full 3-D orientation of the vehicle [Cohen, '96].

Quin, '92 discussed an example of a manufactured multi-antenna array dedicated to attitude determination. This platform consists of four microstrip antennas connected to a 24-channel single frequency receiver. Six channels are assigned to each antenna so that up to six satellites can be tracked.

Lu '95 discussed Incorporating the geometric constraints due to the known antenna array geometry on the vehicle.

El-Mowafy and Schwartz, '95 described different antenna configurations on the vehicle in order to provide an instantaneous ambiguity resolution for attitude determination. Vehicle attitude determination techniques with multi-antenna GPS receivers were used in this research in an improved IS-DGPS design in order to have a more robust lane sensing system.

# Chapter 3

# GPS Technology

## The Global Positioning System (GPS)

The Global Positioning System (GPS) is a satellite based all-weather radionavigation system developed by the United States Department of Defense (DoD) to provide precise positioning and velocity to an unlimited number of users anywhere on the planet [Parkinson, '96]. This chapter gives an overview of GPS, describes various positioning techniques, describes the various errors encountered in the measurements, presents the Differential GPS (DGPS) technique for accurate positioning with emphasis on Real-Time Kinematics (RTK), and presents the concept of vehicle attitude determination using GPS.

# 3.1 GPS System Architecture

GPS consists of three segments known as the space segment, the control segment and the user segment. The space segment consists of 24 satellites on 6 different orbits, (Figure 3.1) orbiting at about 20,000 km above Earth. The control segment, which consists of 5 monitoring ground stations, monitors transmissions and orbital behavior of the satellites. The master station, in Colorado Springs, up links to the satellites orbital elements, satellite clock information and model parameters for the atmosphere that will be transmitted back to earth by the satellites. The user segment consists of many users in a variety of disciplines using the L-band transmissions from the GPS satellites.
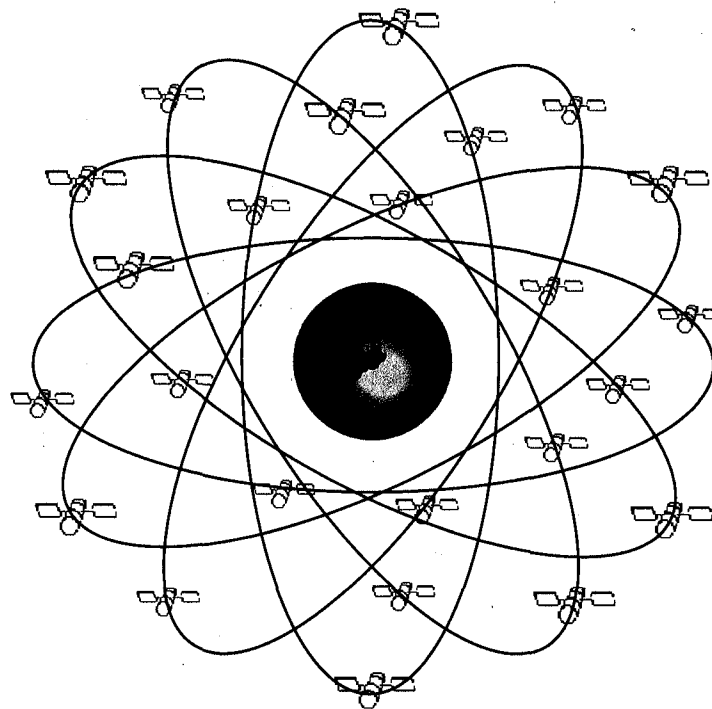


**Figure 3.1**: GPS satellite constellation

# 3.2 GPS Signal

All satellite transmissions are coherently derived from the fundamental frequency of 10.23 MHz, and are made available by a set of onboard extremely accurate atomic clocks. This accuracy is so critical since positioning in GPS relies on measuring the time that takes the signal to get from the satellite to the user's receiver.

The GPS signal is elaborate because it has to provide various positioning observables, error correction parameters and encrypted codes for authorized users. The GPS satellite transmits a radio signal that consists of two simple sine wave carriers that are phase modulated by some codes. The oscillator on board the satellites generates, with very high stability, a fundamental frequency $f_0$ = 10.23 MHz. From this fundamental frequency, two carriers in the L-band, denoted L1 and L2 are derived by integer multiplication of $f_0$ (Table 3.1). The two carriers are modulated, using the BPSK (Binary Phase Shift Keying) technique [Leick, '95], by the Coarse/Acquisition-code (C/A-code), the Precision-code (P-code) and the Navigation Message. The codes are known +1/-1 sequences of bits. The C/A-code is repeated every one millisecond and the P-code is repeated every 266.4 days. The Navigation Message contains satellite Keplerian orbital elements, clock information and atmospheric model parameters. The components of the signal and their frequencies are summarized in Table 3.1.

As we will see, GPS positioning is done using the following observables, the C/A-code, the P-code, the L1 carrier phase, and the L2 carrier phase or a combination of these observables. Positioning with the C/A-code is the quickest and the least accurate. The P-code provides much higher positioning accuracy than the C/A code because its frequency

is 10 times higher than that of the C/A code. However, the P-code is encrypted so that only authorized users can access it.

The L1 carrier is modulated by both C/A and P codes while the L2 carrier is modulated by only the P-code. The mathematical formula for the two carriers can be written as

$$L1 = a_1 \cdot P(t) \cdot W(t) \cdot D(t) \cdot \cos f_1(t) + a_1 \cdot C/A(t) \cdot D(t) \cdot \sin f_1(t) \qquad (3.1)$$

$$L2 = a_2 \cdot P(t) \cdot W(t) \cdot D(t) \cdot \cos f_2(t) \qquad (3.2)$$

where $D(t)$ is the navigation message code and $W(t)$ is the encryption code.

Figure 3.2 shows a diagram of how the transmitted satellite signal is created [Kleusberg and Teunissen, '96].

**Table 3.1**: Signal components

| Component | Frequency (MHz) |
|---|---|
| Fundamental Frequency | $f_0 = 10.23$ |
| Carrier L1 | $154.f_0 = 1575.42$ |
| Carrier L2 | $120.f_0 = 1227.60$ |
| P code | $f_0 = 10.23$ |
| C/A code | $f_0/10 = 1.023$ |
| Navigation Message | $50.10^{-6}$ |
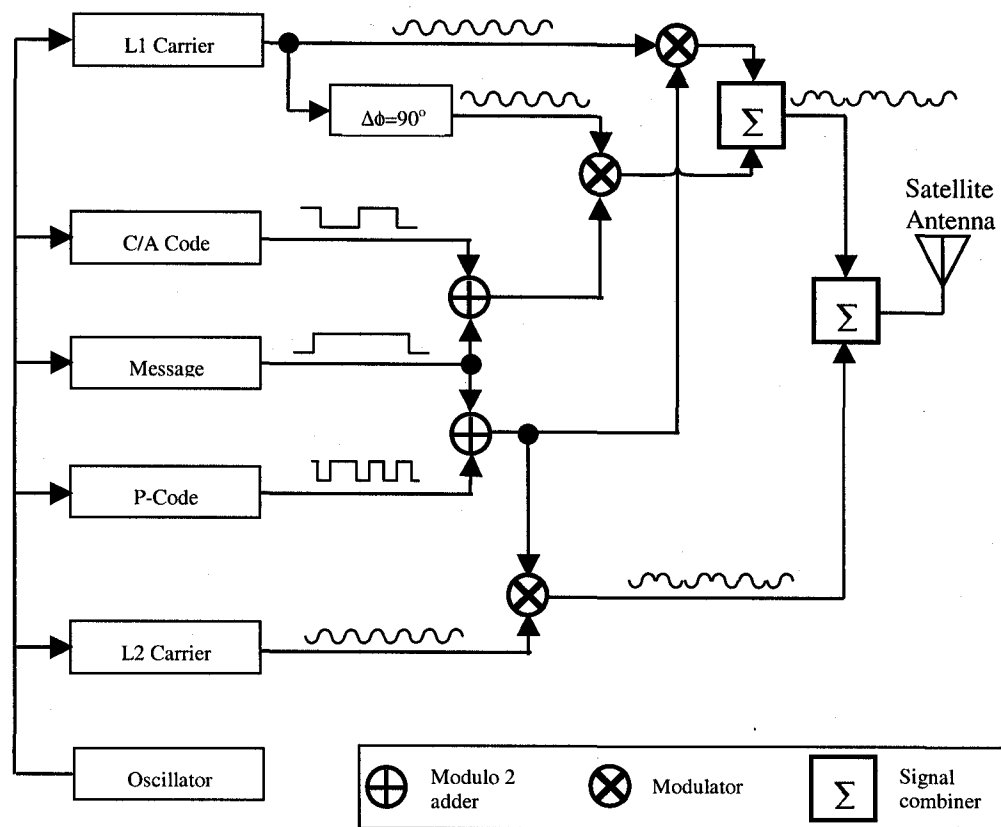
**Figure 3.2**: How the components of the GPS Signal are combined.
Note that the various waveforms are not to scale. [15]

# 3.3 Reference Coordinate Systems

In order to formulate the positioning problem, it is necessary to choose a suitable reference coordinate system in which the states of both the satellite and the receiver can be represented. All the GPS receiver's positioning calculations are done in an Earth Centered Earth Fixed (ECEF) Cartesian coordinate system. The satellite orbital positions are originally obtained from the GPS signal's Navigation Message in the form of Keplerian orbital elements. The algorithm to calculate the satellite's position in the ECEF system from the Keplerian elements is described in Appendix A. Associated with the

ECEF system a World Geodetic System (WGS-84) that models the gravitational irregularities of the Earth and adds a geocentric ellipsoid of revolution. Also, some applications require that the receiver position data be presented in suitable reference system that has a real life meaning, like a local state-plane Northing-Easting-Up coordinate system. This section describes these various coordinate systems.
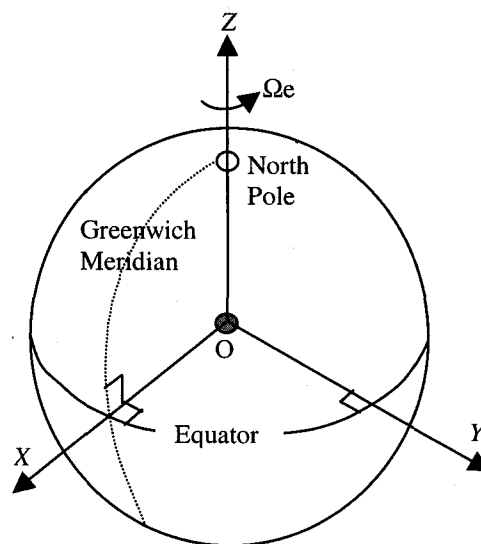


**Figure 3.3**: ECEF coordinate system (*XYZ*)

## 3.3.1 Earth Centered Earth Fixed Frame (ECEF)

For the purpose of computing the position of a GPS receiver, it is convenient to use a coordinate system that rotates with Earth. The GPS receiver conducts its fundamental calculations using an ECEF coordinate system (Figure 3.3). The ECEF *X*-axis points in the direction of the Greenwich Meridian ($0^\circ$ longitude). The *Z*-axis coincides with the spin axis of the earth. The *Y*-axis is orthogonal to these two directions.

## 3.3.2 World Geodetic System 1984 (WGS-84)

The DoD defined a global geocentric coordinate system called the World Geodetic System (WGS-84). It includes a model of the irregular gravity field and is physically defined by the coordinates of 1500 terrestrial sites. Associated with WGS-84 is a geocentric equipotential ellipsoid of revolution. The position of the GPS receiver can be obtained as geodetic coordinates, latitude, longitude and height.

The ECEF coordinate system is affixed to the WGS-84 reference ellipsoid with the point corresponding to the center of Earth. Transformation from geodetic coordinates to Cartesian coordinates, and visa versa, can be done in closed form [Kaplan, '96].

## 3.3.3 Local Northing and Easting Coordinate System

Some engineering projects, like highway construction and mapping, require that a local Cartesian coordinate system is used. Each State in the US has local State-plane coordinates defined. For instance, California is divided into six zones, each has a Northing-Easting-Up coordinate system with the origin located in the Pacific Ocean.

A number of commercially available transformation programs are capable of transforming between WGS-84 and state-plane coordinate systems. Sometimes, some transformation programs transform coordinates between the North American Datum 1983 (NAD-83) and State-plane coordinates [Reference 3]. For our purposes, the NAD-83 coincides with the WGS-84.

# 3.4 GPS Positioning with the Code Observable

GPS uses trilateration, measurement of the distance from the satellites to a receiver, using the signals emitted by the satellites. Since signals travel at the speed of light, the key to the accuracy of GPS is precise knowledge of the time and location of the satellites.

Ideally, if the system was error free and the satellite and receiver clocks were synchronized, the positioning process becomes simple. The receiver receives and demodulates the signal coming from the satellite, in order to extract the C/A or P code and the Navigation Message. Meanwhile, the receiver internally generates a replica of that code. The receiver then time-shifts its replica code until it matches the satellite's code using an autocorrelation function. This time-shift $\Delta t$ is the time it took for the satellite code to travel down to the receiver (Figure 3.4). Multiplying the time-shift by the speed of light $c$ gives the range $\rho$ between the satellite and the receiver's antenna. Since the satellite and user's receiver clocks were accurate and synchronized, we only need to measure ranges to three satellites in order to solve for the three components $(x,y,z)$ of the position of the receiver's antenna in the ECEF coordinate frame (Figure 3.5). The three range equations would be

$$\begin{aligned}
\rho_1 &= c * \Delta t_1 = \sqrt{(X_1 - x)^2 + (Y_1 - y)^2 + (Z_1 - z)^2} \\
\rho_2 &= c * \Delta t_2 = \sqrt{(X_2 - x)^2 + (Y_2 - y)^2 + (Z_2 - z)^2} \\
\rho_3 &= c * \Delta t_3 = \sqrt{(X_3 - x)^2 + (Y_3 - y)^2 + (Z_3 - z)^2}
\end{aligned} \qquad (3.3)$$

where $X_1, Y_1, Z_1, \ldots, Z_3$ are the ECEF coordinates of the three satellites.
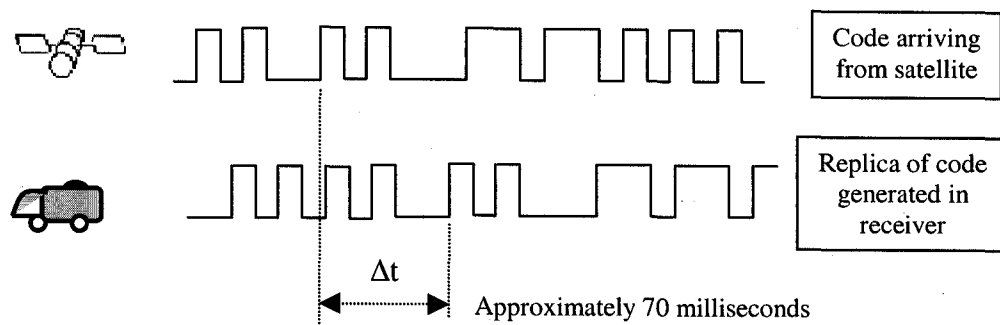
**Figure 3.4**: Code time-shift measurement
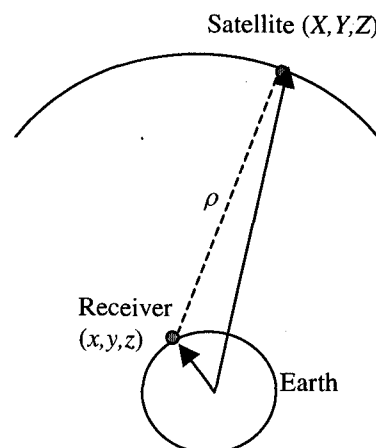


**Figure 3.5**: GPS positioning concept

Although, the satellite has a very stable atomic clock, it still has a bias $dt$. Fortunately, a model is given for this bias, in the Navigation Message, which can be used to estimate the associated error [Hofmann et al., '97], that is

$$dt = a_0 + a_1(t - t_c) + a_2(t - t_c)^2 \tag{3.4}$$

where $a_0$ is satellite clock offset; $a_1$ is satellite clock drift; $a_2$ is satellite clock frequency drift; $t_c$ is satellite clock reference epoch.

Since the clock in the receiver is an inexpensive crystal clock, which is set approximately to GPS time, it has an offset $dT$ from true GPS time. Because of this offset, the measured distance between the satellite and the receiver is slightly longer or shorter than the true range. The receiver can overcome this problem by treating the receiver clock bias as an unknown. Then, distance measurements to four satellites instead of three are required. These distances are called pseudoranges $P$, which are the true ranges $\rho$ plus a small range correction, and are given as

$$P = \rho + c * (dT + dt) \ . \tag{3.5}$$

Then, four equations are generated to solve for the four unknowns, which are the three components of position and the receiver clock error. The four equations are

$$
\begin{aligned}
P_1 + c \cdot dt_1 &= \sqrt{(X_1 - x)^2 + (Y_1 - y)^2 + (Z_1 - z)^2} + c \cdot dT \\
P_2 + c \cdot dt_2 &= \sqrt{(X_2 - x)^2 + (Y_2 - y)^2 + (Z_2 - z)^2} + c \cdot dT \\
P_3 + c \cdot dt_3 &= \sqrt{(X_3 - x)^2 + (Y_3 - y)^2 + (Z_3 - z)^2} + c \cdot dT \\
P_4 + c \cdot dt_4 &= \sqrt{(X_4 - x)^2 + (Y_4 - y)^2 + (Z_4 - z)^2} + c \cdot dT
\end{aligned} \tag{3.6}
$$

One way to solve this set of nonlinear equations is by linearizing around an approximate value $(x_0, y_0, z_0)$ for the unkown receiver coordinates. Then,

$$
\begin{aligned}
x &= x_0 + \Delta x \\
y &= y_0 + \Delta y \\
z &= z_0 + \Delta z
\end{aligned}
\tag{3.7}
$$

where now, the unknowns are $\Delta x$, $\Delta y$, and $\Delta z$. The receiver-satellite range is a function of the receiver coordinates

$$
\rho_i = \sqrt{(X_i - x)^2 + (Y_i - y)^2 + (Z_i - z)^2} \equiv f(x, y, z).
\tag{3.8}
$$

The receiver-satellite approximate range is a function of the approximate receiver coordinates

$$
\rho_{0i} = \sqrt{(X_i - x_0)^2 + (Y_i - y_0)^2 + (Z_i - z_0)^2} \equiv f(x_0, y_0, z_0).
\tag{3.9}
$$

Then, $f(x,y,z)$ can be expanded into a Taylor series with respect to the approximate point $(x_0, y_0, z_0)$ as

$$
\begin{aligned}
f(x, y, z) &\equiv f(x_0 + \Delta x, y_0 + \Delta y, z_0 + \Delta z) = \\
f(x_0, y_0, z_0) &+ \frac{\partial f(x_0, y_0, z_0)}{\partial x_0} \cdot \Delta x + \frac{\partial f(x_0, y_0, z_0)}{\partial y_0} \cdot \Delta y + \frac{\partial f(x_0, y_0, z_0)}{\partial z_0} \cdot \Delta z + \cdots
\end{aligned}
\tag{3.10}
$$

where the expansion is truncated after the linear term. The partial derivatives are

$$
\begin{aligned}
\frac{\partial f(x_0, y_0, z_0)}{\partial x_0} &= -\frac{X_i - x_0}{\rho_{0i}} \\
\frac{\partial f(x_0, y_0, z_0)}{\partial y_0} &= -\frac{Y_i - y_0}{\rho_{0i}} \\
\frac{\partial f(x_0, y_0, z_0)}{\partial z_0} &= -\frac{Z_i - z_0}{\rho_{0i}}
\end{aligned}
\tag{3.11}
$$

Finally, the linearized equation set is

$$P_1 - c \cdot dt_1 - \rho_{01} = -\frac{X_1 - x_0}{\rho_{0i}} \cdot \Delta x - \frac{Y_1 - y_0}{\rho_{0i}} \cdot \Delta y - \frac{Z_1 - z_0}{\rho_{0i}} \cdot \Delta z + c \cdot dT$$

$$P_2 - c \cdot dt_2 - \rho_{02} = -\frac{X_2 - x_0}{\rho_{0i}} \cdot \Delta x - \frac{Y_2 - y_0}{\rho_{0i}} \cdot \Delta y - \frac{Z_2 - z_0}{\rho_{0i}} \cdot \Delta z + c \cdot dT$$

$$P_3 - c \cdot dt_3 - \rho_{03} = -\frac{X_3 - x_0}{\rho_{0i}} \cdot \Delta x - \frac{Y_3 - y_0}{\rho_{0i}} \cdot \Delta y - \frac{Z_3 - z_0}{\rho_{0i}} \cdot \Delta z + c \cdot dT$$

$$P_4 - c \cdot dt_4 - \rho_{04} = -\frac{X_4 - x_0}{\rho_{0i}} \cdot \Delta x - \frac{Y_4 - y_0}{\rho_{0i}} \cdot \Delta y - \frac{Z_4 - z_0}{\rho_{0i}} \cdot \Delta z + c \cdot dT$$

$$(3.12)$$

Solving this linear set gives $\Delta x$, $\Delta y$, $\Delta z$ and $dT$ and then $x$, $y$ and $z$ can be obtained. If more than four satellites are available a least square technique is applied.

Writing (3.12) in matrix form, we have

$$\Delta \rho = H \cdot \Delta X \tag{3.13}$$

where

$$\Delta \rho = \begin{bmatrix} P_1 - c \cdot dt_1 - \rho_{01} \\ P_2 - c \cdot dt_2 - \rho_{02} \\ P_3 - c \cdot dt_3 - \rho_{03} \\ P_4 - c \cdot dt_4 - \rho_{04} \end{bmatrix}, H = \begin{bmatrix} -\frac{X_1 - x_0}{\rho_{0i}} & -\frac{Y_1 - y_0}{\rho_{0i}} & -\frac{Z_1 - z_0}{\rho_{0i}} & 1 \\ -\frac{X_1 - x_0}{\rho_{0i}} & -\frac{Y_2 - y_0}{\rho_{02}} & -\frac{Z_2 - z_0}{\rho_{02}} & 1 \\ -\frac{X_3 - x_0}{\rho_{03}} & -\frac{Y_3 - y_0}{\rho_{03}} & -\frac{Z_3 - z_0}{\rho_{03}} & 1 \\ -\frac{X_4 - x_0}{\rho_{04}} & -\frac{Y_4 - y_0}{\rho_{04}} & -\frac{Z_4 - z_0}{\rho_{04}} & 1 \end{bmatrix}, \Delta X = \begin{bmatrix} \Delta x \\ \Delta y \\ \Delta z \\ \Delta T \end{bmatrix}.$$

Notice that, $H$ would not be square if more than four satellites are included. Then, the generalized inverse is used to obtain $\Delta X$

$$\Delta X = (H^T \cdot H)^{-1} \cdot H^T \cdot \Delta \rho. \tag{3.14}$$

Unfortunately, GPS calculations are corrupted by other error sources tending to reduce its accuracy. These errors will be described and analyzed in Sections 3.5 and 3.7.

# 3.5 GPS Error Sources

A GPS receiver fundamentally measures pseudoranges, which is a range measurement corrupted by various types of errors and biases. Satellite and receiver clock biases, satellite location errors, atmospheric effects, multipath errors and hardware noises are all factors that contribute to range measurement error. Ranging errors are grouped into six classes:

- Ephemeris data errors in the transmitted location of the satellite

- Satellite clock errors including SA

- Ionospheric effect errors

- Tropospheric effect errors

- Multipath errors

- Receiver errors caused by clock bias, thermal noise and software accuracy.

## 3.5.1 Ephemeris Data Errors

Ephemeris errors result when the GPS Navigation Message does not transmit the correct satellite location. This error reflects a position prediction that tends to grow with time from the last station upload. The radial component of this error is fortunately small. The tangential part is larger but does not effect ranging accuracy to the same degree. The rms ranging error attributable to ephemeris is 2.1 meters [Bowen et al., '96]. Portion of the SA error ($\varepsilon$-process) is added to the ephemeris. The $\varepsilon$-process is the truncation of the orbital information in the Navigation Message so that the coordinates of the satellites

cannot accurately be computed. However, all errors in the ephemeris tend to be slowly changing with time. Although SA could be applied to the ephemeris message, this technique apparently has not been used. This is because any errors in the ephemeris would be slowly changing, and hence, strongly correlated over many minutes. Correction for these errors would be valid for long periods of time.

## 3.5.2 Satellite Clock Error

The satellite atomic clock is accurate to 1 part in $10^{13}$. In the absence of Selective Availability, these errors are small and change slowly, 1-2 m, and have correlation times of about 5 minutes. A big part of this error can be eliminated by the clock correction coefficients broadcasted in the Navigation Message, as was mentioned before. Selective Availability (SA) is the dominant error source without differential corrections [Van Graas and Braasch, '96]. The SA process was placed by the Department of Defense (DoD) in order to deny navigation accuracy for unauthorized parties. Accuracy denial is done by dithering the satellite clock ($\delta$-process) and manipulating the ephemrides ($\varepsilon$-process) in the Navigation Message. In the presence of SA, clock errors of 20-30 m are not unusual. This error is exclusively a time correlated error. The period of oscillations is on the order of 2-5 minutes, while the standard deviation is approximately 23 m [Parkinson and Enge, '96].

## 3.5.3 Ionospheric Error

The ionosphere is the first layer of the atmosphere the GPS signal encounters. It is the portion of the atmosphere 50-1000 km above the earth. Free electrons in the ionosphere produces a group delay in the GPS signal and an advance in the carrier phase, so the effects on the pseudorange and phase observables are equal but with opposite signs. It varies with the time of the day, the angle the signal is penetrating the ionosphere, and the sun's activities. Excluding SA, the ionosphere is the most dominant error source for satellite ranging. Typically, delays are in the 4-10 m range. The ionospheric effect is dispersive which leads to the fact that different frequencies are affected differently. Its error $v$ is inversely proportional to the square of the frequency $f$ of the signal,

$$v = \left( \frac{40.3}{c \cdot f^2} \right) \cdot TEC$$ [Spilker, '96], and proportional to $TEC$, the number of Total

free Electron Content in a m$^3$. Without DGPS corrections, 50 –75% of this error can be removed by using a standard model where its coefficients are available in the Navigation Message [Parkinson and Enge, '96]. DGPS should reduce this error to less than 1 m for reference–user separation of less than 100 km. With differential corrections, the size of the residual pseudorange error for the ionosphere depends strongly on the separation of the user and the reference (spatial decorrelation) and the elevation angle of the satellites. Ionospheric spatial decorrelation has been measured to be less than 0.2 m for 100 km. A dual L1/L2 frequency receiver can directly measure the delay and make the correction to be accurate to about 1 m.

## 3.5.4 Tropospheric Error

The troposphere is the portion of the atmosphere closest to the earth (0-50 km above earth). It causes a delay in the GPS signal. The troposphere is electrically neutral meaning it is neither ionized nor dispersive. This means that it is frequency independent, so, it affects both components, L1 and L2, of the GPS signal in the same way. Also, the tropospheric refraction has the same delaying effect on both the code and the phase of the carrier. Refraction in the troposphere has a dry component closely correlated with the atmospheric pressure and a wet component associated with the water vapor density in the atmosphere. The dry component accounts for the larger portion of the range error and can be easily estimated. The wet component can also be estimated with sophisticated water vapor radiometers. The density of the troposphere governs the severity of its effect on the signal. When a satellite is close to the horizon, the delay of the signal is maximized, whereas at zenith, the delay is minimized. Most of this error can be removed using a simple model, where its coefficients are acquired from the navigation message. Without differential corrections, this model typically removes 90% of the delay. Tropospheric error decorrelates strictly with distance. The residual tropospheric effect after a model has been applied starts to decorrelate at about 15 km separation, since the volume of the atmosphere is not uniform over large distances [Van Sickle, '97]. With DGPS, the reference and user receivers traverse volumes of the atmosphere with different meteorological parameters, so, differencing might leave a residue if the separation between receivers is large.

## 3.5.5 Multipath Error

Multipath error arises when GPS signals travel over multiple paths from the satellite to the receiver (Figure 3.6). With DGPS, the base station's and the user's receiver antennas are located at different sites. They could be subject to different uncorrelated multipath disturbances. Hence, while differencing in DGPS, the Root-Mean-Square of the multipath error increases by a factor of $\sqrt{2}$ because



**Figure 3.6**: Multipath effect

$$RMS\_error = \sqrt{(individual\_error)^2 + (individual\_error)^2} = \sqrt{2} \times (individual\_error).$$

For mobile application, such as RTK, the antenna motion relative to reflecting surfaces may significantly decrease the time correction of the multipath signal, thereby allowing it to be reduced by filtering [Hofmann et al., '97].

## 3.5.6 Receiver Errors

An error of 10-100 m can be attributed to the receiver clock error, depending on the oscillator type. The receivers are usually equipped with relatively inexpensive quartz clocks with a 10 year life span. A good clock has an accuracy of 1 part in $10^8$ to 1 part in $10^{10}$ (error of 0.25 seconds in about 70 years) [Van Sickle, '97].

## 3.5.7 Error Table

Table 3.2 lists the error sources and their estimated average values for a C/A-code receiver after applying the models using the parameters obtained from the Navigation Message.

**Table 3.2**: Range errors

| Error Source | Error in (m) |
|---|---|
| Ephemeris Data | 2.1 |
| Satellite Clock + SA | 20.0 |
| Ionosphere | 4.0 |
| Troposphere | 0.5 |
| Multipath | 1.0 |
| Receiver measurement | 0.5 |
| **Total** | 20.6 |

The statistical sum of the contributions from each of the error sources are combined in a measure called the *UERE* (User Equivalent Range Error) which is transmitted via the Navigation Message.

## 3.5.8 C/A-Code Positioning Equation

Taking into account all the errors, the C/A code observable equation is

$$P^j(t_0) = \rho_A^j(t_0) + d\rho_A^j(t_0) + c \cdot dt(t_0) - c \cdot dT_A(t_0) + T + I + v_A(t_0). \tag{3.15}$$

Or in a simplified version

$$P^j(t_0) = \rho_A^j(t_0) + \Delta\rho_A^j(t_0) + c \cdot dt(t_0) - c \cdot dT_A(t_0) + v_A(t_0) \qquad (3.16)$$

where $P^j(t_0)$ is the satellite-receiver pseudorange; $\rho_A^j(t_0)$ is the true satellite-receiver range; $d\rho_A^j(t_0)$ is the radial orbital error; $c \cdot dt(t_0)$ is the satellite clock bias; $c \cdot dT_A(t_0)$ is the receiver clock bias; $T$ & $I$ are the Tropospheric and Ionospheric errors; $\Delta\rho_A^j(t_0)$ is the radial orbital error; and $v_A(t_0)$ is combination of receiver noise and multipath effect.

# 3.6 Carrier Phase Positioning

The most accurate positioning is done with the carrier phase observable. A certain number of carrier cycles exists between a satellite and the receiver (Figure 3.7). Knowing that the wavelenght of the L1 carrier cycle is 19.02 cm, if the number of cycles can be accounted for at all times, then, centimeter accuracy would be feasible.

The number of cycles that exist between the satellite and the receiver changes as they move toward or away from each other. The receiver cannot measure the original number of cycles when it locks on the satellite signal, but it can track the fractional phase change with subcentimeter accuracy. The receiver generates a signal similar to the carrier signal coming from the satellite, and then measures the fractional phase difference between them as the satellite and the receiver move away from or closer to one another.

Denoting $\phi^s(t)$ as the phase of the received carrier (L1 or L2) and $\phi_R(t)$ the phase of a reference carrier generated by the receiver, the following phase equations are obtained
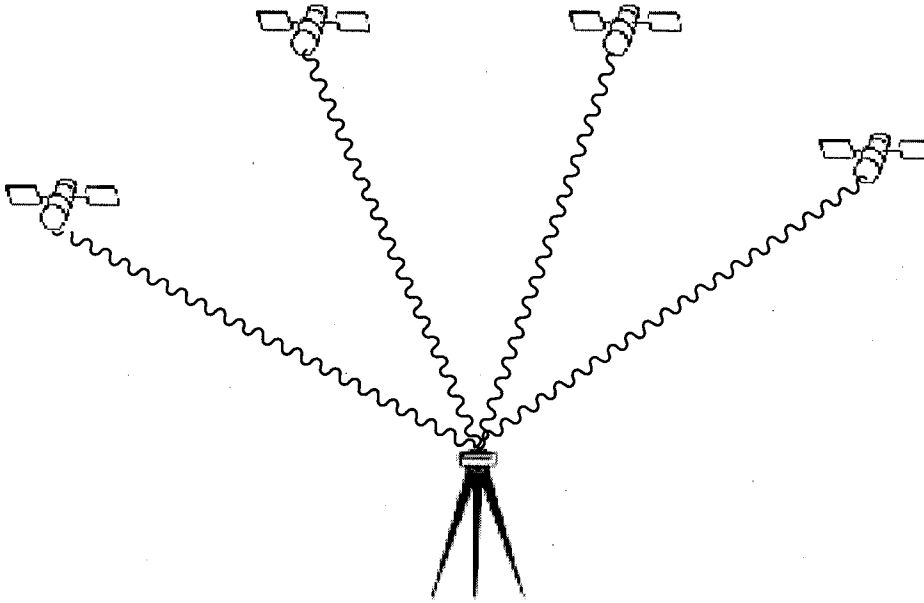
**Figure 3.7**: The Carrier phase observable

$$\phi^S(t) = f \cdot t - f \cdot \frac{\rho}{c} - \phi_0^S \tag{3.17}$$

$$\phi_R(t) = f \cdot t - \phi_{0R}. \tag{3.18}$$

The initial phases $\phi_0^S$ and $\phi_{0R}$ are caused by clock errors and are equal to

$$\phi_0^S = f \cdot dt \tag{3.19}$$

$$\phi_{0R} = f \cdot dT. \tag{3.20}$$

Hence, the beat phase is

$$\phi_R^S(t) = \phi^S(t) - \phi_R(t) = -f \cdot \frac{\rho}{c} - f \cdot dt + f \cdot dT. \tag{3.21}$$

Turning on a receiver at epoch $t_0$, the instantaneous fractional beat phase is measured. But, the initial number of cycles $N$ between satellite and receiver is unknown (Figure 3.8). $N$, which is also called the integer ambiguity, remain the same as long as there is no loss of lock. The beat phase at epoch $t$ is
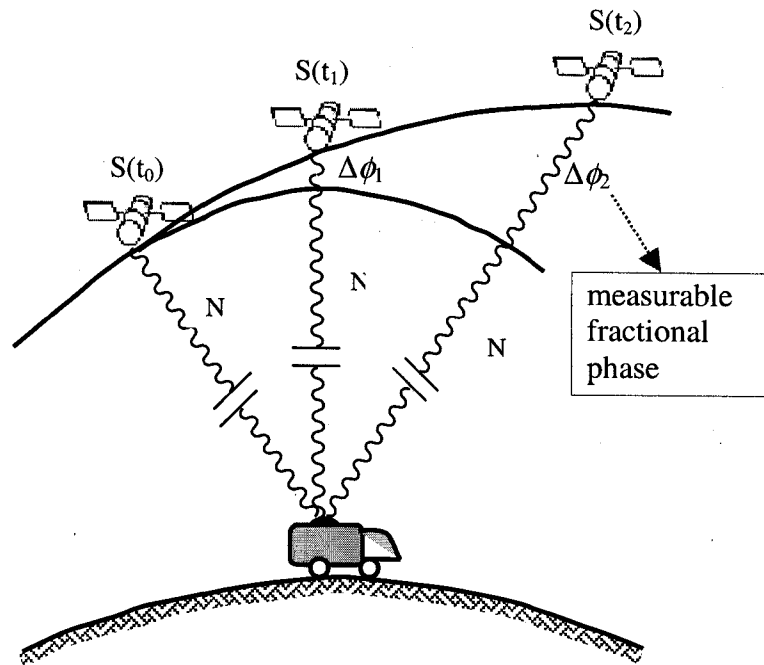
**Figure 3.8:** Geometrical interpretation of phase ranges

$$\phi_R^S(t) = \Delta\phi_R^S\big|_{t_0}^{t} + N \tag{3.22}$$

where $\Delta\phi_R^S\big|_{t_0}^{t}$ is the measurable fractional phase at epoch $t$ augmented by the number of integer cycles since the initial epoch $t_0$. Equating the beat phase in both equations (3.21) and (3.22), and using $\Phi = -\Delta\phi_R^S$ gives

$$\Phi = \rho - c\cdot dt + c\cdot dT + \lambda\cdot N \tag{3.23}$$

where $\Phi$ is in meters and $\lambda$ is the wavelength. Adding the atmospheric effect, the orbital error and the combination of multipath error and noises gives

$$\Phi = \rho + d\rho - c\cdot dt + c\cdot dT + \lambda\cdot N - I + T + \varepsilon. \tag{3.24}$$

This was the equation for carrier phase observation.

# 3.7 GPS Error Analysis

Understanding the flow of GPS errors in the observation equations and their relationship to the geometry of the satellites in view, provides understanding on how these errors get transformed into a receiver positioning error. This section presents the GPS error equation, as developed by [Parkinson, '96], beginning with the fundamental measurements, proceeding with analysis of the effects of various errors and finally incorporating the concept of dilution of precision (*DOP*).

The true measurement is the GPS signal arrival time delayed by the vacuum transit time and ionospheric and tropospheric effects

$$t_A = t_T + \frac{\rho}{c} + \frac{T}{c} + \frac{I}{c} \tag{3.25}$$

where $t_A$ = true arrival time; $t_T$ = true transmit time; $\rho$ = true range in meters; $c$ = speed of light in vacuum; $T$ = tropospheric delay in meters; $I$ = ionospheric delay in meters.

The measured arrival time reflects the user's clock bias and other measurement errors, and is written as

$$t_{Au} = t_A + b_u + \frac{v}{c} \tag{3.26}$$

where $t_{Au}$ = arrival time measured by the user; $b_u$ = user clock bias estimate; $v$ = receiver noise, multipath, interchannel errors in meters.

The satellite clock correction transmitted by the satellite can also be in error (dominant error is selective availability SA). The satellite time equation can be written as

$$t_{Ts} = t_T + B \tag{3.27}$$

where $t_{Ts}$ = transmission time in satellite message; $B$ = true error in satellite's transmission time including SA.

The true range $\rho$ is the absolute value of the vector difference between the true satellite position and the true user position

$$\rho = \left| \bar{r}_s - \bar{r}_u \right| = \bar{1}_s \bullet \left[ \bar{r}_s - \bar{r}_u \right] \tag{3.28}$$

where $\bar{r}_s$ = true satellite position; $\bar{r}_u$ = true user position; $\bar{1}_s$ = true unit vector from user to satellite.

The user receiver actually measures the pseudorange $P$ by the following

$$P = c.\left( t_{Au} - t_{Ts} \right). \tag{3.29}$$

Using (3.29), (3.25), (3.26) and (3.27) gives

$$P = \rho + c.\left( b_u - B \right) + \left( T + I + v \right) \tag{3.30}$$

$$P = \bar{1}_s \bullet \left[ \bar{r}_s - \bar{r}_u \right] + c.\left( b_u - B \right) + \left( T + I + v \right). \tag{3.31}$$

To account for the estimated value (^) and the estimate error ($\Delta$), each of the above terms is to be broken into two parts as follows

$\bar{r}_s = \hat{\bar{r}}_s - \Delta \bar{r}_s$    where $\hat{\bar{r}}_s$ = satellite position from the Navigation Message in m,

$\bar{r}_u = \hat{\bar{r}}_u - \Delta \bar{r}_u$    where $\hat{\bar{r}}_u$ = user estimated position in m,

$\bar{1}_s = \hat{\bar{1}}_s - \Delta \bar{1}_s$    where $\hat{\bar{1}}_s$ = unit vector, user to satellite estimated from $\hat{\bar{r}}_s$ and $\hat{\bar{r}}_u$,

$b_u = \hat{b}_u - \Delta b_u$    where $\hat{b}_u$ = user clock bias estimate,

$B = \hat{B} - \Delta B - S$ where $\hat{B}$ = satellite transmitted clock bias; $\Delta B$ = the natural satellite clock error predicted in the Navigation Message; $S$ = error transmit time due to SA,

$$T = \hat{T} - \Delta T \quad \text{where } \hat{T} = \text{estimated or modeled tropospheric delay,}$$

$$I = \hat{I} - \Delta I \quad \text{where } \hat{I} = \text{estimated or modeled ionospheric delay.}$$

Equation (3.31) can then be modified to account for the estimated values

$$P_j = \left( \hat{\bar{1}}_{sj} - \Delta \bar{1}_{sj} \right) \bullet \left( \hat{\bar{r}}_{sj} - \Delta \bar{r}_{sj} - \hat{\bar{r}}_u - \Delta \bar{r}_u \right) + c.\left( \hat{b}_u - \Delta b_u - \hat{B}_j + \Delta B_j + S_j \right) +$$
$$\left( \hat{T}_j - \Delta T_j + \hat{I}_j - \Delta I_j + v_j \right) \tag{3.32}$$

where $j$ is the satellite number. This equation can be written as

$$\hat{\bar{1}}_{sj} \bullet \hat{\bar{r}}_u - c \cdot b_u - \hat{\bar{1}}_{sj} \bullet \Delta \bar{r}_u + c \cdot \Delta b_u = \hat{\bar{1}}_{sj} \bullet \hat{\bar{r}}_{sj} - P_j + \left[ \hat{I}_j + \hat{T}_j - c \cdot \hat{B}_j \right] - \hat{\bar{1}}_{sj} \bullet \Delta \bar{r}_{sj} -$$
$$\Delta \bar{1}_{sj} \bullet \left( \hat{\bar{r}}_{sj} - \hat{\bar{r}}_u \right) + c \cdot \left( \Delta B_j + S_j \right) - \left( \Delta I_j + \Delta T_j \right) + v_j + \left( higher \cdot order \cdot terms \right). \tag{3.33}$$

To write Equation (3.33) in matrix form, we define the following matrices for $k$ satellites

$$\underline{G}_{kx4} = \begin{bmatrix} \hat{\bar{1}}_{s1} & 1 \\ \hat{\bar{1}}_{s2} & 1 \\ \vdots & \vdots \\ \hat{\bar{1}}_{sk} & 1 \end{bmatrix}, \qquad \underline{A}_{kx3k} = \begin{bmatrix} \hat{\bar{1}}_{s1}^T & & & 0 \\ & \hat{\bar{1}}_{s2}^T & & \\ & & \ddots & \\ 0 & & & \hat{\bar{1}}_{sk}^T \end{bmatrix}$$

$$\hat{\bar{x}}_{4\times1} = \begin{bmatrix} \hat{\bar{r}}_u \\ -c \cdot \bar{b}_u \end{bmatrix}, \qquad \Delta \bar{x}_{4\times1} = \begin{bmatrix} \Delta \bar{r}_u \\ -c \cdot \Delta b_u \end{bmatrix}, \qquad \bar{R}_{3k\times1} = \begin{bmatrix} \hat{\bar{r}}_{s1} \\ \hat{\bar{r}}_{s2} \\ \vdots \\ \hat{\bar{r}}_{sk} \end{bmatrix}, \qquad \Delta \bar{R}_{3k\times1} = \begin{bmatrix} \Delta \bar{r}_{s1} \\ \Delta \bar{r}_{s2} \\ \vdots \\ \Delta \bar{r}_{sk} \end{bmatrix},$$

$$-\hat{\overline{P}}_{c_{k\times 1}} = \begin{bmatrix} -P_1 + \left(\hat{I}_1 + \hat{T}_1 - \hat{B}_1\right) \\ -P_2 + \left(\hat{I}_2 + \hat{T}_2 - \hat{B}_2\right) \\ \vdots \\ -P_k + \left(\hat{I}_k + \hat{T}_k - \hat{B}_k\right) \end{bmatrix} = \begin{bmatrix} -P_{c1} \\ -P_{c2} \\ \vdots \\ -P_{ck} \end{bmatrix}, \underline{\varepsilon}_{kx3k} = \begin{bmatrix} \Delta\overline{1}_1^T & & & 0 \\ & \Delta\overline{1}_2^T & & \\ & & \ddots & \\ 0 & & & \Delta\overline{1}_k^T \end{bmatrix}, \overline{P}_{3k\times 1} = \begin{bmatrix} \overline{r}_u \\ \overline{r}_u \\ \vdots \\ \overline{r}_u \end{bmatrix}.$$

Writing Equation (3.33) in matrix form, we have

$$\underline{G}\cdot\hat{\overline{x}} - \underline{G}\cdot\Delta\overline{x} = \underline{A}\cdot\overline{R} - \hat{\overline{P}}_c - \underline{A}\cdot\Delta\overline{R} + c\cdot\left(\Delta\overline{B} + c\cdot\overline{S} - \Delta\overline{I} - \Delta\overline{T} + \overline{v}\right) + \varepsilon\cdot\left(\overline{R} - \overline{P}\right) \quad (3.34)$$

The user is interested in determining $\hat{\overline{x}}$. If he does not know the residual errors $\Delta\overline{R}, \Delta\overline{B}, \Delta\overline{I}$ & $\Delta\overline{T}$, he ignores them and calculates the position based on

$$\underline{G}\cdot\hat{\overline{x}} = \underline{A}\cdot\overline{R} - \hat{\overline{P}}_c. \quad (3.35)$$

Then, for $k = 4$ satellites

$$\hat{\overline{x}} = \underline{G}^{-1}\cdot\left(\underline{A}\cdot\overline{R} - \hat{\overline{P}}_c\right), \quad (3.36)$$

and for $k > 4$ satellites, using the generalized matrix inverse of $\underline{G}$.

$$\hat{\overline{x}} = \left(\underline{G}^T\underline{G}\right)^{-1}\cdot\underline{G}^T\cdot\left(\underline{A}\cdot\overline{R} - \hat{\overline{P}}_c\right). \quad (3.37)$$

These were the fundamental position calculations.

$\underline{G}$ is the geometry matrix, constructed from the set of approximate directions to the satellites, as is the matrix $\underline{A}$. $\overline{R}$ is constructed from the location of the satellites that has been transmitted via the Navigation Message. $\hat{\overline{P}}_c$ is the corrected pseudorange to each satellite. The fundamental error equation becomes

$$\underline{G}\cdot\Delta\overline{x} = \left(-c\cdot\Delta\overline{B} - c\cdot\overline{S} + \Delta\overline{I} + \Delta\overline{T} - \overline{v}\right) - \varepsilon\cdot\left(\overline{R} - \overline{P}\right) + \underline{A}\cdot\Delta\overline{R} \equiv \Delta\overline{P}_c. \quad (3.38)$$

Then the position error $\Delta\overline{x}$ in meters, is

for $k = 4$ satellites:     $\Delta\overline{x} = \underline{G}^{-1}\cdot\Delta\overline{P}_c$ \quad (3.39)

for $k > 4$ satellites: $\qquad \Delta \bar{x} = \left( \underline{G}^T \underline{G} \right)^{-1} \cdot \underline{G}^T \cdot \Delta \bar{P}_c .$ $\qquad\qquad\qquad\qquad$ (3.40)

From these equations we can see that satellite geometry, represented by matrix $G$, affects the accuracy of the error. As a matter of fact, if four satellites are in view, the determinant of $G$ is proportional to the scalar triple product $\left[ (\hat{\bar{1}}_{s4} - \hat{\bar{1}}_{s1}), (\hat{\bar{1}}_{s3} - \hat{\bar{1}}_{s1}), (\hat{\bar{1}}_{s2} - \hat{\bar{1}}_{s1}) \right]$ which can be interpreted as the volume of the space created by the receiver-satellite vectors. The bigger the volume, the higher the determinant, the smaller the error. This brings the powerful concept of geometric dilution of precision $GDOP$.

If we take the covariance of the position, we get

$$\text{cov}(position) = E\left[\Delta \bar{x} \cdot \Delta \bar{x}^T \right] = \left( \underline{G}^T \underline{G} \right)^{-1} \cdot \underline{G}^T \cdot E\left[\Delta \bar{P} \cdot \Delta \bar{P}^T \right] \cdot \underline{G} \cdot \left( \underline{G}^T \underline{G} \right)^{-1} \text{ for } k > 4 \quad (3.41)$$

$$\text{cov}(position) = E\left[\Delta \bar{x} \cdot \Delta \bar{x}^T \right] = \underline{G}^{-1} \cdot E\left[\Delta \bar{P} \cdot \Delta \bar{P}^T \right] \cdot \underline{G}^{-T} \qquad \text{for } k = 4. \qquad (3.42)$$

Because $G$ does not have a random component, it was brought outside the expectation operator. If all ranging errors have the same variance $[\sigma_R{}^2]$ (m$^2$) and are uncorrelated zero mean, ($E[\Delta P_i \Delta P_j] = 0$, $i \neq j$), then, the expectation $E[\Delta P \cdot \Delta P^T] = \sigma_R{}^2 \cdot I$, where $I$ is 4x4 identity matrix. Then

$$\text{cov}(position) = E\left[\Delta \bar{x} \cdot \Delta \bar{x}^T \right] = \sigma_R{}^2 \cdot \left[ \underline{G}^T \cdot \underline{G} \right]^{-1} \qquad\qquad\qquad (3.43)$$

where $\left[ \underline{G}^T \cdot \underline{G} \right]^{-1}$ is the matrix of multipliers of ranging variance to give position variance and is known as the GDOP or geometric dilution of precision matrix. If the position coordinates are the ordered right-hand set, East, North and Up, then

$$\text{cov}(position) = \sigma_R{}^2 \begin{bmatrix} (EastDOP)^2 & & & cov\,ariance.terms \\ & (NorthDOP)^2 & & \\ & & (VerticalDOP)^2 & \\ cov\,ariance.terms & & & (TimeDOP)^2 \end{bmatrix} . \quad (3.44)$$

Equation (3.44) tells us that, an error with a variance of $\sigma_R{}^2$ in the satellite-receiver range would lead to an error with a covariance $\text{cov}(position)$ in the receiver position.

The scalar GDOP is defined to be the square root of the trace of the GDOP matrix

$$GDOP(geometric) = \sqrt{(NorthDOP)^2 + (EastDOP)^2 + (VDOP)^2 + (TimeDOP)^2} \quad (3.45)$$

Also, we have

$$HDOP(horizontal) = \sqrt{(NorthDOP)^2 + (EastDOP)^2} \quad\quad\quad (3.46)$$

and

$$PDOP(position) = \sqrt{(NorthDOP)^2 + (EastDOP)^2 + (VDOP)^2} \quad . \quad\quad (3.47)$$

The concept of *GDOP* is a powerful tool for GPS. All receivers use some algorithm base on *GDOP* to select the best set of satellites to track among the group of up to 11 satellites in view. Positioning accuracy can then be estimate as the ranging accuracy *UERE* multiplied by a dilution factor. This dilution factor (*DOP*) depends solely on geometry. *UERE* and *DOP* factor allow an estimation of the achievable point positioning accuracy.

With Differential GPS, as explained in the following sections, in order for the reference receiver to calculate the corrections, it solves the reversed problem. Its antenna is located in a known position. Then, it solves equation

$$G\hat{\bar{x}}_T = A \cdot \bar{R} - \bar{P}_c - \Delta\hat{\bar{P}}_R \quad\quad\quad\quad (3.48)$$

where $\Delta \hat{\bar{P}}_R$ is the estimated ranging error, transmitted to the user then

$$\Delta \hat{\bar{P}}_R = A \cdot \bar{R} - \bar{P}_c - G\hat{\bar{x}}_T .$$

(3.49)

This is the fundamental reference station calculation.

# 3.8 Differential GPS (DGPS)

DGPS is based on a simple idea. If the coordinates of one fixed receiver are accurately known, then its distance from each satellite in view can be easily computed. Remember that, the accurate positions of the satellites are derived from the Navigation Message. Comparing this computed distance or true range with the erroneous measured pseudorange gives the error or the correction amount. The error is found for every satellite in view, and then broadcasted by the fixed receiver via telemetry. This fixed receiver is referred to as base or reference station (Figure 3.9). Any number of roving receivers could pick up the broadcasted information and correct their own measured pseudoranges from the satellite, by that correction amount. In this way, the roving receivers improve the accuracy of their measured pseudoranges.

If the base and user receivers are in the same vicinity (within 30 km), they will see, more or less, the same errors and can reduce them with the DGPS technique. DGPS is successful in many applications because the largest GPS errors vary slowly with time and are strongly correlated over distance.
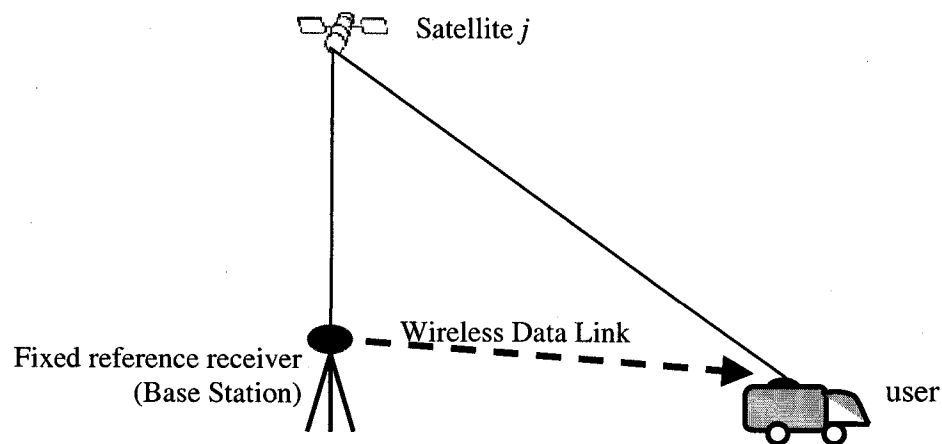
**Figure 3.9**: Differential GPS (DGPS)

The transmission of correction data between the reference receiver and the remote receivers is standardized as proposed by the Radio Technical Commission for Maritime Services (RTCM) [Hofmann et al., '97].

The differential correction message is broadcasted every 2 to 30 seconds. The longer the time interval between correction values, the less accurate they become. The DGPS positioning accuracy gets reduced as the correction ages. This phenomenon is referred to as the latency in applying the corrections. For instance, if the latency is 10 seconds, then the pseudorange error expected to grow to approximately 0.2 m, [Parkinson and Enge, '96].

If the delay of application of the corrections (latency) is zero, then the process is called Relative Positioning, where the reference receiver transmits the raw observables to the remote receiver. Then, the remote receiver time-matches the received observables and its own and then does all the differencing calculations, as presented in Section 3.12.

# 3.9 GPS Error Types

In order to know the effect of the DGPS technique on each GPS error, the errors are classified into three different types [Parkinson and Enge, '96]. DGPS would either eliminate the error, reduce it or have no effect on it. The three types are

- Type 1: Errors that decorrelates with distance

- Type 2: Errors that decorrelates with time or latency

- Type 3: Errors that are uncorrelated (not correctable with DGPS).

Type 1 errors are caused by atmospheric effects and improperly modeled orbits. They are highly spatially correlated over distances up to about 20 km. Type 2 errors are mainly due to Selective Availability (SA) which is highly correlated with time. The ionospheric error is both type 1 and type 2. Type 3 errors are uncorrelated with either distance or latency. They are mainly multipath and receiver noise errors.

Generally, in DGPS the reference base station is separated from the user in two ways, geographically, which leads to that the user and the reference might not see exactly the same error (spatial decorrelation - Type 1 errors) depending on the distance between them, and by delay of application of the corrections (temporal decorrelation or latency – Type 2 errors). Because SA is relatively large and has fairly random velocity and acceleration magnitudes, it totally dominates the latency-induced error growth.

DGPS cancels the part of the error that is correlated between the reference station and the user. In carrier phase DGPS, the reference receiver $A$ calculates the phase range differential correction $\Phi c^{j}(t_{o})$ for satellite $j$ at reference epoch $t_{o}$, which is written as

$$\Phi c^{j}(t_o) = -\Phi_A^{j}(t_o) + \rho_A^{j}(t_o) \tag{3.50}$$

or

$$\Phi c^{j}(t_o) = -\Delta\rho_A^{j}(t_o) - c \cdot dt_A^{j}(t_o) + c \cdot dT_A(t_o) - \lambda \cdot N_A^{j} - \varepsilon_A^{j}(t_o). \tag{3.51}$$

The correction $\Phi c^{j}(t_o)$ changes with time and distance from the base station. The best way to describe the effect of the temporal and spatial decorrelation is with a second order relationship between the differential correction calculated by the base station at time $t_0$ and the best correction at time $t$ is as follow

$$\Phi c(t) = \Phi c(t_0) + \dot{\Phi} c(t_0)(t - t_0) + \ddot{\Phi} c(t_0)\frac{(t - t_0)^2}{2} + \frac{\partial(\Delta\rho)}{\partial x} \cdot \delta x + \delta\rho \tag{3.52}$$

where

1. $\Phi c(t)$ is the correction at time $t$,

2. $\Phi c(t_0)$ is the correction estimated by the reference station,

3. $\dot{\Phi} c(t_0)(t - t_0)$ is the portion of the correction due to the rate of change of $\Phi c(t_0)$,

4. $\ddot{\Phi} c(t_0)\frac{(t - t_0)^2}{2}$ is the portion of the correction due to the acceleration of $\Phi c(t_0)$,

5. $\frac{\partial(\Delta\overline{\rho})}{\partial\overline{x}} \cdot \delta x$ is a first order term representing the portion of the correction due to

   the spatial separation between the base and user receivers, and

6. $\delta\rho$ is the uncorrelated error from receiver noise and multipath.

Term 5, which is the spatial or geographical decorrelation, cannot be estimated by either receiver. Term 6 is different for each receiver. Term 4 is normally ignored and results in a few centimeter error according to [Lapucha and Baker, '95]. The rate of

change $\dot{\Phi}c(t_0)$ is calculated using previous values of $\Phi c(t_0)$. Then, the correction formula reduces to a $1^{st}$ order Taylor series written as

$$\Phi_c(t) = \Phi_c(t_0) + \dot{\Phi}_c(t_0)(t - t_0).$$ (3.53)

Similarly, the reduced correction formula for the C/A code observable can be written as

$$PRC^j(t) = PRC^j(t_0) + RRC^j(t_0) \cdot (t - t_0)$$ (3.54)

where $PRC^j(t)$ is the PseudoRange Correction and $RRC^j(t_0)$ (Rate Range Correction) is the rate of change of that correction.

## 3.10 DGPS Using the C/A Code

The pseudorange equation for the reference receiver at point $A$ for satellite $j$ is

$$P_A^j(t_0) = \rho_A^j(t_0) + \Delta\rho_A^j(t_0) + c \cdot dt(t_0) - c \cdot dT_A(t_0) + V_A(t_0)$$ (3.55)

where $\Delta\rho_A^j(t_0)$ is the combination of ionospheric, tropospheric and orbital errors. True range $\rho_A^j(t_0)$ is known since the location of the receiver is known. So, the pseudorange correction $PRC$ is the difference between the true and measured ranges

$$PRC^j(t_0) = -P_A^j(t_0) + \rho_A^j(t_0)$$ (3.56)

or

$$PRC^j(t_0) = -\Delta\rho_A^j(t_0) - c \cdot dt(t_0) + c \cdot dT_A(t_0) - V_A(t_0).$$ (3.57)

$PRC$ is always being calculated but transmitted once every several seconds. The rate of change of $PRC$ within these several seconds is the $RRC$ (range rate correction) must be also calculated and transmitted with the $PRC$. From a time series of range corrections, the

range rate correction $RRC$ can be evaluated by numerical differentiation. Thus, the code range correction at an arbitrary epoch $t$ is approximated by

$$PRC^j(t) = PRC^j(t_0) + RRC^j(t_0) \cdot (t - t_0) \tag{3.58}$$

where $t$-$t_0$ is the latency that is essential for best accuracy.

Now, the code ranges measured at the rover are

$$P_X^j(t) = \rho_X^j(t) + \Delta\rho_X^j(t) + c \cdot dt(t) - c \cdot dT_X(t) + v_X(t) \tag{3.59}$$

Applying the range correction to the measured pseudorange yields

$$P_X^j(t)_{corr.} = P_X^j(t) + PRC^j(t) \tag{3.60}$$

or

$$P_X^j(t)_{corr.} = \rho_X^j(t) + (\Delta\rho_X^j(t) - \Delta\rho_A^j(t)) + c \cdot (dt_X(t) - dt_A(t)) - c \cdot (dT_X(t) - dT_A(t)) + (v_X(t) - v_A(t)) \tag{3.61}$$

For moderate length baselines (tens of kilometers), $\Delta\rho_X^j(t)$ and $\Delta\rho_A^j(t)$ at both stations are highly correlated and virtually identical. Also, the error of the satellite clock is a slowly varying error, so it will cancel out. $(v_X(t) - v_A(t))$ is the combined multipath and noise error that will not cancel out. It will be ignored for the rest of this section. The corrected range becomes

$$P_X^j(t)_{corr.} = \rho_X^j(t) - c \cdot (dT_X(t) - dT_A(t)) \tag{3.62}$$

or

$$P_X^j(t)_{corr.} = \rho_X^j(t) - c \cdot \Delta dT_{AX}(t) \tag{3.63}$$

where $\Delta dT_{AX}(t) = dT_X(t) - dT_A(t)$ is the combined error of the receiver clock at times $t_o$ and $t$. The effect due to SA, ionospheric and tropospheric refractions have been eliminated.

At least four satellites are needed to solve for the coordinates of point $X$ and the combined receiver clock error.

# 3.11 DGPS Using Single Frequency Carrier Phases

Using the L1-carrier phase observable, the pseudorange derived from single frequency carrier phases measured at base station $A$ is

$$\Phi_A^j(t_o) = \rho_A^j(t_o) + \Delta\rho_A^j(t_o) - c \cdot dt_A^j(t_o) + c \cdot dT_A(t_o) + \lambda \cdot N_A^j + \varepsilon_A^j(t_o). \qquad (3.64)$$

The phase range correction calculated at $A$, at reference epoch $t_o$ is given by

$$\Phi c^j(t_o) = -\Phi_A^j(t_o) + \rho_A^j(t_o) \qquad (3.65)$$

which is also equal to

$$\Phi c^j(t_o) = -\Delta\rho_A^j(t_o) - c \cdot dt_A^j(t_o) + c \cdot dT_A(t_o) - \lambda \cdot N_A^j - \varepsilon_A^j(t_o). \qquad (3.66)$$

The phase differential correction $\Phi c^j(t)$ at an arbitrary epoch $t$ is approximated by

$$\Phi c^j(t) = \Phi c^j(t_o) + \dot{\Phi} c^j(t_o) \cdot (t - t_o). \qquad (3.67)$$

Now, the phase ranges measured for any receiver $X$ at epoch $t$ can be modeled as

$$\Phi_X^j(t) = \rho_X^j(t) + \Delta\rho_X^j(t) - c \cdot dt_X^j(t) + c \cdot dT_X(t) + \lambda \cdot N_X^j + \varepsilon_X^j(t). \qquad (3.68)$$

Applying the range correction to the measured phase range yields

$$\Phi_X^j(t)_{Corr.} = \Phi_X^j(t) + \Phi c^j(t) \qquad (3.69)$$

$$\Phi_X^j(t)_{Corr.} = \rho_X^j(t) + \left(\Delta\rho_X^j(t) - \Delta\rho_A^j(t_o)\right) + \lambda\left(N_X^j - N_A^j\right) +$$
$$c\left(dt_X^j(t) - dt_A^j(t_o)\right) - c\left(dT_X(t) - dT_A(t_o)\right) + \left(\varepsilon_X^j(t) - \varepsilon_A^j(t_o)\right) \tag{3.70}$$

At close distance between $A$ and $X$ (within 30 km), the combined errors $\Delta\rho_A^j(t)$ and $\Delta\rho_X^j(t)$ are very similar. The satellite clock error is a slowly varying error, so, it cancels out. The multipath and noise are ignored. The corrected range becomes

$$\Phi_X^j(t)_{Corr.} = \rho_X^j(t) - c \cdot \left(dT_X(t) - dT_A(t_o)\right) + \lambda\left(N_X^j - N_A^j\right). \tag{3.71}$$

Combining the ambiguities and both receiver clock errors gives

$$\Phi_X^j(t)_{Corr.} = \rho_X^j(t) + \lambda\Delta N_{XA}^j - c \cdot \Delta dT_{AX}(t). \tag{3.72}$$

The unknown ambiguities $\lambda\Delta N_{XA}^j$ are usually resolved using an ambiguity resolution technique [Hatch, '90]. $\Delta dT_{AX}(t)$ is the combined error of the base and user clocks.

The effect due to SA, ionospheric and tropospheric refractions have been reduced or eliminated. Once the ambiguities are resolved, at least four satellites are needed to solve for the coordinates of point $X$ and the combined receiver clock error. Table 3.3 shows the effect of DGPS in reducing or eliminating the residual errors of the carrier phase observable with zero baseline-zero latency, latency and geographic decorrelation.

**Table 3.3**: Errors that are eliminated or reduced by DGPS.

| Error Source | Without DGPS Correction | Zero Baseline, Zero Latency | Decorrelation with Latency (m/s) | Geographic Decorrelation (m/100km) |
|---|---|---|---|---|
| Receiver Noise | <0.01 | <0.01 | 0.0 | 0.0 |
| Multipath | 0.05 | 0.05 | 0.0 | 0.0 |
| Satellite Clock | 21.0 | 0.0 | 0.21 | 0.0 |
| Satellite Orbit | 3.0 | 0.0 | negligible | <0.05 |
| Ionosphere | 2.0-10.0 | 0.0 | negligible | <0.2 |
| Troposphere | 2.0 | 0.0 | negligible | <0.2 |

# 3.12 Relative Positioning

DGPS is called relative positioning when the corrections are applied with zero latency. The best accuracy with GPS is achieved by using carrier phase relative positioning. Relative positioning is based on simultaneous measurements at both sites. Figure 3.10 shows $A$ as the reference receiver at a known position and receiver $B$ as the user at an unknown position to be determined. Basically, since the position of receiver $A$ is known, we are after the $AB$ baseline vector, then, we can determine the coordinates of $B$. Single difference is the term used when two receivers and one satellite are involved (Figure 3.10a). The phase equations are

$$\Phi_A^k = \rho_A^k - c \cdot dt^k + c \cdot dT_A + \lambda \cdot N_A^k - I_A^k + T_A^k + \varepsilon_A \tag{3.73}$$

and

$$\Phi_B^k = \rho_B^k - c \cdot dt^k + c \cdot dT_B + \lambda \cdot N_B^k - I_B^k + T_B^k + \varepsilon_B . \tag{3.74}$$

Taking the difference between these two equations with assuming the ionospheric and tropospheric effects are equal for both receivers and ignoring $\varepsilon_A$ and $\varepsilon_B$ gives the single difference equation

$$\Phi_B^k - \Phi_A^k = \rho_B^k - \rho_A^k + c \cdot dT_B - c \cdot dT_A + \lambda \cdot N_B^k - \lambda \cdot N_A^k. \qquad (3.75)$$

Notice that since the same satellite is involved, the satellite clock error cancels out. Writing this equation in a shorthand notation form gives

$$\Phi_{AB}^k = \rho_{AB}^k - c \cdot dT_{AB} + \lambda \cdot N_{AB}^k. \qquad (3.76)$$



a: Single Difference          b: Double Difference
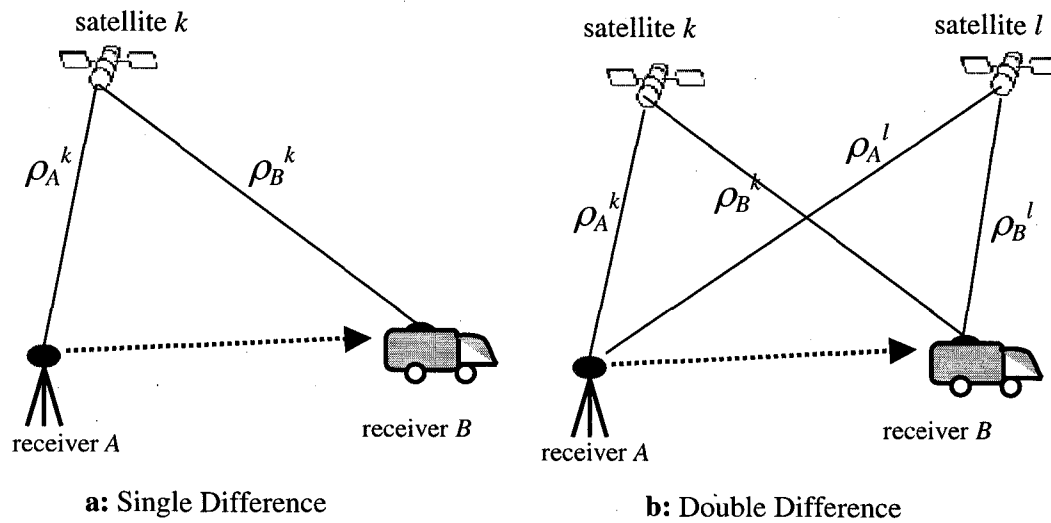
**Figure 3.10:** Relative positioning

Double difference is the term used when using two satellites $k$ and $l$ and the two receivers (Figure 3.10b). Two single difference equations can be written

$$\Phi_{AB}^k = \rho_{AB}^k - c \cdot dT_{AB} + \lambda \cdot N_{AB}^k \qquad (3.77)$$

$$\Phi_{AB}^l = \rho_{AB}^l - c \cdot dT_{AB} + \lambda \cdot N_{AB}^l. \qquad (3.78)$$

Differencing these two equations gives the double difference equation

$$\Phi^l_{AB} - \Phi^k_{AB} = \rho^l_{AB} - \rho^k_{AB} + \lambda \cdot N^l_{AB} - \lambda \cdot N^k_{AB}. \tag{3.79}$$

Writing (3.79) in shorthand notation

$$\Phi^{kl}_{AB} = \rho^{kl}_{AB} + \lambda \cdot N^{kl}_{AB}. \tag{3.80}$$

Notice that the receiver clock error combination $c \cdot dT_{AB}$ cancels out. Double difference is the most used technique in relative positioning.

In static mode where $B$ is also stationary, as in surveying applications, the problem is simple because it is not crucial how fast $B$ receives the observables from $A$ and how fast the calculation process is. On the contrary, in RTK the observables measured by reference receiver $A$ must be radio linked with minimum latency and high accuracy to the receiver $B$ to do the direct differencing calculations. In addition to the calculations, the rover has to do time matching in order to use the same epoch's observables from both receivers. This process is complicated since a lot of data is transmitted to the rover $B$, with each reference data set has to be time-matched with the rover's so that, direct differencing calculations can be done.

Lapucha and Baker, '95 argued against RTK with carrier phase relative positioning because of the operational limitations that still exist in the real-time environment. These limitations are due to time-matching delays that adds a few seconds to the data link delay. They suggested using the carrier phase DGPS method without direct differencing (without relative positioning). The result is an uninterrupted and more robust DGPS positioning with slightly degraded accuracy. To make up for some of the accuracy degradation, they included the correction accelerations by using a second order extrapolation model.

# 3.13 Ambiguity Resolution

GPS receivers are only capable of measuring the fractional part of the GPS carrier phase observable, which leaves ambiguous the initial number of integer cycles between the receiver and the satellite. This cycle ambiguity must be resolved (fixed to an integer value) before precise carrier-phase measurements can be achieved. The encouraging news is that, this cycle ambiguity remains constant as long as no cycle slip or loss of lock occurs.

In vehicle guidance and automatic control applications, it is necessary to be able to resolve the ambiguities while the vehicle is in motion. This process is known as On-The-Fly (OTF) ambiguity resolution. Several methods and algorithms have been presented and used to solve the OTF problem. These methods include the least square ambiguity search technique [Hatch, '90], the ambiguity function method (AFM) [Counselman and Gourevitch, '81], the fast ambiguity resolution approach (FARA) [Frei and Beutler, '90] and the fast ambiguity search filter (FASF) [Chen and Lachapelle, '94].

Ambiguity resolution is done in two steps. First, the generation of potential ambiguity combinations that should be considered by the algorithm. This part is done by setting an initial search volume that has a high degree of certainty of containing the correct location. Second, the method to select the integer ambiguity combination which fits the measurements.

# 3.14 Limitations of DGPS

The limitation of RTK with DGPS, in both its forms, DGPS with latency and relative positioning, are the following

- The need to have adequate data links between the reference and rover receivers is the single factor that prevents reliability in real-time positioning. UHF frequency, which is usually used to transmit the differential corrections, has a drawback that the range of waves is limited to the line of sight between transmitter and receiver. Natural barriers, buildings, structures and trees block the line of site between the receivers. In addition, rovers can't go beyond the limit of the transmitter, usually 25 km.

- The cost of establishing reference base stations, to cover the entire field of operation, and radio link equipment, sometimes, make the project not cost effective.

- With DGPS, at least four common satellites must be tracked simultaneously at both sites throughout the session, that might be tough to achieve if the distance between reference and rover is great.

- Large geographical distances and altitude changes between reference and rover receivers have a decorrelation effect on atmospheric error values.

- Ambiguity resolution On-The-Fly OTF requires time matching and heavy computation that the receiver might not be able to handle sometimes.

# 3.15 Vehicle Attitude Determination with GPS

Vehicle attitude is the orientation of vehicle's fixed body frame with respect to a reference frame, usually a North-East-Up local frame. A GPS multi-antenna receiver is normally used to determine the absolute position of the vehicle along with its attitude [Cohen, '96]. One of the applications for this receiver is in avionics to determine the attitude of a plane (Figure 3.11). A dual-antenna receiver is basically two sets of satellite tracking channels sharing the same receiver clock and processor, and is usually a single frequency carrier phase receiver with a master antenna and a slave antenna. Usually, each antenna is wired to a set of 8 satellite tracking channels. The receiver normally produces the azimuth angle as well as the position of the master antenna. Three or four antenna receivers provide the position along with all orientation angles, roll, pitch and yaw, of the vehicle.

The attitude information is obtained by differencing between the antennas of the receiver. The fixed location of the antennas on the vehicle results in a constraint that can be used to increase the efficiency of attitude ambiguity resolution.
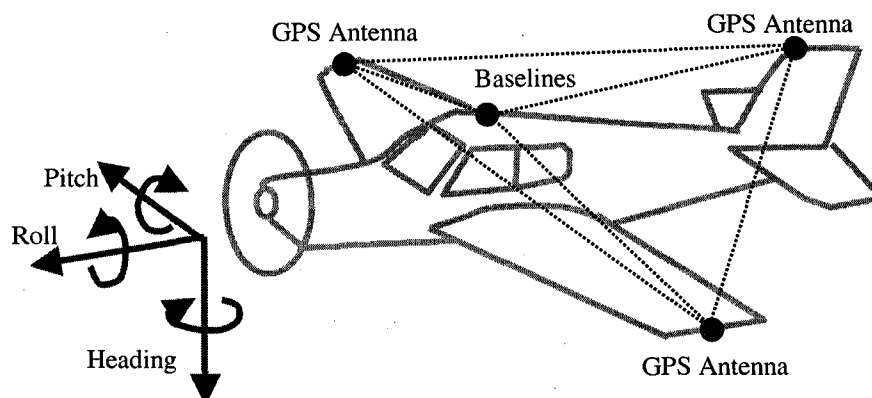


**Figure 3.11**: Plane attitude [Cohen, '96]

# Chapter 4

# In-Situ Differential GPS (IS-DGPS)

This chapter and the next one present the main contribution of this dissertation. The GPS concepts and techniques presented in Chapter 3 were used to introduce the new method, IS-DGPS. This chapter presents IS-DGPS using a single antenna GPS receiver.

IS-DGPS depends on the GPS system for positioning and on the road magnetic markers for generating the differential correction values necessary for eliminating or reducing the errors associated with GPS measurements (Figure 4.1). The concept of IS-DGPS is to generate the satellite-vehicle range correction values at every road marker and to use these values afterward to correct the measured ranges, until a new road marker is detected and a fresh set of correction values are calculated. Basically, IS-DGPS is similar in concept to DGPS, since it calculates the differential corrections at discrete times and uses a first order extrapolation model, as in Equation (3.51) or (3.52).

Figure 4.2 explains the concept of IS-DGPS in estimating the position with a simulation on a vehicle moving from west to east. The true trajectory of the vehicle is the horizontal line with the north coordinate equals to zero meters. The IS-DGPS estimated

trajectory is represented by the line with asterisks. Each asterisk represents an estimated position of the vehicle. As you see in Figure 4.2, the estimated trajectory drifts away from the true trajectory but suddenly gets pulled back to it when a road marker is encountered. At every marker, the receiver calculates a fresh set of corrections and correction rates. These corrections and their rates have the best accuracy when they are applied immediately to the measured ranges. Notice that, as a result, the best corrected position estimate occurs immediately after encountering the marker. As these correction values age, their accuracy deteriorates and the estimated trajectory drifts away from the true trajectory until a new marker is encountered, a fresh set of the differential correction values is calculated and a pull back to the true trajectory occurs. This drift is mainly due to the growth of second and higher order terms of the Selective Availability time variant error, since only the correction value's first order Taylor series element is estimated. The drift amounts to an error of a few centimeters with the phase observable.
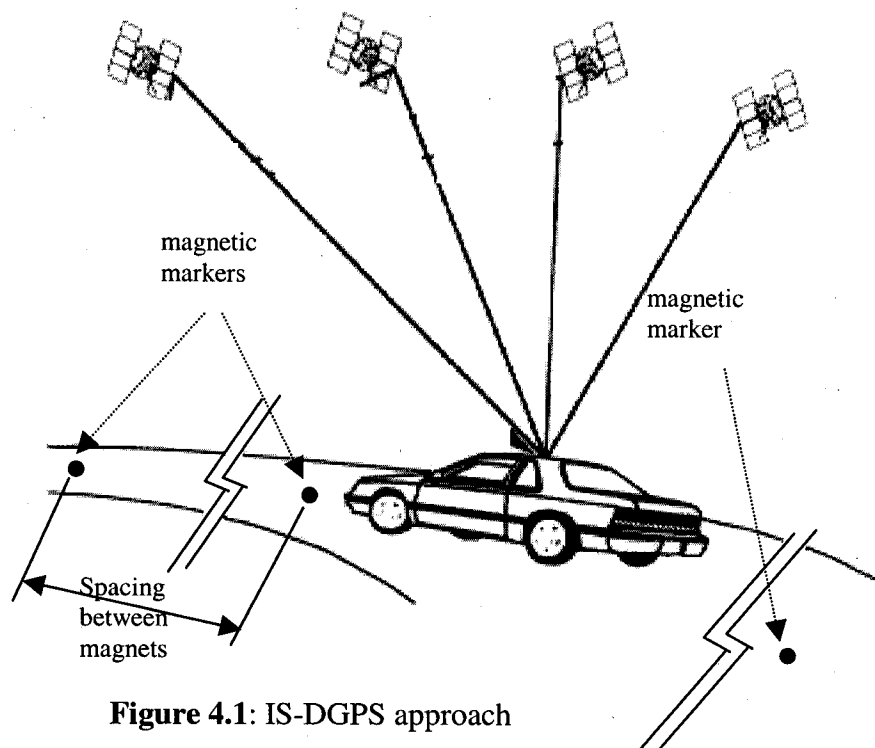
**Figure 4.1**: IS-DGPS approach
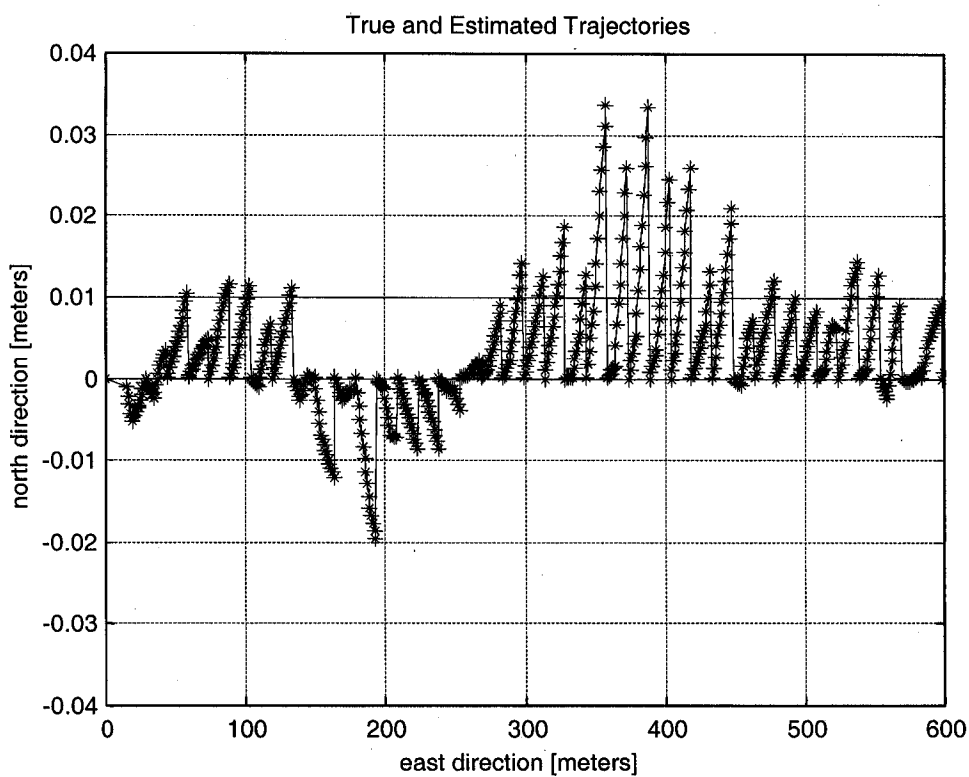


**Figure 4.2**: IS-DGPS differential correction concept

# 4.1 IS-DGPS With Code Pseudoranges

Usually, the C/A-code observable does not provide adequate accuracy for vehicle guidance and control. Positioning errors of one meter and above are normal. However, we are discussing it because the conducted experiments showed a surprisingly promising result where a maximum error of 42 cm. This result leads to the conclusion that the C/A-code observable could be used for guidance applications if a low-cost C/A code receiver is integrated with other sensors, such as a low-cost Inertial Navigation System (INS). This dissertation, however, shows that IS-DGPS with carrier phase does provide the accuracy needed for vehicle guidance and control purposes. The rest of this section presents the IS-DGPS formulation using the C/A-code observable.

When a moving vehicle passes over surveyed marker $A$ at epoch $t_o$ (Figure 4.3), the code range observation equation can be written as

$$P_A^j(t_o) = \rho_A^j(t_o) + \Delta\rho_A^j(t_o) - c \cdot dt_A^j(t_o) + c \cdot dT_A(t_o) + v_A^j(t_o) \tag{4.1}$$

Knowing the coordinates of the marker and the geometry of the vehicle, the
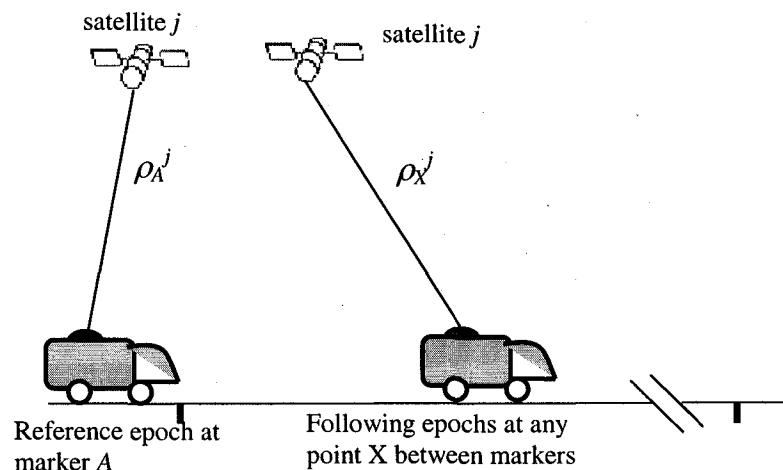


**Figure 4.3**: IS-DGPS concept

coordinates of the antenna can be quickly calculated. The coordinates of satellite $j$ are known from the Navigation Message. The known coordinates of the antenna and the satellite are used to obtain the true range $\rho_A^j$. Then, the Pseudo-Range Correction value (*PRC*) for satellite $j$ at reference epoch $t_o$ becomes

$$PRC^j(t_o) = -P_A^j(t_o) + \rho_A^j(t_o) \tag{4.2}$$

or

$$PRC^j(t_o) = -\Delta\rho_A^j(t_o) + c \cdot dt_A^j(t_o) - c \cdot dT_A(t_o) - v_A^j(t_o). \tag{4.3}$$

The rate of change of the correction is called Range Rate Correction (*RRC*) and can be estimated from previous *PRC*'s [Hofmann et al., '97]. Thus, the code range correction at an arbitrary epoch $t$ is approximated by

$$PRC^j(t) = PRC^j(t_o) + RRC^j(t_o) \cdot (t - t_o) + \frac{\partial(\Delta\rho)}{\partial x} \cdot \delta x + \delta\rho \tag{4.4}$$

where $t$-$t_o$ is the latency in applying the correction.

The term $\dfrac{\partial(\Delta\rho)}{\partial x} \cdot \delta x$ in Equation (4.4) is the first order spatial separation portion of the correction and is virtually zero with our short baselines (less than 100 meters). The last term $\delta\rho$ is ignored since it represents receiver noise and multipath errors. Consequently, Equation (4.4) reduces to

$$PRC^j(t) = PRC^j(t_o) + RRC^j(t_o) \cdot (t - t_o) \tag{4.5}$$

where $PRC^j(t)$ would be the instantenous correction at time $t$.

Now, the code ranges measured at an unknown point $X$ is modeled as

$$P_X^j(t) = \rho_X^j(t) + \Delta\rho_X^j(t) - c \cdot dt_X^j(t) + c \cdot dT_X(t) + v_X^j(t). \tag{4.6}$$

Applying the range correction to the measured pseudorange at any point $X$ yields

$$P_X^j(t)_{Corr.} = P_X^j(t) + PRC^j(t).$$  (4.7)

Hence,

$$P_X^j(t)_{Corr.} = \rho_X^j(t) + \left(\Delta\rho_X^j(t) - \Delta\rho_A^j(t_o)\right) + c \cdot \left(dt_X^j(t) - dt_A^j(t_o)\right) - c \cdot \left(dT_X(t) - dT_A(t_o)\right) + \left(v_X^j(t) - v_A^j(t_o)\right)$$  (4.8)

The combined error $\Delta\rho_X^j(t)$ and $\Delta\rho_A^j(t_0)$ are virtually equal. The error of the satellite clock is a slowly varying error, so it will be greatly reduced. Ignoring noise and multipath $v_X - v_A$, the corrected range would be

$$P_X^j(t)_{Corr.} = \rho_X^j(t) - c\left(dT_X(t) - dT_A(t_o)\right),$$  (4.9)

or in short hand notation

$$P_X^j(t)_{Corr.} = \rho_X^j(t) - c.\Delta dT_{AX}(t)$$  (4.10)

where $\Delta dT_{AX}(t)$ is the combined error of the receiver clock at times $t_0$ and $t$.

The effect due to Selective Availability, have been reduced and the effect of the ionospheric and tropospheric refractions have been eliminated. At least four satellites are needed to solve for the coordinates of point $X$ and the combined receiver clock error. The full discussion of the solution to Equation (4.10) was presented in Section 3.4.

The frequency of the reference markers has to be such that an adequately accurate RRC is generated. The work in this dissertation was based on three second spacing between the markers. Using 20 mph as a nominal speed for slowly moving specialty vehicles such as snow plows or roadway maintenance vehicles, the markers should be 26.8 meters apart in order to secure a correction every three seconds. At 60 mph, the

markers can be 80.5 meters apart. After six seconds, three corrections are obtained and can be used to calculate an *RRC* value that will be used to calculate an instantaneous correction $PRC^j(t)$ during the next three seconds. Both *PRC* and *RRC* are updated every three seconds. A more detailed discussion on the frequency of markers is given in Section 4.6.

# 4.2 IS-DGPS With Single Frequency Carrier Phases

Using the L1-carrier phase observable, the pseudorange derived from single frequency carrier phases measured at the surveyed marker $A$ is

$$\Phi_A^j(t_o) = \rho_A^j(t_o) + \Delta\rho_A^j(t_o) - c \cdot dt_A^j(t_o) + c \cdot dT_A(t_o) + \lambda \cdot N_A^j + \varepsilon_A^j(t_o). \tag{4.11}$$

The phase differential correction value $\Phi c^j$, of satellite $j$ calculated at marker $A$, at reference epoch $t_o$ is given by

$$\Phi c^j(t_o) = -\Phi_A^j(t_o) + \rho_A^j(t_o). \tag{4.12}$$

This correction value is also equal to

$$\Phi c^j(t_o) = -\Delta\rho_A^j(t_o) - c \cdot dt_A^j(t_o) + c \cdot dT_A(t_o) - \lambda \cdot N_A^j - \varepsilon_A^j(t_o). \tag{4.13}$$

The phase correction $\Phi c^j(t)$ at an arbitrary epoch $t$ is approximated by

$$\Phi c^j(t) = \Phi c^j(t_o) + \dot{\Phi} c^j(t_o) \cdot (t - t_o) + \frac{\partial(\Delta\rho)}{\partial x} \cdot \delta x + \delta\rho. \tag{4.14}$$

Using the same argument as in Section 4.1, the third term on the right hand side of (4.14) is virtually zero with our short baselines and the last term is ignored. Then, Equation (4.14) reduces to

$$\Phi c^j(t) = \Phi c^j(t_o) + \dot{\Phi} c^j(t_o) \cdot (t - t_o). \tag{4.15}$$

Now, the phase ranges measured at any point $X$ after the surveyed marker $A$ at epoch $t$ can be modeled as

$$\Phi_X^j(t) = \rho_X^j(t) + \Delta\rho_X^j(t) - c \cdot dt_X^j(t) + c \cdot dT_X(t) + \lambda \cdot N_X^j + \varepsilon_X^j(t). \tag{4.16}$$

Notice that the ambiguity stays the same, that is, $N_A^j = N_X^j$. Applying the range correction to the measured phase range yields

$$\Phi_X^j(t)_{Corr.} = \Phi_X^j(t) + \Phi c^j(t). \tag{4.17}$$

Thus,

$$\begin{aligned}\Phi_X^j(t)_{Corr.} &= \rho_X^j(t) + \left(\Delta\rho_X^j(t) - \Delta\rho_A^j(t_o)\right) + \lambda\left(N_X^j - N_A^j\right) + \\ &\quad c\left(dt_X^j(t) - dt_A^j(t_o)\right) - c\left(dT_X(t) - dT_A(t_o)\right) + \left(\varepsilon_X^j(t) - \varepsilon_A^j(t_o)\right)\end{aligned} \tag{4.18}$$

The combined errors $\Delta\rho_A^j(t)$ and $\Delta\rho_X^j(t)$ are equal since there is no spatial decorrelation, the satellite clock error is a slowly varying error, so, it gets reduced and the ambiguities cancel out as long as a cycle slip or a loss of lock does not occur. The multipath and noise are ignored at this point, but will be discussed in a Section 4.8. The corrected phase becomes

$$\Phi_X^j(t)_{Corr.} = \rho_X^j(t) - c \cdot \left(dT_X(t) - dT_A(t_o)\right) \tag{4.19}$$

or

$$\Phi_X^j(t)_{Corr.} = \rho_X^j(t) - c \cdot \Delta dT_{AX}(t). \tag{4.20}$$

At least 4 satellites are needed to solve for the coordinates of point X and the combined clock error. If more than 4 satellites are used, a least square technique could be used (see Equation (3.12)).

Table 4.1 shows the advantage that IS-DGPS has over base station DGPS in reducing or eliminating the residual errors that DGPS leaves behind. IS-DGPS eliminates or reduces the errors in the shaded blocks in Table 4.1.

The table has four columns that represent the various GPS errors in four different cases. Column 1 represents GPS errors without any DGPS correction. Columns 2, 3 and 4 represent errors residuals after DGPS corrections. Column 2 represents error residuals with perfect DGPS correction (no latency & no spatial decorrelation). Column 3 represents error residuals due to DGPS with latency decorrelation. Finally, Column 4 represents error residuals due to DGPS with spatial decorrelation.

In IS-DGPS, since the baseline between $A$ and $X$ is very short, the GPS satellite signal travels through the same portion of the atmosphere. Thus, the geographic or spatial decorrelation error residuals, shown in Column 4, vanish. On the other hand, in regular DGPS, the size of the spatial decorrelation error residual left behind depends on how far the base station is from the user. The decorrelation with latency in Column 3, can be improved with IS-DGPS by adjusting the spacing between markers accordingly. In addition, receiver noise and multipath errors, shown in Column 2, are attenuated since only one GPS receiver is involved.

**Table 4.1**: Errors in shaded blocks that are eliminated or reduced by IS-DGPS.

| Error Source | Without DGPS Correction | Zero Baseline, Zero Latency | Decorrelation with Latency (m/s) | Geographic Decorrelation (m/100km) |
|---|---|---|---|---|
| Receiver Noise | <0.01 | <0.01 | 0.0 | 0.0 |
| Multipath | 0.05 | 0.05 | 0.0 | 0.0 |
| Satellite Clock | 21.0 | 0.0 | 0.21 | 0.0 |
| Satellite Orbit | 3.0 | 0.0 | Negligible | <0.05 |
| Ionosphere | 2.0-10.0 | 0.0 | Negligible | <0.2 |
| Troposphere | 2.0 | 0.0 | Negligible | <0.2 |

# 4.3 IS-DGPS requirements and assumptions

One of the requirements of the IS-DGPS technique is to be able to recognize a reference marker and its particular (x,y,z) coordinates from among all markers, especially in the case of initialization while the vehicle is moving. The detected magnet must not be confused with neighboring ones since GPS accuracy before a differential fix could be more than 40 meters. Using polarity in an alternating fashion, where, the detected reference magnet would have an opposite polarity to the neighboring magnets would solve the problem (Figure 4.4). In this way, the detected marker can be quickly identified



Ranges of GPS positioning error without differential correction
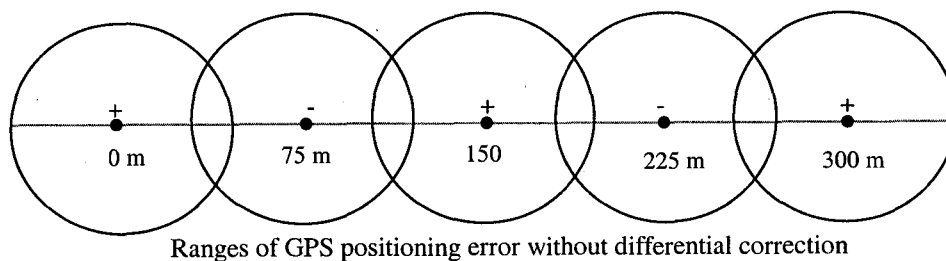
**Figure 4.4**: Reference magnet detection and identification

and its position can be fetched from the reference marker database.

For the slowly moving highway specialty vehicles such as a snowplow, the magnetic markers are placed with a shorter spacing. That creates a potential for confusing marker identity at initialization. Placing the markers in pairs (Figure 4.5) provides four different combinations of polarity codes with each combination repeating every 160 meters. This arrangement guarantees a successful system initialization anywhere on the road. Placing the markers in triplets would provide eight different polarity combinations for easy identification.
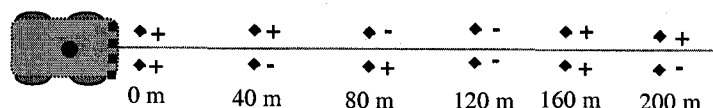


**Figure 4.5**: Arrangement for closely placed markers

If the single marker configuration was used, the assumption is that the direction of travel of the vehicle is parallel to the lane direction or the tangent that passes through the surveyed marker (Figure 4.6). Two points T1 and T2 on the tangent would be surveyed in order to know its slope. If this assumption is not made, the heading of the vehicle must be
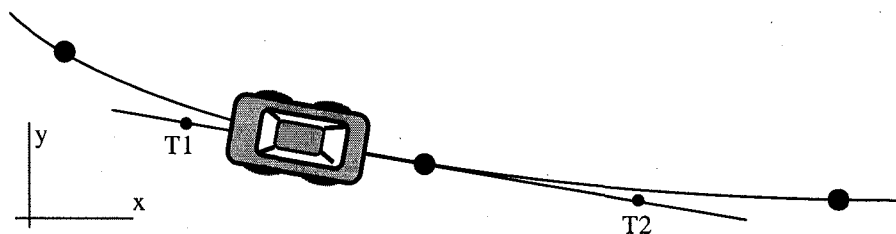


**Figure 4.6**: Vehicle orientation with the centerline

found (azimuth angle) using other sensors.

When a marker is detected, the receiver is triggered to take a GPS reading. Since there is latency $\Delta t$ involved between detecting the marker and taking a GPS measurement, we need to account for the traveled distance $v.\Delta t$ between detecting a reference marker and the point of taking the GPS measurement (Figure 4.7). This distance can be estimated using a signal from the odometer and a software timer. The location of the antenna used to calculate the correction values is $\mathbf{A2} = \mathbf{A1} + \mathbf{v}.\Delta t$. The GPS reading can also take place before the detection of the marker. Then, the calculation of the correction value and its rate takes place.
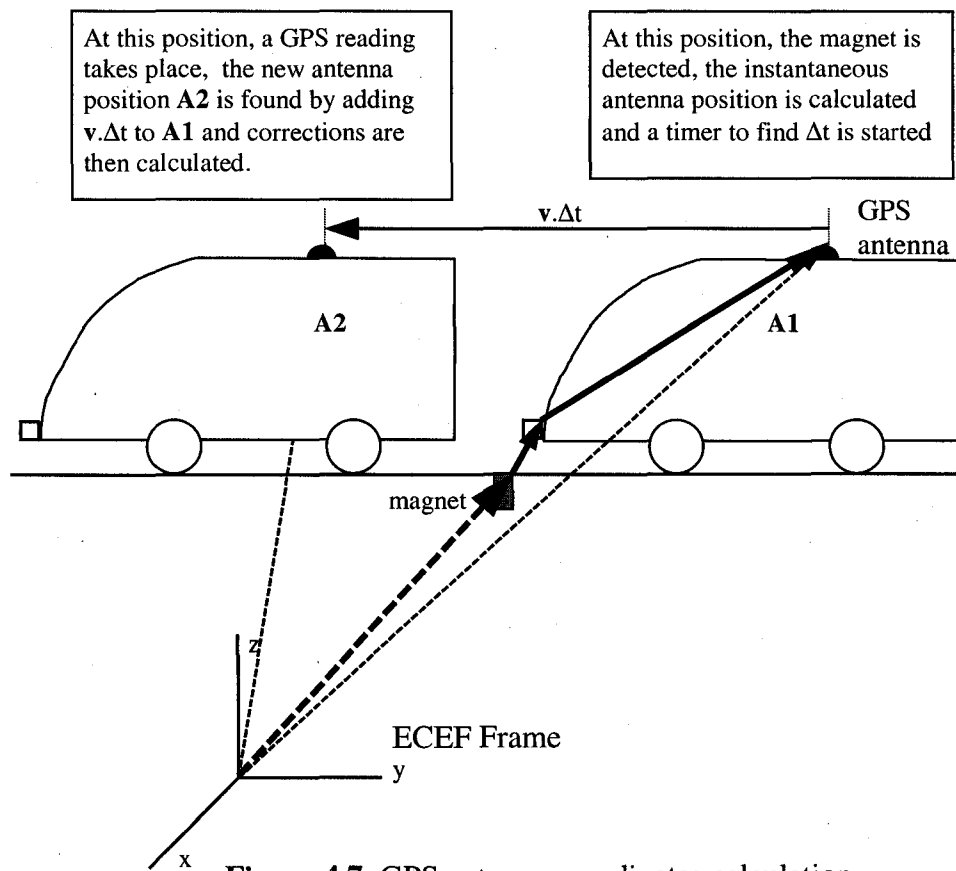


**Figure 4.7**: GPS antenna coordinates calculation

# 4.4 Experimental Evaluation of IS-DGPS

The focus of the experimental evaluation was to determine the accuracy obtainable by the IS-DGPS technique. The purpose of the experiments was not to control or guide a vehicle. In order to perform such an experimental evaluation in a cost effective fashion, a radio controlled ¼ scale model car, with no real steering mechanism was sufficient (Figure 4.8). Also, there was no need to test the technique on an actual vehicle.

The vehicle must travel on a predetermined and accurately mapped trajectory so that error measures can be obtained between the desired and the actual trajectory of the vehicle. The predetermined trajectory was chosen to be a perfect circle with a radius of 18 m. The car was attached to an 18-meter long rope close to its center of gravity. The other end of the rope was attached to a light pole in the center of a large parking lot (Figure 4.9). The experiment took place at UCD Campus parking Lot 47A. The car was originally designed to have four independent wheels with a separate DC motor on each wheel. The outer wheels of the car were disabled so that the car, while the rope is pulling it inward toward the pole, would travel in a circular trajectory. The car carried a Novatel RT-2 carrier phase GPS receiver, the GPS antenna, a laptop PC and power batteries. The car carried the GPS antenna on its top and an OMRON EE-SPZ301-A optical sensor at the bottom, placed vertically under the antenna. The car travels at 2.26 m/s. Twenty light reflective markers were placed on the trajectory, one every 5.65 meters, which secures a differential correction every three seconds. The light reflective markers and the optical sensor were used because drilling holes on the parking lot ground to install magnetic

markers was not feasible. The same results would have been obtained using either sensing system.

A base station was established at the UC-Davis airport on an accurately surveyed control point by the National Geodetic Survey Department (NGS). The name of the control point is Daveport. The airport is 1.5 miles away from Lot 47A. The car's and base station's Novatel RT-2 L1/L2 dual frequency carrier phase receivers, that have an accuracy of 2 cm, were used to accurately survey the marker locations and map the circular trajectory in post-processing mode using the double difference relative positioning technique.

Eight satellites were used. Both C/A-code and carrier phase data were logged. The positioning algorithm was done according to the theoretical formulation presented in Sections 4.1 and 4.2. The satellite orbital data obtained from the ephemeris was used to solve for the satellite's positions in the ECEF coordinate system. The receiver positioning solution was coded according to Section 3.4. Matlab was used for all calculations.
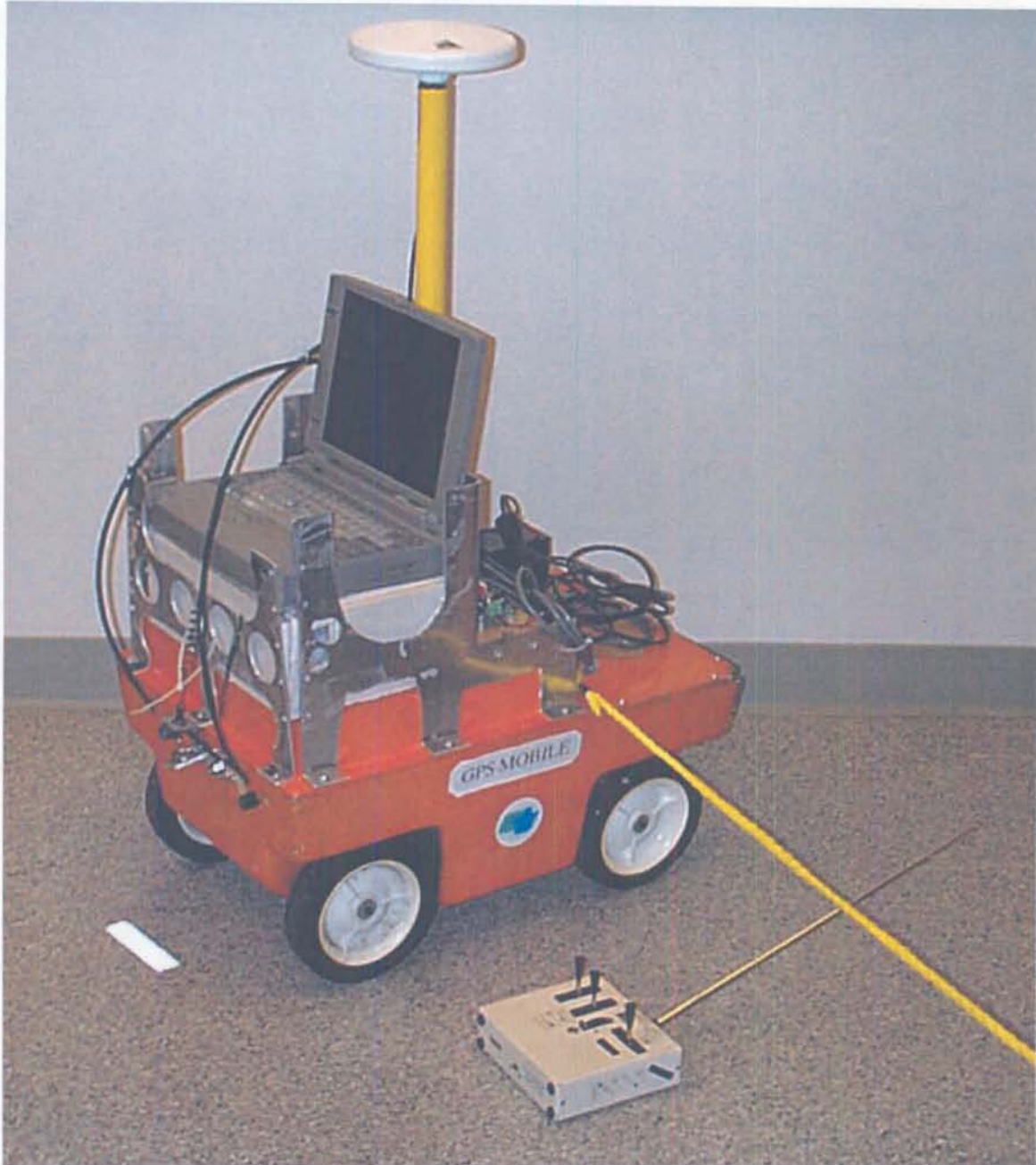
**Figure 4.8**: Radio controlled ¼ scale model car

18-meter rope

pole

UCD Parking Lot 47A

1.5 miles

Base Station at UCD Airport
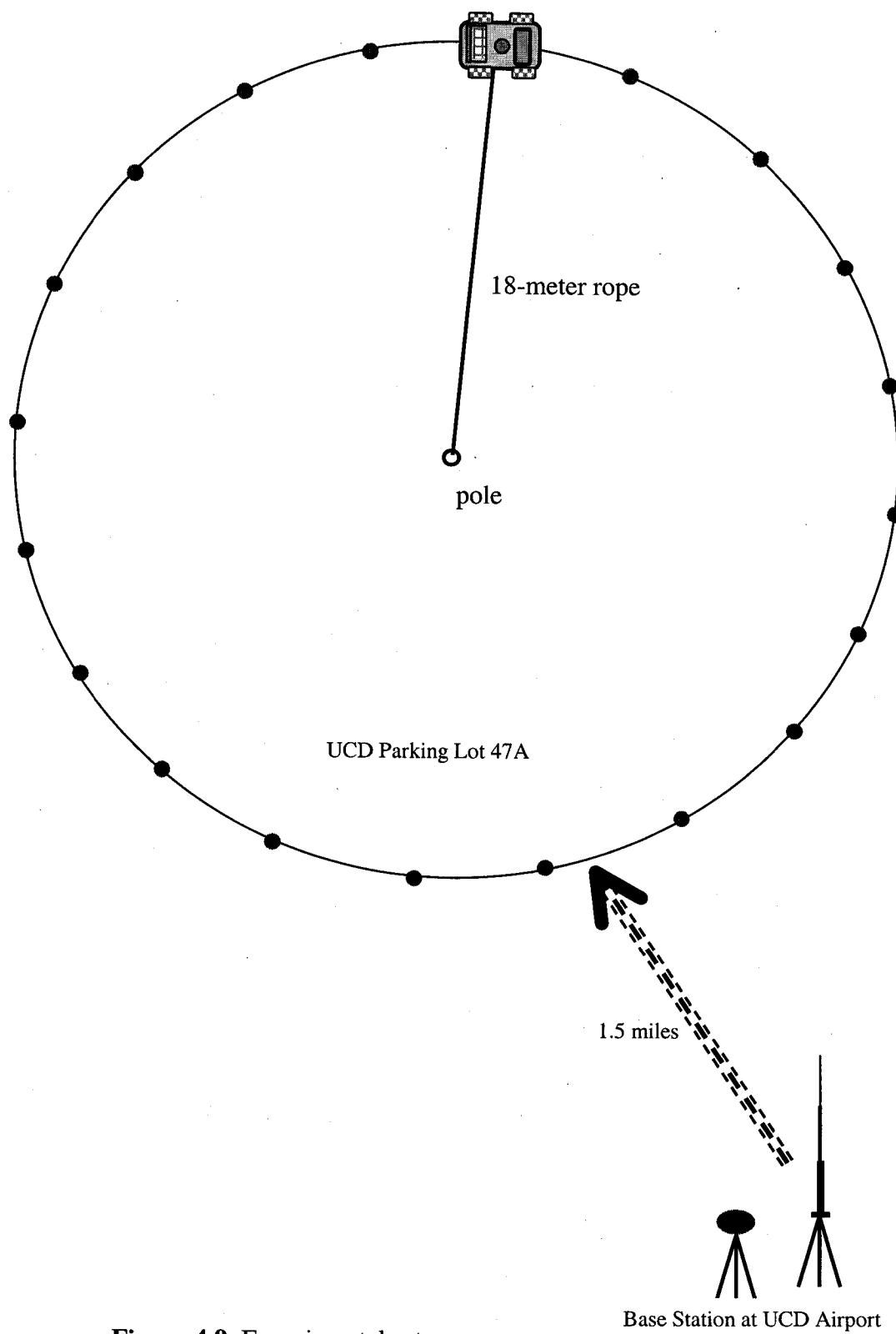
**Figure 4.9**: Experimental setup

# 4.5 Experimental Results

The IS-DGPS method was applied using both the C/A code and the carrier phase observables. Using the C/A code, the expectation was to have a positioning error of more than a meter. Usually, the C/A code is not used for guidance or automatic control. It was reported, merely, as a reference and for future research (see Section 6.6.1). However, the results showed that the positioning accuracy using the C/A code was better than expected. Figure 4.10 shows the true post-processing and the IS-DGPS C/A code trajectories. Figure 4.11 shows the lateral deviation of the estimated C/A circular trajectory from the true trajectory. The error using the C/A code had a standard deviation of 16 cm with a maximum error of 42 cm.

Using the L1 carrier phase observable, Figure 4.12 shows the true post-processing and actual carrier phase IS-DGPS trajectories. Figure 4.13 shows the lateral deviation of the estimated circular trajectory of the vehicle from the true, 2 cm accurate, trajectory. The results showed a standard deviation of 4.5 cm.

The experimental setup was not ideal since the car did not have proper compliance and shock absorption. That resulted in some jerky and rough ride, which rattled the GPS antenna while the car was in motion. Hence, these results would be better under real car conditions. A maximum error of 5 to 6 cm would be easily obtainable with the carrier phase observable.
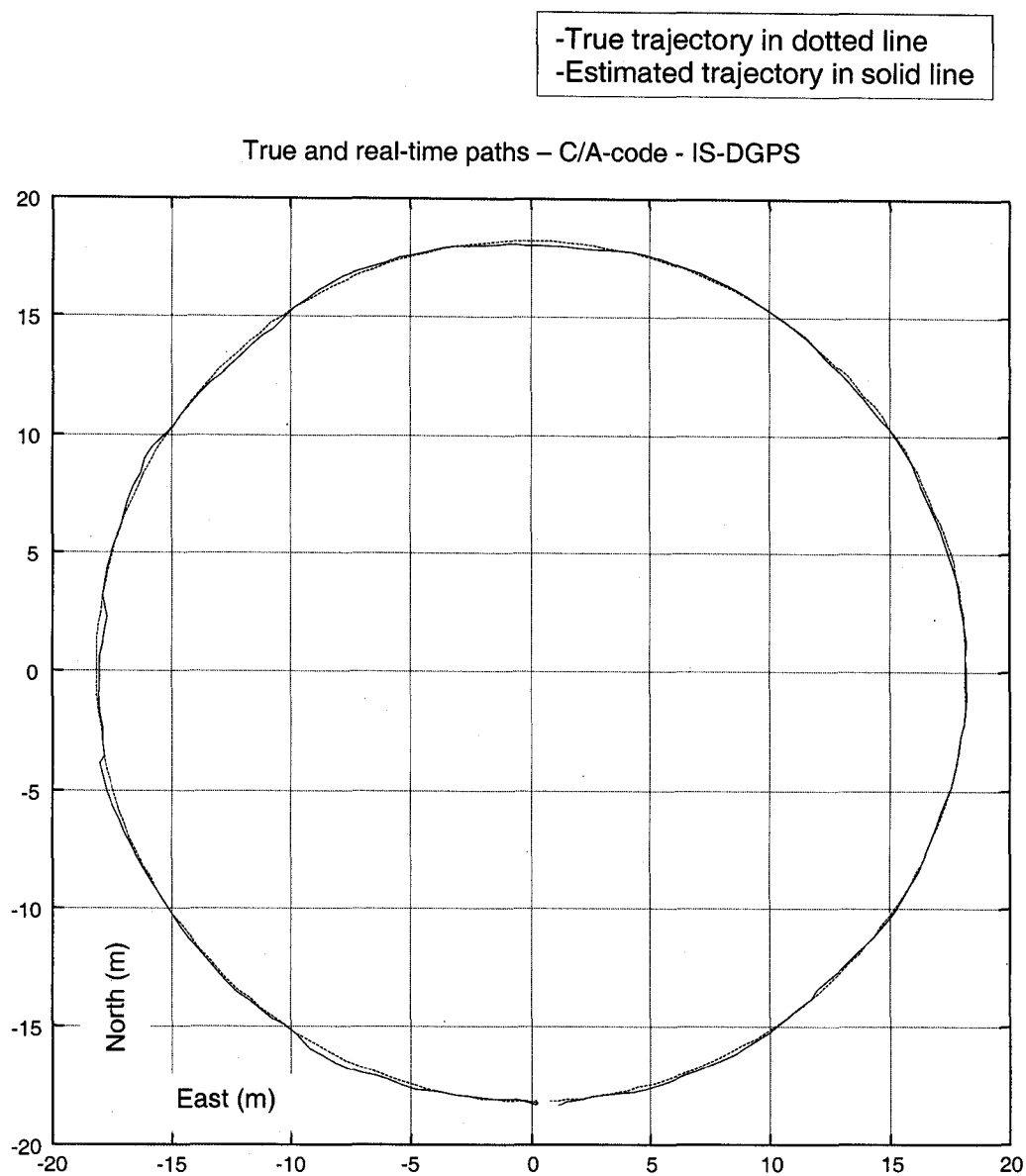
Figure 4.10: True post-processing trajectory and C/A IS-DGPS estimated trajectory
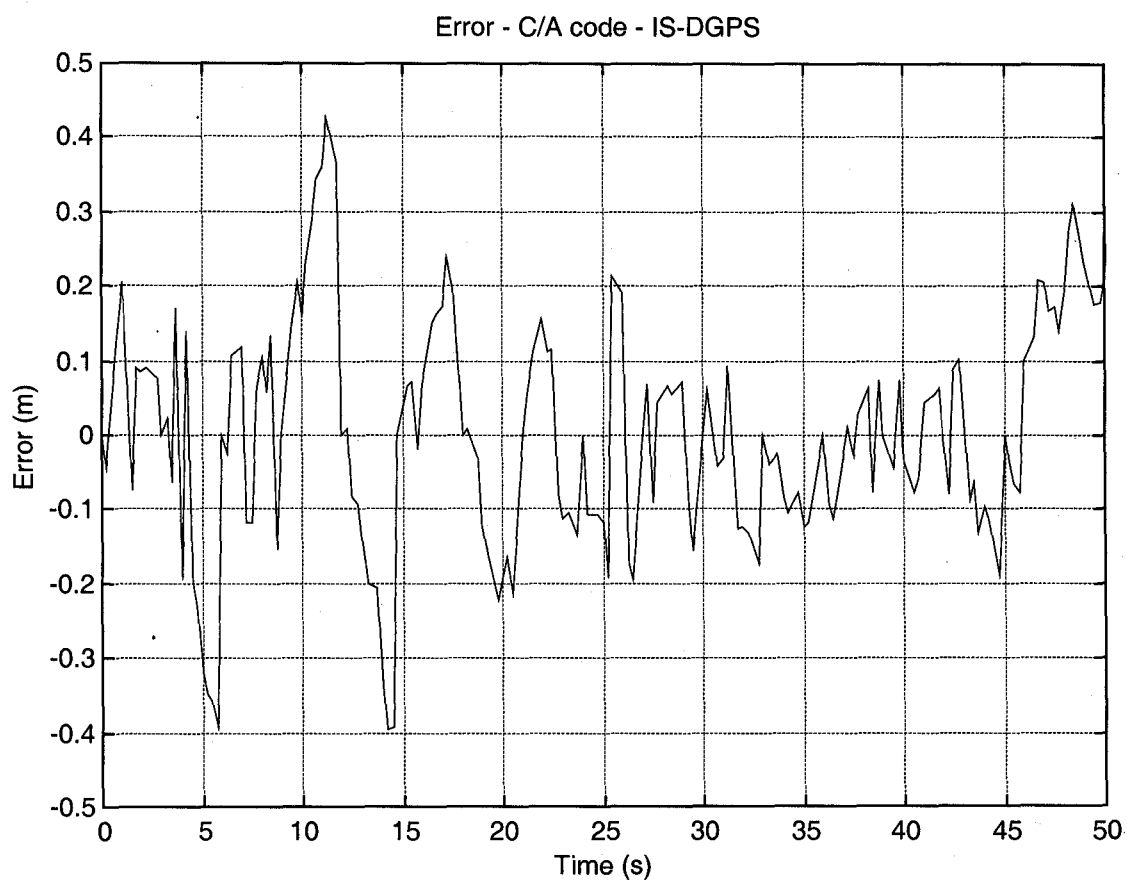
**Figure 4.11**: Lateral deviation of IS-DGPS C/A-code estimated circle from the true circle.

-True trajectory in dotted line
-Estimated trajectory in solid line

True and real-time paths - L1 phase - IS-DGPS
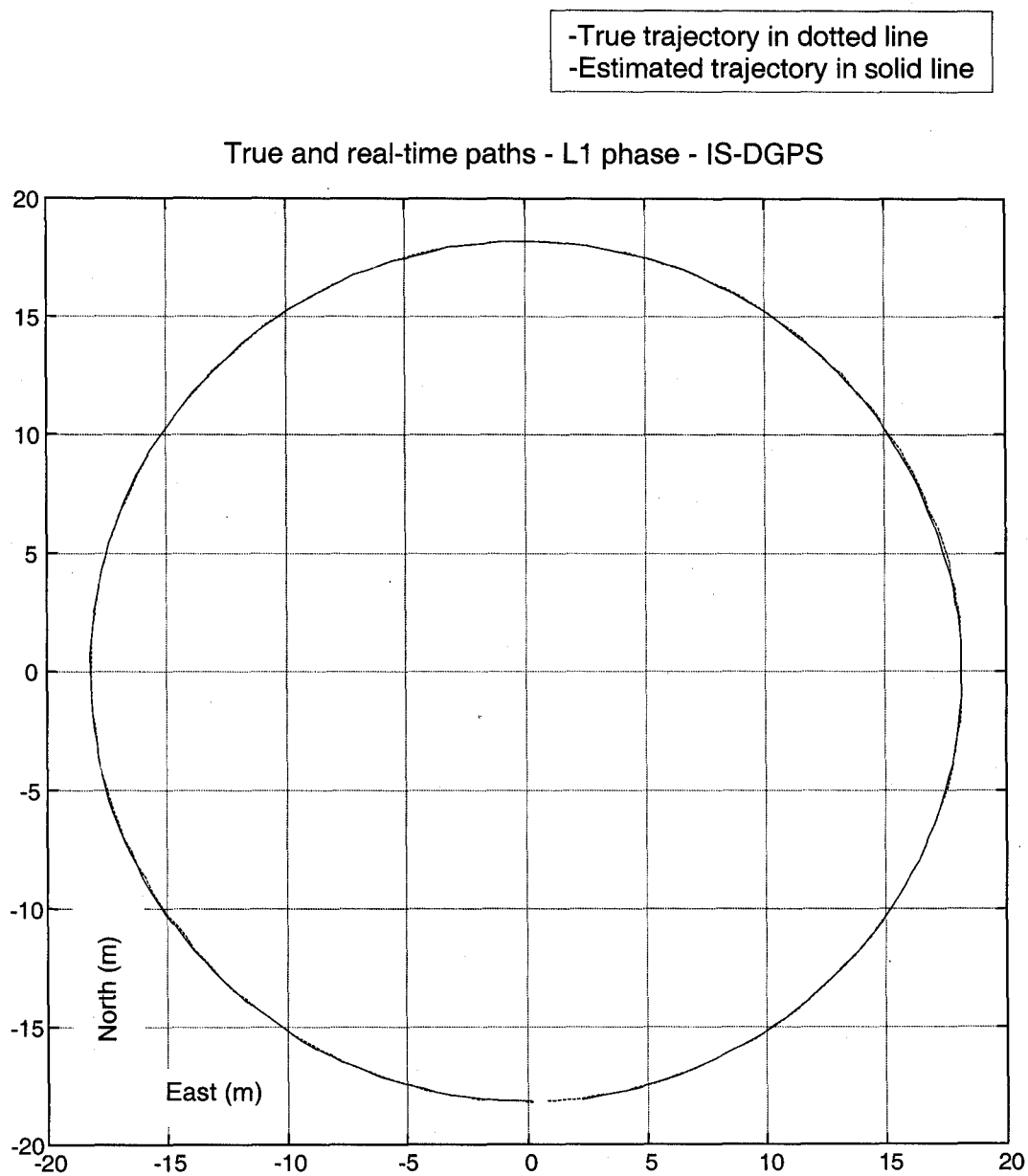


**Figure 4.12**: True post-processing and L1 carrier phase IS-DGPS trajectories.
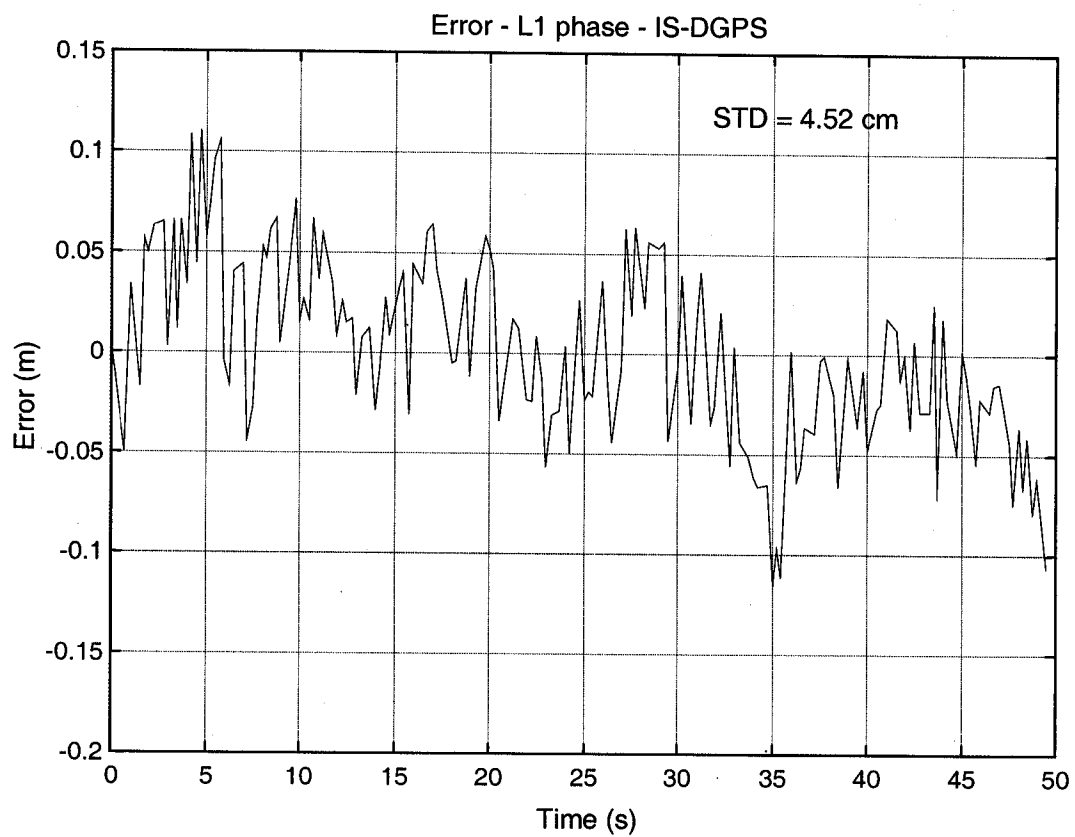
**Figure 4.13**: Lateral deviation of IS-DGPS L1 phase estimated circle from the true circle.

# 4.6 Marker Frequency

The required accuracy to achieve successful vehicle guidance in the DAS or automatic control on the AHS dictates the length of the distance separating road markers or the time interval T between differential corrections (Figure 4.14). Simulations were carried out in order to see the relation between the error and the time interval between corrections. Three, four, five and six second time intervals between corrections were considered. The results are presented in Figure 4.15.
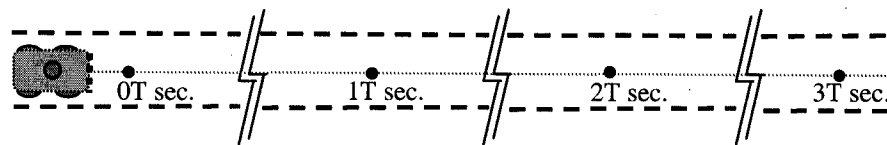


**Figure 4.14**: Frequency of reference magnetic markers

The dominant factor on the frequency of the reference markers is the Selective Availability effect, since it changes with time causing continuous deterioration in the positioning accuracy [Van Grass and Braasch, '96]. The frequency of the reference markers has to be such that an adequately accurate rate of change of the correction value is generated. The experimental work and the simulations, throughout this dissertation, were based on three second spacing between the markers. Using 20 mph as a nominal speed for slowly moving specialty vehicles such as snow plows, the markers should be 26.8 meters apart in order to secure a correction every three seconds. At 60 mph, the markers can be 80.5 meters apart. After six seconds, three correction values can be used

to calculate a rate of change of the corrections that will be used during the next three seconds. Both, the corrections and their rates are updated every three seconds.

As expected, the results in Figure 4.15 showed that the error did not increase linearly with the correction period. That is due to the ignored 2$^{nd}$ and higher orders Taylor series terms in the correction value equation

$$\Phi c(t) = \Phi c(t_0) + \dot{\Phi} c(t_0)(t - t_0) + \ddot{\Phi} c(t_0)\frac{(t - t_0)^2}{2} + higher \cdot order \cdot terms.$$
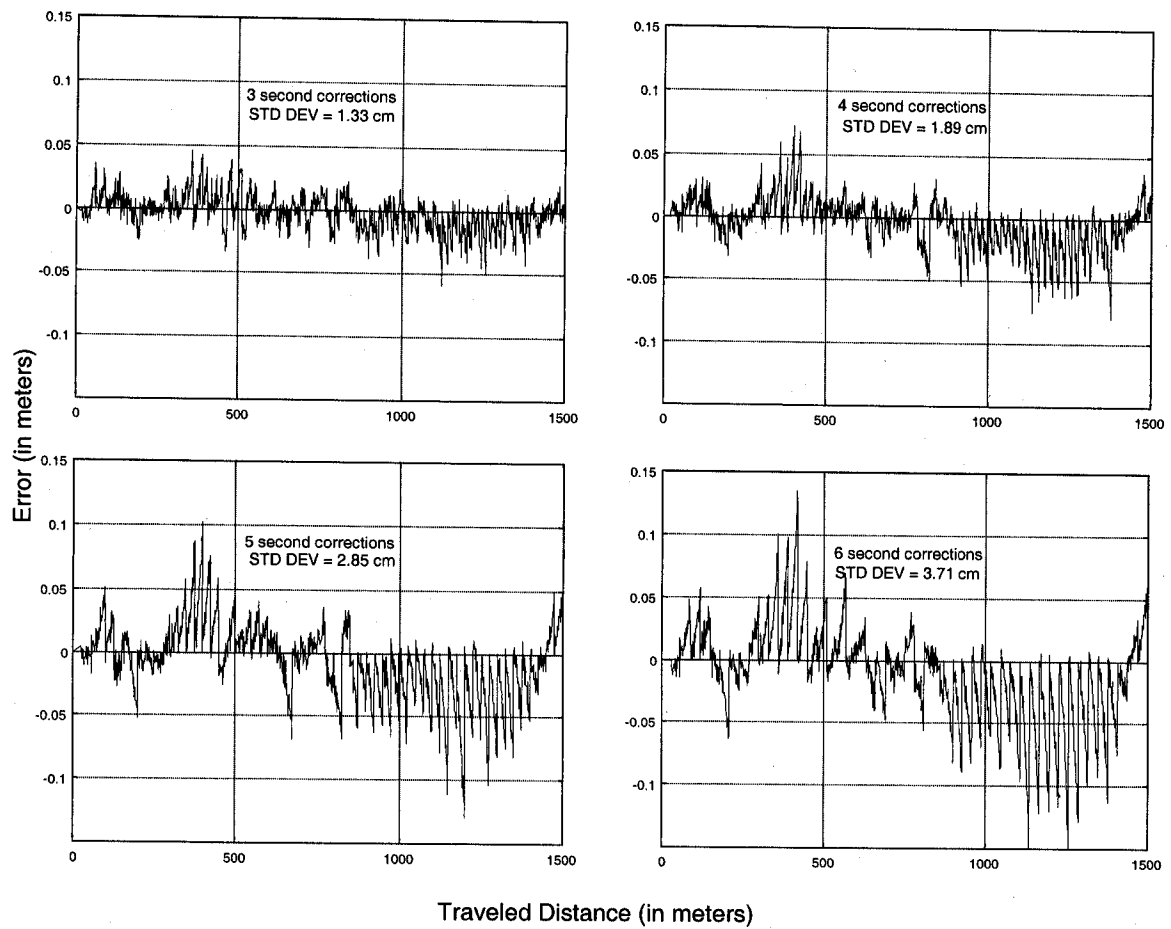
**Figure 4.15**: Lateral error of the estimated trajectory using 3, 4,5 & 6 seconds between corrections

# 4.7 Magnetic Marker Positioning Uncertainty

The marker sensing devices are magnetometers, which can acquire signals at any vehicle speed. A magnetic marker can be referred at as magnetic dipole. Then, the M-field B at an observation point P(x,y,z) is

$$B = \frac{\mu M}{4\pi r^3}\left(3xza_x + 3yza_y + \left(2z^2 - x^2 - y^2\right)a_z\right) \tag{4.21}$$

where $r = \sqrt{x^2 + y^2 + z^2}$

$\mu \equiv$ permeability of free space

$M \equiv$ magnetic moment.

Sensing the location of the magnetic marker is done by watching the vertical component of $B$ as it peaks when the magnetometer bar is on top of the marker, or by watching the horizontal component of the magnetic signal as it changes between positive and negative values.

The uncertainty in locating the magnetic marker by the magnetometer system contributes to the overall vehicle's positioning error of IS-DGPS. A magnetometer system is capable of locating a magnetic marker to within ±1.5 centimeters laterally and ±3.0 centimeters longitudinally [Zhang and Parsons, '91]. This uncertainty is analogous to uncertainty in the coordinates of the base station antenna in DGPS, except that, in IS-DGPS, the uncertainty is variable from marker to marker and the uncertainty is only in the horizontal coordinate and not in the vertical coordinate.

In formulating the problem we ignore all other GPS errors and introduce only an error in the coordinates of two consecutive markers $A$ and $B$. Using the code observation equation for simplicity, we have

$$P_A = \rho_A^j = \left\| r_A - r^j \right\| \tag{4.22}$$

where $r_A$ and $r^j$ are the coordinate vectors of marker $A$ and satellite $j$. More explicitly

$$\rho_A^j = \sqrt{(X_A - X^j)^2 + (Y_A - Y^j)^2 + (Z_A - Z^j)^2} \equiv f(x, y, z). \tag{4.23}$$

The error is introduced through linearizing around a point that is away from point $A$ by the uncertainty amount. Using vector terminology, we linearize around an approximate value $(X_{A0}, Y_{A0}, Z_{A0})$ for the receiver coordinates. Then, the Taylor series expansion truncated after the linear term becomes

$$P_A = \rho_{A0} - (u_A^j)^T \Delta r_A \tag{4.24}$$

where $u_A^j$ is the unit vector between the receiver at point $A$ and satellite $j$. $\Delta r_A$, which is considered the uncertainty in the $r_A$ vector, was the offset from point $A_0$ introduced after linearizing. If we consider $A_0$ as the true location of the marker, then $(u_A^j)^T \Delta r_A$ is considered to be the range error introduced when the magnetometer mislocates the marker. Similarly, at point $B$

$$P_B = \rho_{B0} - (u_B^j)^T \Delta r_B. \tag{4.25}$$

At any point $X$ after marker $B$, the range in the observation equation has a two part error due to the uncertainty in locating both markers, $A$ and $B$. The first part of the error is $-(u_B^j)^T \Delta r_B$ which accrues from calculating the differential correction value at point $B$.

The second part accrues when the rate of change of the correction value is calculated using the erroneous differential correction values of $A$ and $B$. The observation equation at any point $X$ becomes

$$P_X = \rho_{X0} - (u_B^j)^T \Delta r_B - \frac{(u_B^j)^T \Delta r_B - (u_A^j)^T \Delta r_A}{\Delta t}(t - t_0) \qquad (4.26)$$

where $\Delta t$ is the period of the corrections and $(t - t_0)$ is the age of the correction. The term $(u_B)^T \Delta r_B$ means that the exact same error in the horizontal East-North coordinates at point $B$ gets transferred to point $X$. The size of the $2^{nd}$ error term in (4.26) depends on how $A$ and $B$ were mislocated. In addition, the $(t - t_0)$ factor means that the total error has the tendancy to increase as it ages between markers. The worst possibility is when a marker is mislocated to one side and the following marker to the other side.

The effect of the uncertainty in locating the road magnetic markers can also be introduced and studied with simulation. The Matlab GPS simulation toolbox by [GPSOFT, '98] was used to simulate the GPS satellites, the various errors and a vehicle traveling on a known trajectory. Uncertainty in locating the markers was generated and randomly introduced at every marker, with a value between ±1.5 cm laterally and ±3.0 cm longitudinally. A straight east-west path was chosen as a nominal vehicle trajectory. Simulation runs were carried out with and without the marker location uncertainty. The simulation results, presented in Figure 4.16a & b, asserted the theoretical analysis findings and sometimes showed a larger lateral error than the introduced one. There was a difference of 0.7 cm between standard deviations of the vehicle lateral position of runs with no marker positioning error and runs with an error introduced.
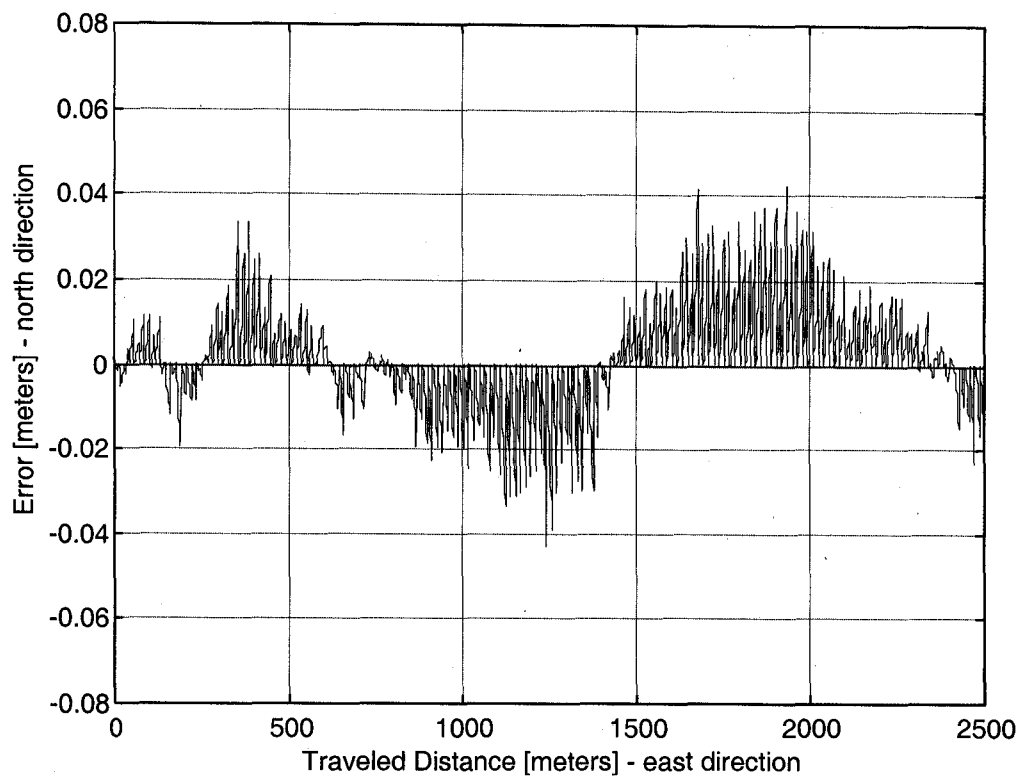
**Figure 4.16 a:** Lateral error without marker location uncertainty.
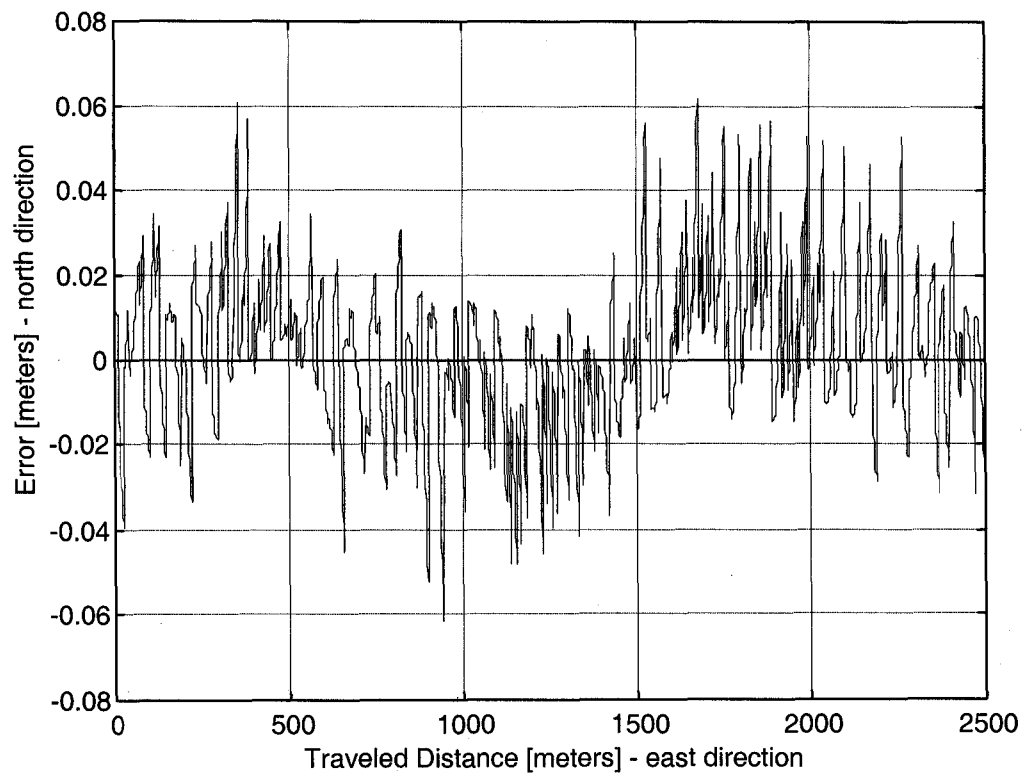


**Figure 4.16 b:** Lateral error with marker location uncertainty.

# 4.8 Multipath Error Mitigation

The multipath effects on carrier phases with short baselines could have an error to within a few centimeters [Counselman and Gourevitch, '81]. However, there is an error in DGPS multipath that does not get differenced out since the ground base receiver and user receiver, which are at independent sites, get affected differently. In DGPS, multipath error increases statistically by a factor of $\sqrt{2}$ when doing the differencing (see Section 3.5.5). In the case of IS-DGPS, only one receiver is involved, hence, only one multipath problem is dealt with. Multipath is considered the only other enemy for IS-DGPS after Selective Availability.

There are some remedies to help fixing the multipath problem. The antenna should be placed on the vehicle above the highest reflector to prevent waves arriving from the horizon from getting reflected to the antenna. Also, the antenna can be placed in a choke ring so that the multipath signals get reflected away.

Multipath reflections are geometry dependent and time-variant. The receiver of the traveling vehicle and multipath generating objects, such as mountains, buildings, and water surfaces might experience a slowly changing geometry, so that the multipath error would have some temporal correlation. Hence, since IS-DGPS always has very short baselines, the correlated part of the multipath error would be differenced out along with the other differentiable errors. Generally, multipath exhibits random low-frequency and high-frequency features. IS-DGPS has the potential of attenuating the low-frequency part.

# Chapter 5

# IS-DGPS with a Multi-Antenna Setup

As was mentioned in the third chapter of this dissertation, relative positioning is the most accurate way to perform differential GPS. This is because relative positioning eliminates the latency in applying the differential corrections. Also, it was mentioned that multi-antenna receivers are normally used to measure the attitude of the vehicle (roll, pitch & yaw) along with its absolute position. In this chapter, IS-DGPS is implemented by combining the relative positioning technique, a multi-antenna GPS system and the road markers (Figure 5.1). This approach would improve the positioning accuracy by eliminating the error drift that takes place between markers due to Selective Availability. In addition, the approach reduces the critical dependency on the markers that exists in the case of single antenna approach. Another important advantage with the multi-antenna approach is that the 3-D attitude of the vehicle would be obtainable. Vehicle attitude is vital information that is needed for the display of the vehicle's position on the road in a DAS (Driver Assistance System). Also, attitude data serves as input in the implementation of automatic steering on the AHS vehicles. This chapter describes the

GPS multi-antenna system, presents the formulation for a two- and three-antenna GPS receivers and addresses the ambiguity resolution problem. It should be mentioned that the concept is not limited to multi-antenna receivers. It could also be applied with multi-receiver setup using the double difference technique.
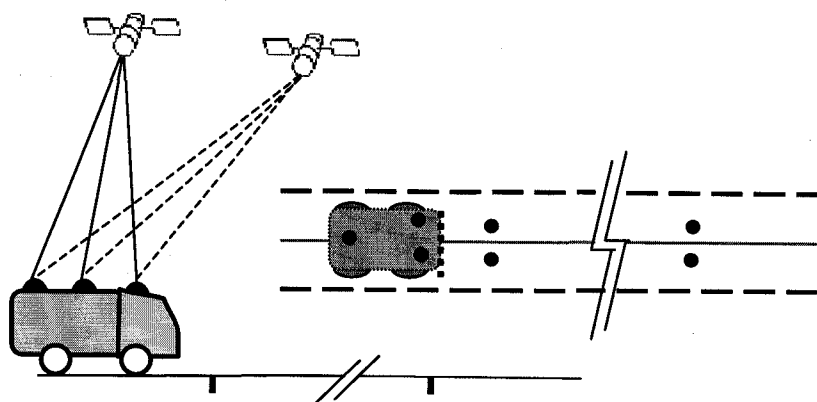


**Figure 5.1**: Multiple antenna approach

# 5.1 System Description

With the multi-antenna method, the magnetic markers are placed in pairs in order to determine accurately the position of all GPS antennas on the vehicle when the markers are detected. In addition, as mentioned in Chapter 4, dual markers are used for a successful identification of the detected markers at initialization.

The antennas would be placed on the vehicle at positions, with an optimal geometric configuration, such that a stable solution is obtained and accurate positioning can be performed. Discussion on various antenna configurations is presented in Section 5.8. One of the key elements to good positioning accuracy is the baseline distance separating the antennas. A relatively long baseline provides a better geometry between antennas and

satellites and less sensitive difference equations. The shorter the baseline, the faster the ambiguities can be resolved by reducing the search space [Euler and Hill, '95]. Specialty vehicles are usually quite large which potentially permits positioning the antennas up to six meters apart.

# 5.2 Multi-Antenna IS-DGPS Concept

A signal traveling from a GPS satellite arrives at the antenna closer to that satellite slightly before reaching the other antenna (Figure 5.2). Both antennas 1 and 2 will be tracking their corresponding fractional phases $\Phi_1^j$ and $\Phi_2^j$. The difference between the
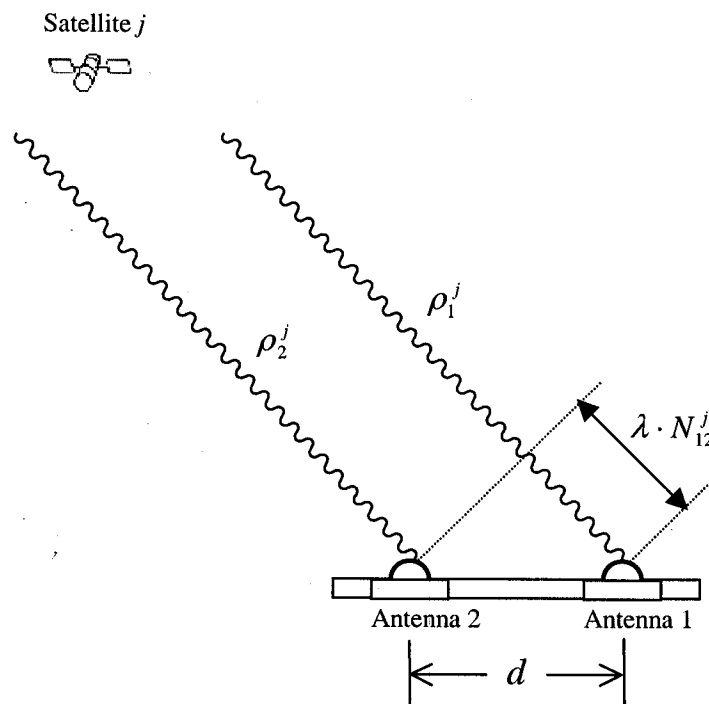
Satellite $j$

**Figure 5.2**: Multi-antenna concept

two ambiguities of both antennas is a fixed integer number $N_{12}^j = N_1^j - N_2^j$, where $N_{12}^j$ depends on the distance between the two antennas and the angle of the initial satellite-receiver line of sight. Since the two antennas share the same oscillator, the receiver clock bias will be eliminated when differencing. Since single differencing is used, the satellite clock bias that includes Selective Availability (SA) gets differenced out. This means that, the accuracy drift due to SA in the distance separating the markers, that existed with a single antenna system, is eliminated. The baseline between the two antennas is so small that all atmospheric and orbital error will totally vanish when differencing.

The ambiguity resolution problem here is somewhat similar to the one for attitude determination. When the road markers are detected, the true antenna-satellite range $\rho_A^j$ and $\rho_{A'}^j$ are calculated for both antennas. Dividing the ranges by the wavelength (19.02 cm) gives the floating solution to the individual ambiguities $N_1^j$ and $N_2^j$. Then, a search space is established around points $A$ and $A'$ by using a range of $\pm 0.9$ cycles around the floating ambiguity solution of every satellite. Then, the least square method is used to find the integer ambiguities.

When performing positioning, after the ambiguities are resolved, the unknowns are the coordinates of the two antennas. The following sections present the detailed formulation.

# 5.3 Dual-Antenna Formulation

The two antennas are placed laterally on the top of the vehicle (Figure 5.3). When the magnetometer bar is on top of magnetic nail set $a$, the antenna positions are at points $A$ and $A'$. The carrier phase equations for both antennas can be written as

$$\Phi_A^j = \rho_A^j + \Delta\rho_A^j - c \cdot dt_A^j + c \cdot dT + \lambda N_A^j + \varepsilon_A^j \tag{5.1}$$

$$\Phi_{A'}^j = \rho_{A'}^j + \Delta\rho_{A'}^j - c \cdot dt_{A'}^j + c \cdot dT + \lambda N_{A'}^j + \varepsilon_{A'}^j . \tag{5.2}$$

After detecting both markers, the coordinates of points $A$ and $A'$ can be determined from both the coordinates of marker set $a$ and the geometry of the vehicle.
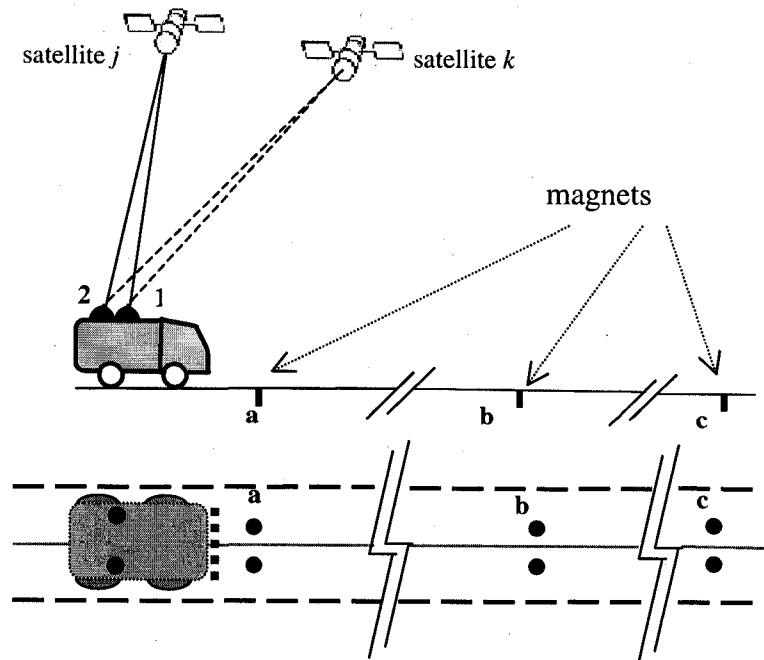


**Figure 5.3**: Dual antenna system

The ranges $\rho_A^j$ and $\rho_{A'}^j$ would then be calculated using the coordinates of the antennas at $A$ and $A'$ and satellite $j$'s coordinates. Since the two antennas and channels share the same receiver clock then its bias $dT$ will be differenced out. Differencing the

two Equations (5.1) and (5.2), while ignoring the noise and multipath effects $\varepsilon_A^j$ $\varepsilon_{A'}^j$ gives

$$\Phi_{AA'}^j = \rho_{AA'}^j + \lambda \cdot N_{AA'}^j. \tag{5.3}$$

This single difference equation (5.3) has only one unknown, the carrier phase integer ambiguity difference $N_{AA'}^j$.

In relationship to the satellite-vehicle geometry, Equation (5.3) of some satellites might be sensitive. This should not be a problem because only five satellites are needed to solve for the coordinates of the antennas and up to ten satellites can be present at one time. In addition, considering more than two antennas would lead to a more robust system (Section 5.5).

As was demonstrated in Chapter 3, the cycle ambiguity is an integer. The solution to Equation (5.3) might give a number with a fraction. Fixing the number to the correct integer value is called ambiguity resolution, which is discussed in the next section.

If one epoch is not enough to fix the ambiguity to an integer, more equations can be generated at the following markers and used in a least square algorithm. When the vehicle travels over the following marker set $b$, a similar set of equations like (5.3) can be generated. Notice that the ambiguities at $B$ are the same as those at $A$ if no loss of lock or a cycle slip takes place; that is

$$\Phi_{BB'}^j = \rho_{BB'}^j + \lambda \cdot N_{AA'}^j. \tag{5.4}$$

After the ambiguities are resolved, and assuming lock is maintained on the same satellites, positioning can be done at any point $x$. Six unknowns must be solved for,

namely the coordinates of antenna 1 and antenna 2 at points X and X' respectively. Every satellite provides an equation similar to (5.3) written as

$$\Phi_{XX'}^{j} = \rho_{XX'}^{j} + \lambda \cdot N_{AA'}^{j} + \varepsilon_{XX'}^{j}.$$ (5.5)

Another important equation to follow can be generated from the baseline geometric constraint between the two antennas, since they are both rigidly attached to the vehicle:

$$d = \sqrt{(x_X - x_{X'})^2 + (y_X - y_{X'})^2 + (z_X - z_{X'})^2}$$ (5.6)

where $d$ is the constant distance between the two antennas.

Since there are six unknowns, at least five satellites are needed. Five satellites generate five single difference equations and the geometric constraint provides the sixth equation. These equations can be solved by linearizing around an approximate value of the coordinates of X and X' (See Section 5.4). If more satellites are available then a least square technique can be used. The heading of the vehicle is then easily obtained from the coordinates of X and X' in local (Northing-Easting) frame.

# 5.4 Ambiguity Resolution

As was mentioned in Chapter 3, GPS receivers are only capable of measuring the fractional part of the GPS carrier phase observable. In regular reference-user relative positioning, the initial number of unknown integer cycles between the receiver and the satellite must be determined before precise carrier phase positioning can be achieved [Hofmann et al., '97]. The carrier phase ambiguity resolution problem for attitude applications is slightly different and has been examined by many researchers, as was

mentioned in Section 2.2.4 of the literature review. Since the antennas are rigidly attached to the vehicle, the separating distance between them (baseline) is used as a geometric constraint to speed up the ambiguity resolution. In the case of multi-antenna IS-DGPS, the ambiguity resolution problem is similar to the one for attitude determination.

Figure 5.4 shows a flow chart of the steps involved to resolve the ambiguities [Harvey, '98]. We start with choosing the best 4 satellites based on the best PDOP. The ambiguities are estimated by the ranges between the satellites and points $A$ and $A'$ in cycles. Since the obtained position for the antennas, when detecting the marker set, have some error, the initial ambiguity coming from dividing the range by the wavelength is a real number that has a fraction (the floating ambiguity $N_{float} = \rho_{oA}/\lambda$ ). A search space must be set up around the antennas, that would include all possibilities for the coordinates of the two antennas that correspond to integer ambiguity combinations (Figure 5.5). The search volume would include a discrete set of points that are candidates for the true position of antennas $A$ and $A'$ (Figure 5.6). Setting a window of $\pm 0.9$ cycles around the floating ambiguity gives one or two possible integer ambiguities. Doing that for all eight ambiguities gives $r_1.r_2.r_3.r_4.r_5.r_6.r_7.r_8$ possible ambiguity combinations for a maximum of $2^8 = 256$ combinations. Widening the window would increase the number of combinations. The list of the combination is created and arranged in a most likelihood fashion. Then, the combinations of these adjusted ambiguities $N_{adjust}$ are tested one by

one. First, the adjusted ambiguities are used to calculate the corresponding adjusted range $\overline{\rho} = \lambda \cdot N_{adjust}$ for $A$ and $A'$.

Writing the distance equations between four satellites ($j$, $k,l$ and $m$) and the two antennas $A$ and $A'$, we have

$$
\begin{aligned}
\overline{\rho}_A^{\,j} &= \sqrt{(X^{\,j} - x_A)^2 + (Y^{\,j} - y_A)^2 + (Z^{\,j} - z_A)^2} \\
\overline{\rho}_A^{\,k} &= \sqrt{(X^{\,k} - x_A)^2 + (Y^{\,k} - y_A)^2 + (Z^{\,k} - z_A)^2} \\
\overline{\rho}_A^{\,l} &= \sqrt{(X^{\,l} - x_A)^2 + (Y^{\,l} - y_A)^2 + (Z^{\,l} - z_A)^2} \\
\overline{\rho}_A^{\,m} &= \sqrt{(X^{\,m} - x_A)^2 + (Y^{\,m} - y_A)^2 + (Z^{\,m} - z_A)^2} \\
\overline{\rho}_{A'}^{\,j} &= \sqrt{(X^{\,j} - x_{A'})^2 + (Y^{\,j} - y_{A'})^2 + (Z^{\,j} - z_{A'})^2} \\
\overline{\rho}_{A'}^{\,k} &= \sqrt{(X^{\,k} - x_{A'})^2 + (Y^{\,k} - y_{A'})^2 + (Z^{\,k} - z_{A'})^2} \\
\overline{\rho}_{A'}^{\,l} &= \sqrt{(X^{\,l} - x_{A'})^2 + (Y^{\,l} - y_{A'})^2 + (Z^{\,l} - z_{A'})^2} \\
\overline{\rho}_{A'}^{\,m} &= \sqrt{(X^{\,m} - x_{A'})^2 + (Y^{\,m} - y_{A'})^2 + (Z^{\,m} - z_{A'})^2}
\end{aligned}
\tag{5.6}
$$

Equations (5.6) should be solved for the coordinates of $A$ and $A'$ using a least square technique. This equation could have been split into two equations, one for $A$ and one for $A'$, since they are not coupled. But as we will see later, when we test for the correct ambiguities by checking the distance $d$ between the two antennas, the combination of eight ambiguities is checked at once. The correct set of $A$ and $A'$ coordinates correspond to a single set of eight ambiguities.

First, Equation (5.6) should be linearized around an estimate value of $A$ and $A'$ coordinates using 1$^{st}$ order Taylor series expansion. The coordinates could be the original values at $A$ and $A'$. Following the linearization procedure of Section 3.4, we get

$$
\overline{\rho}_A^{\,j} - \rho_{oA} = -\frac{X^{\,j} - x_{oA}}{\rho_{oA}^{\,j}} \cdot \Delta x_A - \frac{Y^{\,j} - x_{oA}}{\rho_{oA}^{\,j}} \cdot \Delta y_A - \frac{Z^{\,j} - x_{oA}}{\rho_{oA}^{\,j}} \cdot \Delta z_A
\tag{5.7a}
$$

$$\overline{\rho}_{A'}^{j} - \rho_{oA'} = -\frac{X^{j} - x_{oA'}}{\rho_{oA'}} \cdot \Delta x_{A'} - \frac{Y^{j} - x_{oA'}}{\rho_{oA'}} \cdot \Delta y_{A'} - \frac{Z^{j} - x_{oA'}}{\rho_{oA'}} \cdot \Delta z_{A'} \qquad (5.7b)$$

Similar equations would be written for the other three satellites. Writing the whole set of Equations (5.7) in matrix form, we get

$$\Delta\rho = H \cdot \Delta X \qquad (5.8)$$

or

$$
\begin{bmatrix} \Delta\rho_A^j \\ \Delta\rho_A^k \\ \Delta\rho_A^l \\ \Delta\rho_A^m \\ \Delta\rho_{A'}^j \\ \Delta\rho_{A'}^k \\ \Delta\rho_{A'}^l \\ \Delta\rho_{A'}^m \end{bmatrix}
=
\begin{bmatrix}
-\dfrac{X^j - x_{oA}}{\rho_{oA}^j} & -\dfrac{Y^j - y_{oA}}{\rho_{oA}^j} & -\dfrac{Z^j - z_{oA}}{\rho_{oA}^j} & 0 & 0 & 0 \\[2ex]
-\dfrac{X^j - x_{oA}}{\rho_{oA}^j} & -\dfrac{Y^j - y_{oA}}{\rho_{oA}^j} & -\dfrac{Z^j - z_{oA}}{\rho_{oA}^j} & 0 & 0 & 0 \\[2ex]
-\dfrac{X^j - x_{oA}}{\rho_{oA}^j} & -\dfrac{Y^j - y_{oA}}{\rho_{oA}^j} & -\dfrac{Z^j - z_{oA}}{\rho_{oA}^j} & 0 & 0 & 0 \\[2ex]
-\dfrac{X^j - x_{oA}}{\rho_{oA}^j} & -\dfrac{Y^j - y_{oA}}{\rho_{oA}^j} & -\dfrac{Z^j - z_{oA}}{\rho_{oA}^j} & 0 & 0 & 0 \\[2ex]
0 & 0 & 0 & -\dfrac{X^j - x_{oA'}}{\rho_{oA'}^j} & -\dfrac{Y^j - y_{oA'}}{\rho_{oA'}^j} & -\dfrac{Z^j - z_{oA'}}{\rho_{oA'}^j} \\[2ex]
0 & 0 & 0 & -\dfrac{X^k - x_{oA'}}{\rho_{oA'}^k} & -\dfrac{Y^k - y_{oA'}}{\rho_{oA'}^k} & -\dfrac{Z^k - z_{oA'}}{\rho_{oA'}^k} \\[2ex]
0 & 0 & 0 & -\dfrac{X^l - x_{oA'}}{\rho_{oA'}^l} & -\dfrac{Y^l - y_{oA'}}{\rho_{oA'}^l} & -\dfrac{Z^l - z_{oA'}}{\rho_{oA'}^l} \\[2ex]
0 & 0 & 0 & -\dfrac{X^m - x_{oA'}}{\rho_{oA'}^m} & -\dfrac{Y^m - y_{oA'}}{\rho_{oA'}^m} & -\dfrac{Z^m - z_{oA'}}{\rho_{oA'}^m}
\end{bmatrix}
\cdot
\begin{bmatrix} \Delta x_A \\ \Delta y_A \\ \Delta z_A \\ \Delta x_{A'} \\ \Delta y_{A'} \\ \Delta z_{A'} \end{bmatrix} \cdot
$$

$$(5.9)$$

Since $H$ (8x6) is not square the method of least square is used to solve for $\Delta X$. Then,

$$\Delta X_A = (H_A^T H_A)^{-1} H_A^T \cdot \Delta\rho_A \qquad (5.10)$$

where $(H^T H)^{-1} H^T$ is the generalized inverse. Then, the baseline length $d$ is checked using

$$d = \sqrt{(x_A - x_{A'})^2 + (y_A - y_{A'})^2 + (z_A - z_{A'})^2} \, . \qquad (5.11)$$

If the length of baseline $d$ differs by more that a specified tolerance (say 2 cm) then the combination is rejected and another ambiguity combination is tested. Or, since the number of combination is small, another approach is to calculate all possible $d$'s then the ambiguity combination that gives the closest one to the true value of $d$ is accepted, as long as, the error is within a specified tolerance value.

Once the ambiguities are fixed, then, dropping a satellite or adding others would be a routine procedure. The receiver would have an easy time finding the new ambiguities for the new added satellites.
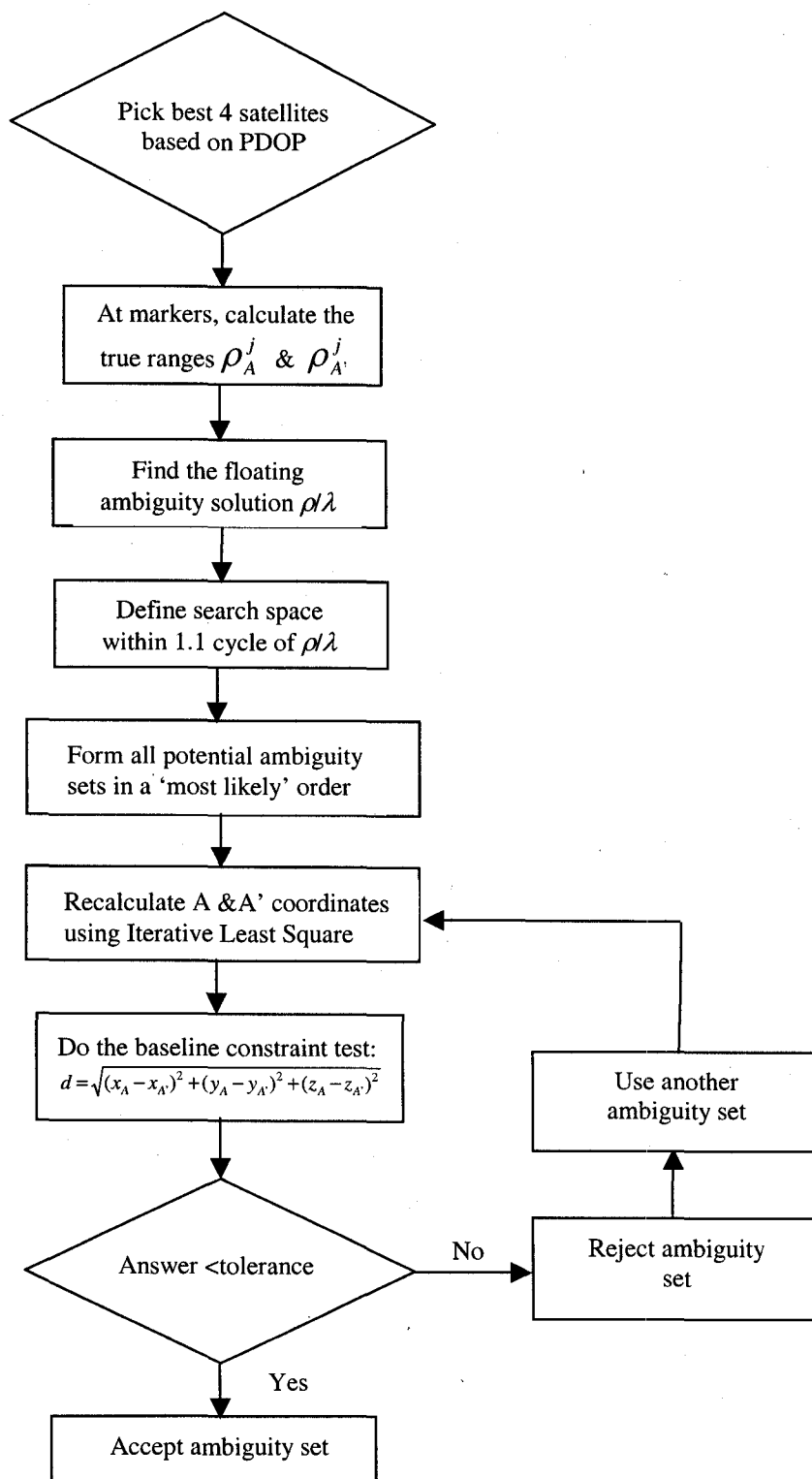
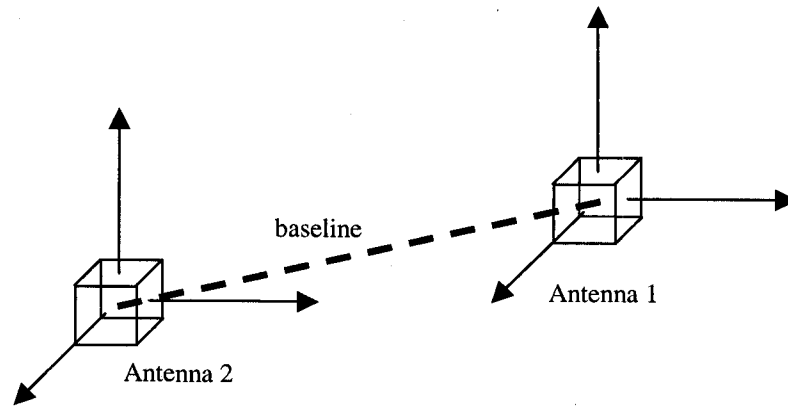**Figure 5.4**: Ambiguity resolution flow chart

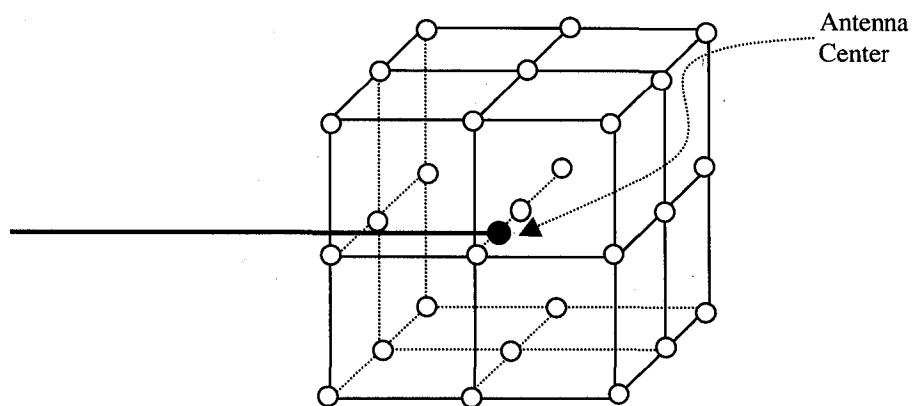**Figure 5.5**: Search volumes for the two antennas



**Figure 5.6**: Search technique [Hoffman et al., '97]

# 5.5 Solving for Vehicle Position and Heading

After the ambiguities are resolved, doing positioning at any point $X$ is done in the following fashion. The observation equation at $X$ is

$$\Phi_{XX'}^j - \lambda \cdot N_{AA'}^j = \rho_{XX'}^j. \tag{5.12}$$

Let

$$Q^j = \Phi_{XX'}^j - \lambda \cdot N_{AA'}^j. \tag{5.13}$$

Then, rewriting Equation (5.12) gives

$$Q^j = \sqrt{(X^j - x_X)^2 + (Y^j - y_X)^2 + (Z^j - z_X)^2} - \sqrt{(X^j - x_{X'})^2 + (Y^j - y_{X'})^2 + (Z^j - z_{X'})^2}. \tag{5.14}$$

Linearizing Equation (5.14) around $Xo$ and $X'o$ gives

$$Q^j - \rho_{oX} + \rho_{oX'} = -\frac{X^j - x_{oX}}{\rho_{oX}^j} \cdot \Delta x_X - \frac{Y^j - x_{oX}}{\rho_{oX}^j} \cdot \Delta y_X - \frac{Z^j - x_{oX}}{\rho_{oX}^j} \cdot \Delta z_X +$$
$$\frac{X^j - x_{oX'}}{\rho_{oX'}^j} \cdot \Delta x_{X'} + \frac{Y^j - x_{oX'}}{\rho_{oX'}^j} \cdot \Delta y_{X'} + \frac{Z^j - x_{oX'}}{\rho_{oX'}^j} \cdot \Delta z_{X'} \tag{5.15}$$

In addition, the baseline geometric constraint equation between the two antennas is

$$d = \sqrt{(x_X - x_{X'})^2 + (y_X - y_{X'})^2 + (z_X - z_{X'})^2}. \tag{5.16}$$

Linearizing around the same points, $Xo$ and $X'o$ gives

$$d - d_o = \frac{x_{oX} - x_{oX'}}{d_o} \cdot \Delta x_X + \frac{y_{oX} - y_{oX'}}{d_o} \cdot \Delta y_X + \frac{z_{oX} - z_{oX'}}{d_o} \cdot \Delta z_X -$$
$$\frac{x_{oX} - x_{oX'}}{d_o} \cdot \Delta x_{X'} - \frac{y_{oX} - y_{oX'}}{d_o} \cdot \Delta y_{X'} - \frac{z_{oX} - z_{oX'}}{d_o} \cdot \Delta z_{X'} \tag{5.17}$$

Using the linearized equation (5.15) with five different satellites and the linearized constraint equation (5.17) produces

$$
\begin{bmatrix} \Delta Q^j \\ \Delta Q^k \\ \Delta Q^l \\ \Delta Q^m \\ \Delta Q^n \\ \Delta d \end{bmatrix} =
\begin{bmatrix}
-\dfrac{X^j - x_{Xo}}{\rho^j_{Xo}} & -\dfrac{Y^j - y_{Xo}}{\rho^j_{Xo}} & -\dfrac{Z^j - z_{Xo}}{\rho^j_{Xo}} & \dfrac{X^j - x_{Xo'}}{\rho^j_{Xo'}} & \dfrac{Y^j - y_{Xo'}}{\rho^j_{oX'}} & \dfrac{Z^j - z_{Xo'}}{\rho^j_{oX'}} \\[2mm]
-\dfrac{X^k - x_{Xo}}{\rho^k_{Xo}} & -\dfrac{Y^k - y_{Xo}}{\rho^k_{Xo}} & -\dfrac{Z^k - z_{Xo}}{\rho^k_{Xo}} & \dfrac{X^k - x_{Xo'}}{\rho^k_{Xo'}} & \dfrac{Y^j - y_{Xo'}}{\rho^j_{oX'}} & \dfrac{Z^j - z_{Xo'}}{\rho^j_{oX'}} \\[2mm]
-\dfrac{X^l - x_{Xo}}{\rho^l_{Xo}} & -\dfrac{Y^l - y_{Xo}}{\rho^l_{Xo}} & -\dfrac{Z^l - z_{Xo}}{\rho^l_{Xo}} & \dfrac{X^l - x_{Xo'}}{\rho^l_{Xo'}} & \dfrac{Y^j - y_{Xo'}}{\rho^j_{X'}} & \dfrac{Z^j - z_{Xo'}}{\rho^j_{oX'}} \\[2mm]
-\dfrac{X^m - x_{Xo}}{\rho^m_{Xo}} & -\dfrac{Y^m - y_{Xo}}{\rho^m_{Xo}} & -\dfrac{Z^m - z_{Xo}}{\rho^m_{Xo}} & \dfrac{X^m - x_{Xo'}}{\rho^m_{Xo'}} & \dfrac{Y^j - y_{Xo'}}{\rho^j_{oX'}} & \dfrac{Z^j - z_{Xo'}}{\rho^j_{oX'}} \\[2mm]
-\dfrac{X^n - x_{Xo}}{\rho^n_{Xo}} & -\dfrac{Y^n - y_{Xo}}{\rho^n_{Xo}} & -\dfrac{Z^n - z_{Xo}}{\rho^n_{Xo}} & \dfrac{X^n - x_{Xo'}}{\rho^n_{Xo'}} & \dfrac{Y^j - y_{Xo'}}{\rho^j_{X'}} & \dfrac{Z^j - z_{Xo'}}{\rho^j_{oX'}} \\[2mm]
\dfrac{x_{Xo} - x_{Xo'}}{d_o} & \dfrac{y_{Xo} - y_{Xo'}}{d_o} & \dfrac{z_{Xo} - z_{Xo'}}{d_o} & -\dfrac{x_{Xo} - x_{Xo'}}{d_o} & -\dfrac{y_{Xo} - y_{Xo'}}{d_o} & -\dfrac{z_{Xo} - z_{Xo'}}{d_o}
\end{bmatrix}
\cdot
\begin{bmatrix} \Delta x_X \\ \Delta y_X \\ \Delta z_X \\ \Delta x_{X'} \\ \Delta y_{X'} \\ \Delta z_{X'} \end{bmatrix}
$$

$$(5.18)$$

where $\Delta Q = Q - \rho_{Xo} + \rho_{X'o}$ and $\Delta d = d - d_o$. Equation (5.18) can be written as

$$\Delta Q = S \cdot \Delta X. \tag{5.19}$$

Then,

$$\Delta X = (S^T \cdot S)^{-1} \cdot S^T \cdot \Delta Q. \tag{5.20}$$

We need to solve Equation (5.20) for $\Delta X$. Then, the true coordinates of $X$ and $X'$ are known by using

$$
\begin{bmatrix} x_X \\ y_X \\ z_X \\ x_{X'} \\ y_{X'} \\ z_{X'} \end{bmatrix} =
\begin{bmatrix} x_{oX} \\ y_{oX} \\ z_{oX} \\ x_{oX'} \\ y_{oX'} \\ z_{oX'} \end{bmatrix} +
\begin{bmatrix} \Delta x_X \\ \Delta y_X \\ \Delta z_X \\ \Delta x_{X'} \\ \Delta y_{X'} \\ \Delta z_{X'} \end{bmatrix}.
\tag{5.21}
$$

# 5.6 Three-Antenna Formulation

Using a three-antenna receiver (Figure 5.7) would give a more stable and more accurate solution. In addition, it provides the 3-D attitude of the vehicle, which could be used in the dynamic control model of the vehicle.
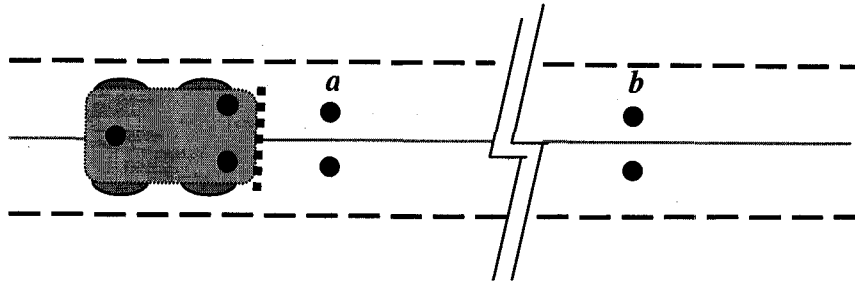


**Figure 5.7**: Three-antenna setup

The geometric configuration of the antennas is important for an optimal operation. Section 5.5 considers different antenna configurations. For now, the calculation is made for a generic configuration (Figure 5.7).

When magnetic marker set *a* are detected, the front antennas are at points *A* and *A'*, the rear antenna is at point *A"* (Figure 5.7). The phase equations are

$$\Phi_A^j = \rho_A^j + \Delta\rho_A^j - c \cdot dt_A^j + c \cdot dT + \lambda \cdot N_A^j + \varepsilon_A^j$$

$$\Phi_{A'}^j = \rho_{A'}^j + \Delta\rho_{A'}^j - c \cdot dt_{A'}^j + c \cdot dT + \lambda \cdot N_{A'}^j + \varepsilon_{A'}^j \qquad (5.22)$$

$$\Phi_{A''}^j = \rho_{A''}^j + \Delta\rho_{A''}^j - c \cdot dt_{A''}^j + c \cdot dT + \lambda \cdot N_{A''}^j + \varepsilon_{A''}^j$$

where $\rho_A^j$, $\rho_{A'}^j$ and $\rho_{A''}^j$ are known since the coordinates of the three antennas are known.

Differencing these three equations gives

$$\Phi_{AA'}^{j} = \rho_{AA'}^{j} + \lambda \cdot N_{AA'}^{j} \tag{5.23}$$

$$\Phi_{AA''}^{j} = \rho_{AA''}^{j} + \lambda \cdot N_{AA''}^{j}. \tag{5.24}$$

Also, the fixed distance constraint equations between the three antennas are

$$d_{1} = \sqrt{(x_{A} - x_{A'})^{2} + (y_{A} - y_{A'})^{2} + (z_{A} - z_{A'})^{2}} \tag{5.25}$$

$$d_{2} = \sqrt{(x_{A} - x_{A''})^{2} + (y_{A} - y_{A''})^{2} + (z_{A} - z_{A''})^{2}}. \tag{5.26}$$

If more than one epoch is needed then, similar equations at the following markers can be used, knowing that the ambiguities stay the same. At marker set **b** we have

$$\Phi_{BB'}^{j} = \rho_{BB'}^{j} + \lambda \cdot N_{AA'}^{j} \tag{5.27}$$

$$\Phi_{BB''}^{j} = \rho_{BB''}^{j} + \lambda \cdot N_{AA''}^{j}. \tag{5.28}$$

Notice that: $N_{AA'}^{j} = N_{BB'}^{j}$ and $N_{AA''}^{j} = N_{BB''}^{j}$.

After the ambiguities are known, and assuming that lock is maintained on the same satellites, at any point $X$ on the road, the following set of equations can be written

$$\Phi_{XX'}^{j} = \rho_{XX'}^{j} + \lambda \cdot N_{AA'}^{j} + \varepsilon_{XX'}^{j} \tag{5.29}$$

$$\Phi_{XX''}^{j} = \rho_{XX''}^{j} + \lambda \cdot N_{AA''}^{j} + \varepsilon_{XX''}^{j} \tag{5.30}$$

$$d_{x1} = \sqrt{(x_{X} - x_{X'})^{2} + (y_{X} - y_{X'})^{2} + (z_{X} - z_{X'})^{2}} \tag{5.31}$$

$$d_{x2} = \sqrt{(x_{X} - x_{X''})^{2} + (y_{X} - y_{X''})^{2} + (z_{X} - z_{X''})^{2}} \tag{5.32}$$

where, the 9 unknowns are the coordinates of the three antennas at $X$, $X'$ and $X''$. Using five satellites produces ten single difference equations. In addition, the two constraint equations can reliably be used in the equation set. The attitude of the vehicle (roll, pitch and yaw) could then be computed from the coordinates of $X$, $X'$ and $X''$.

# 5.7 Using Independent Receivers

Using independent receivers rather than a multi-antenna one, would work. But since the clocks of the various receivers are not synchronized, double differencing is needed to eliminate the receiver clock biases.

# 5.8 Various Antenna Configurations

Additional antennas can provide extra redundancy that makes the positioning process faster and more robust. Some effort in GPS research has gone toward exploring special antenna configurations that would speed up the process of ambiguity resolution for attitude determination.

Configuration **a** in Figure 5.8 is a standard one that is used by researchers on land vehicle positioning and attitude measurements [Han et al., '97]. El-Mowafy and Shwartz, '95 proposed antenna configurations **b** and **c**, in Figure 5.8, to speed up ambiguity resolution. In these configurations the distance between antennas 1 and 2 is less than ½ cycle so that the ambiguity difference is certainly known to be zero. These configurations could be used with IS-DGPS to resolve the ambiguities and add redundancy to the least-square equations. Depending on the shape and size of the vehicle, the antennas could be placed in certain spots and at different heights in order to create more suitable satellite-antenna geometry.

a-General 4-antenna configur.　　b-[El-Mowafy et al., '94]　　c-[El-Mowafy et al., '94]
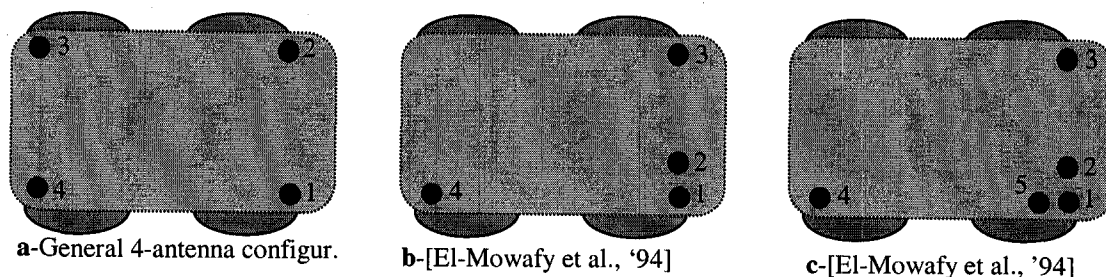
**Figure 5.8**: Various configuration used in attitude determination

# 5.9 Simulation Results

A simulation was conducted using a vehicle with two-antenna setup and a baseline of two meters between the two antennas. The true traveling trajectory was selected to be a straight line going eastward with the north coordinate equals to zero meters (Figure 5.9). Single difference relative positioning was performed at every epoch. Seven satellites were used with various GPS errors introduced, including SA but excluding multipath disturbance.

Figure 5.9 shows the estimated trajectory when the differencing was done at every epoch at a rate of 5 Hz. As expected, the SA effect was canceled due to differencing at every epoch and without any latency. The orbital and atmospheric errors completely vanished. The remaining error between the true and estimated trajectories is mostly within ±2 cm and is due to receiver noise.
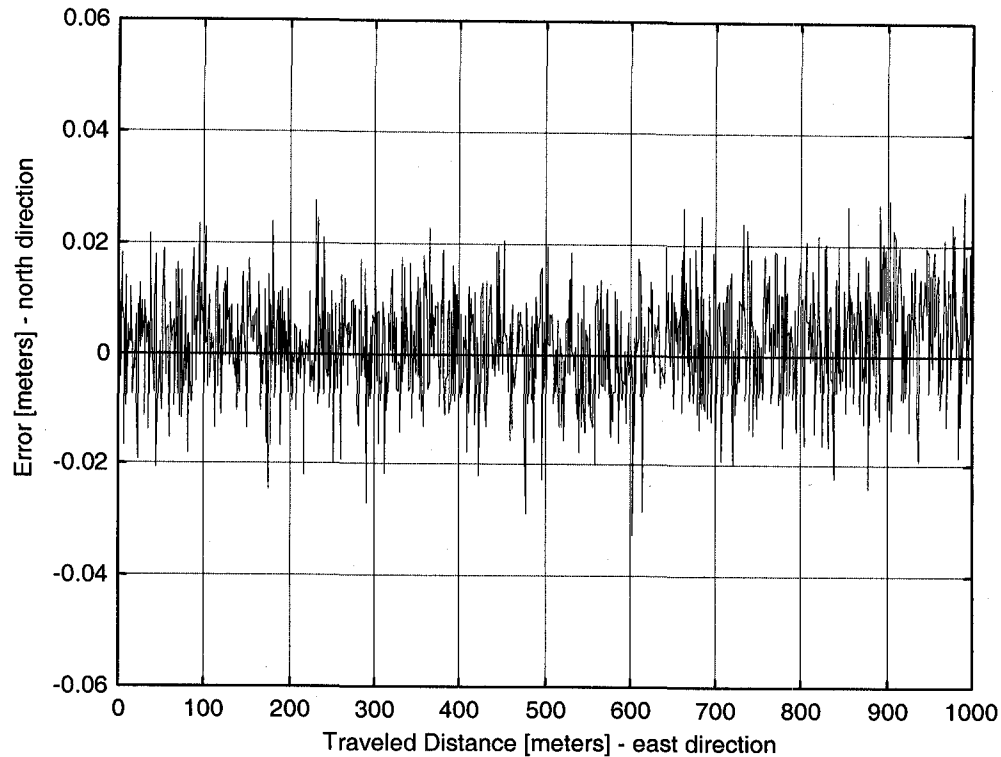
**Figure 5.9**: Dual-Antenna positioning accuracy simulation

# 5.10 Multipath Disturbance

Generally, multipath is a significant limiting error source in attitude determination with GPS. The IS-DGPS method with multiple antennas is susceptible to multipath effect in the same way. The effect can be reduced by taking special precautions on where to place the antennas, installing a common groundplane for all antennas or by the use of choke ring antennas [Hofmann et al., '97].

In order to examine the effect of multipath on the dual-antenna system that was simulated in Section 5.5, a simulation was carried out using the same parameters with the addition of multipath disturbance. This disturbance was created by passing a white noise

through a first-order Butterworth filter [GPSOFT, '98]. The added multipath disturbance

created an extra error of two centimeters as shown in Figure 5.10.
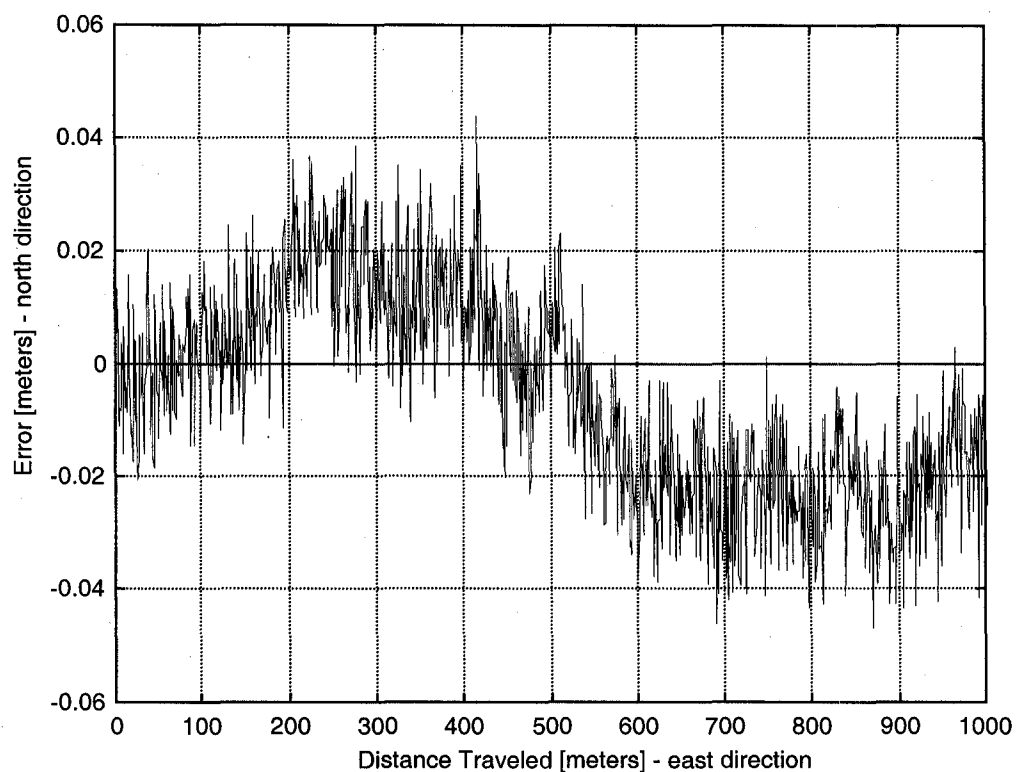


**Figure 5.10**: Dual-Antenna accuracy with added multipath disturbance

# Chapter 6

# Conclusions and Future Work

This dissertation presented a new method for highway lane sensing that targets two distinct applications, Driver Assistance Systems (DAS) and automatic steering for Automated Highway System (AHS) vehicles. Other approaches, that use broadly different technologies, have been proposed. The choice of the adopted method will be based on two major factors - reliability and cost. The system has to perform reliably at any time of the day and in any weather condition. In addition, DAS and AHS are very large scale projects that involve the nation's highways and many vehicles. So, the infrastructural cost of implementation on the highways and the vehicle play a crucial role in the decision.

This chapter draws some conclusions based on the obtained results, discusses the reliability of the new method and the cost involved for implementation and mentions potential topics that could be investigated.

# 6.1 Comments on the Results

Physical experiments and/or computer simulation were used to assess IS-DGPS's performance and to test the involved theory and formulation. The obtained results showed that both methods of assessment were in agreement with the theory and formulation. Also, the two methods provided matching accuracies whenever they were done simultaneously.

In assessing IS-DGPS with the C/A-code, the original expectation was to have an error above one meter, as is the case in regular DGPS. Usually, positioning with the C/A-code is not used for either guidance or automatic control. The experimental result showed a surprising 16 cm standard deviation with a maximum error of 42 cm. As a conclusion of this result, a low cost C/A code GPS receiver could be integrated with other low cost sensors, such as an inertial measurement unit (IMU), to produce a low cost lane sensing system for guidance purposes in the DAS.

The L1 carrier phase results were quite good with a 4.5 cm standard deviation. We feel that the maximum error, seen in the experimental results, reflects anomalies in the apparatus and can be easily avoided.

The multi-antenna receiver approach provided a robust system that is more accurate in determining positions, is less dependent on the markers and provides the attitude of the vehicle.

# 6.2 Lane Sensing Reliability

Detecting magnetic markers was proven to be done reliably and fairly accurately, which makes the concept of IS-DGPS feasible and attractive. Analytically, as well as with simulation, it was shown that uncertainty in locating the magnetic markers has only a slim effect on the positioning accuracy. Current research at UCD is improving the reliability and the accuracy in locating the magnets.

IS-DGPS has less possibility for failure since no signals are transmitted and received over long distances, except for the GPS satellite signals. There is no signal limited ranges that the vehicle cannot go beyond and there is no line of sight requirements.

IS-DGPS has brought the concept of a moving base station which solves the spatial decorrelation problem. Since the baselines are short (tens of meters), the spatial decorrelation effect on the radial orbital and atmospheric errors are totally eliminated. The ionospheric error is the largest error after SA, and it is hard to deal with because of the spatial decorrelation factor. Normally, for one centimeter accuracy positioning, an expensive L1/L2 dual frequency receiver is used, since the ionospheric effect is frequency dependent, and differencing between the L1 and L2 frequencies eliminates the ionospheric effect. With IS-DGPS the ionospheric problem is totally resolved.

IS-DGPS will be a more robust method when selective availability SA is lifted, since SA injects a time varying error that forces the need for short time interval between differential corrections (short distance between markers). SA will be turned off any time, by 2006 at the latest.

# 6.3 Road & Vehicle Infrastructural Cost

The main components of the IS-DGPS system are: a GPS receiver, a set of magnetometers, an electronic road map and sparsely placed road magnets. The prices of GPS receivers and magnetometers are coming down drastically. Hence, from a road and vehicle's infrastructural cost and maintenance point of view, IS-DGPS ranks well among the lane sensing approaches that were described in Chapters 1and 2.

In addition, GPS receivers and electronic road maps are becoming a necessity on vehicles. They will eventually be installed in many vehicles for navigation purposes or as a part of a commercial or a public transportation system. Hence, the additions to the vehicle's infrastructure in IS-DGPS are reasonable, since they are useful in other tasks beside guidance and control.

# 6.4 Future Work

## 6.4.1 Coupling GPS with an IMU or INS

In applications such as vehicle guidance and vehicle automatic control, redundancy of data is critical to guarantee a fault free system. Moreover, GPS signals are vulnerable to jamming, outages and blockages. Combining an Inertial Measurement Unit (IMU) or an Inertial Navigation System (INS) with GPS in a complementary fashion would achieve more reliable and more accurate vehicle's real-time kinematics. An IMU or an INS can also benefit from the magnetic markers, since the accuracy degrading drift, inherent in the inertial elements, is reset at every marker. A GPS and an INS with its drift

canceled by the road markers, can be effectively integrated using a Kalman filter. An INS would be able to provide a consistent and sufficient navigation accuracy indefinitely during satellite signal outage periods, since the markers keep eliminating the drift in the INS. Also, as a result, a less expensive INS can be used instead of an elaborate and expensive one.

## 6.4.2 GPS & GLONASS

GLONASS is the Russian replica of the GPS system (Globalnaya Navigatsionnaya Sputnikovaya Sistema). Some new receivers, in the market today, can use GPS and GLONASS satellites which increases the number of satellites available, hence, adding reliability to the positioning process. The benefits to the IS-DGPS method by using a GPS-GLONASS receiver can be explored. It is important to note that GLONASS does not have Selective Availability.

## 6.4.3 An Integrated System

The GPS equipment we have used in our experimental evaluation has been off the shelf. The data processing in this research was done externally and sometimes manually. An important project to undertake is the design of a GPS receiver that is tightly coupled with the magnetometers, so that, the receiver is automatically triggered and the IS-DGPS algorithms get processed internally.

Finally, various sensors and components could be integrated to add to the robustness and reliability of the system. INS, GPS, transmission odometer, wheel sensors and a magnetic compass, could be tightly integrated to provide an accurate and seamless position and velocity estimation process. Digital road map database, a reliable vehicle dynamic model and various algorithms for signal processing and Kalman filtering could be internally coded. The system would finally provide a reliable signal to an automatic steering controller or a head-up display in the DAS. Figure 6.1 shows a schematic of the various sensors and components of an integrated system.
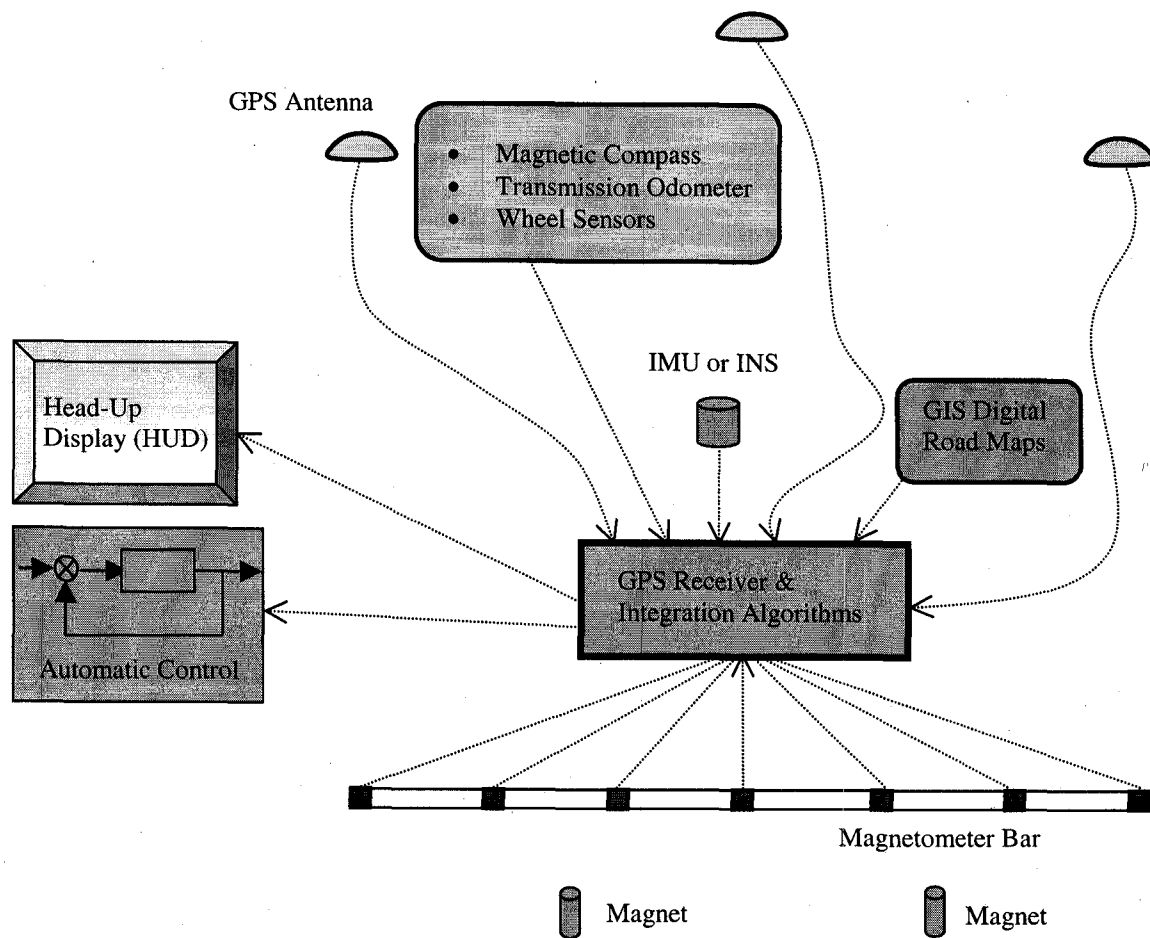


**Figure 6.1**: Schematic of an integrated system

# Appendix A

# Satellite ECEF Positions

This Appendix connects ECEF coordinates $(X,Y,Z)$ to a satellite position described in space by Keplerian orbital elements [Kaplan, '96].

The ECEF coordinate system has its XY-plane coincident with the Earth's equatorial plane. The X-axis points in the direction of $0°$ longitude (Greenwich Meridian). The Z-axis is normal to the equatorial plane in the direction of geographical North Pole.

If the Earth were perfectly spherical and of a uniform density, the Earth's gravity would behave as if the Earth were a point of mass. Let a satellite of mass $m$ be located at position vector $r$ in an Earth Centered Inertial coordinate system. If $G$ is the universal gravitational constant, $M$ is the mass of Earth, and the Earth's gravity acts as a point mass, then, according to Newton's law, the force $F$, acting on the object would be given by

$$F = ma = -G\frac{mM}{r^3}\vec{r} \qquad (A.1)$$

where a is the acceleration of the object. Equation (A.1) can be written as

$$\frac{d^2\vec{r}}{dt^2} = -\frac{\mu}{r^3}\vec{r}$$
(A.2)

where $\mu = G.m = 3986005 \times 10^8\,\text{m}^3/\text{sec}^2$. Equation (A.2) is the expression of so-called "two-body" or Keplerian satellite motion, in which the only force acting on the satellite is the point-mass Earth.

Additional forces acting on satellites include the gravity from the Sun and Moon, solar radiation pressure and the Earth's tidal variation. To model a satellite's orbit very accurately, all these perturbations to the Earth's gravitational field must be modeled. All these perturbing accelerations can be collected in a term $a_d$, so that the equations of motion can be written as

$$\frac{d^2\vec{r}}{dt^2} = -\frac{\mu}{r^3}\vec{r} + a_d.$$
(A.3)

It can be shown that there are six constants of integration in Equation (A.2). Given these constants and an initial time, one can find the position and velocity vectors of a satellite.

In the case of the fully perturbed equation of motion (A.3), it is still possible to characterize the orbit in terms of six integrals of two-body motion, but those six parameters will no longer be constant. Therefore, the Keplerian orbital elements in the GPS ephemeris includes not only six orbital parameters, but also the time of their applicability and a characterization of how they change over time. With this information, a GPS receiver can compute the corrected integral of motion for a GPS satellite at the

time when it is solving the navigation problem. From the corrected integrals, the position vector of the satellite can be computed, as we will show.

The first three Keplerian orbital elements, illustrated in Figure A.1, define the shape of the orbit. They are: $a$ = Semimajor axis of the ellipse, $e$ = eccentricity of the ellipse and $\tau$ = time of perigee passage. The time $t_0$ at which the satellite is at some reference point $A$ in its orbit is known as the "epoch" and as a part of the GPS ephemeris message is called "time of ephemeris". The point $P$ where the satellite is closest to the center of the Earth is known as perigee, and the time at which the satellite passes perigee, $\tau$, is another Keplerian orbital parameter.
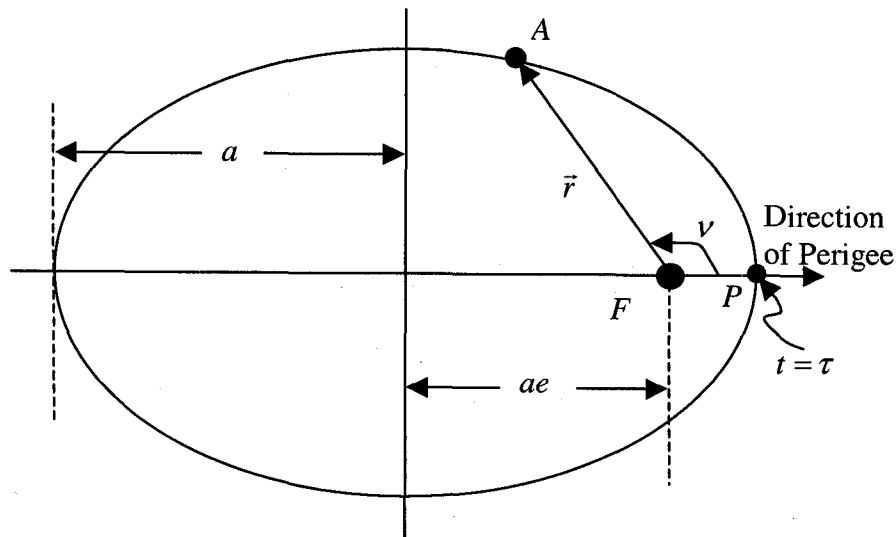


**Figure A.1**: The three Keplerian orbital elements defining the shape of the satellite's orbit.

There is an equivalent parameter used by the GPS system instead of the time of perigee passage known as the mean anomaly at epoch. Mean anomaly is an angle that is related to the true anomaly at epoch, which is illustrated in Figure A.1 as angle $v$. After

defining true anomaly precisely, the transformation to mean anomaly and the demonstration of equivalence to time of perigee passage will be shown.

True anomaly is the angle in the orbital plane measured counterclockwise from the direction of perigee to satellite. From Kepler's laws of two-body motion, it is known that true anomaly does not vary linearly in time for noncircular orbits. Because it is desirable to define a parameter that does vary linearly in time, two definitions are made that transform the true anomaly to the mean anomaly, which is linear in time. The first transformation produces the eccentric anomaly, which is illustrated in Figure A.2, with the true anomaly $v$. Geometrically, the eccentric anomaly $E$ is constructed from the true anomaly first by circumscribing a circle around the elliptical orbit. Next, a perpendicular is dropped from the point A on the orbit to the major axis of the orbit, and this perpendicular is extended upward until it intersects the circumscribed circle at point B. the eccentric anomaly is the angle measured at the center of the circle O, counterclockwise from the direction of the perigee to the line segment OB. In other words, $E = \angle POB$. A useful analytical relationship between eccentric anomaly and true anomaly is as follow

$$E = 2\arctan\left[\sqrt{\frac{1-e}{1+e}}\tan\left(\frac{1}{2}v\right)\right].$$
(A.4)

Once the eccentric anomaly has been computed, the mean anomaly $M$ is given by Kepler's equation

$$M = E - e\sin E.$$
(A.5)
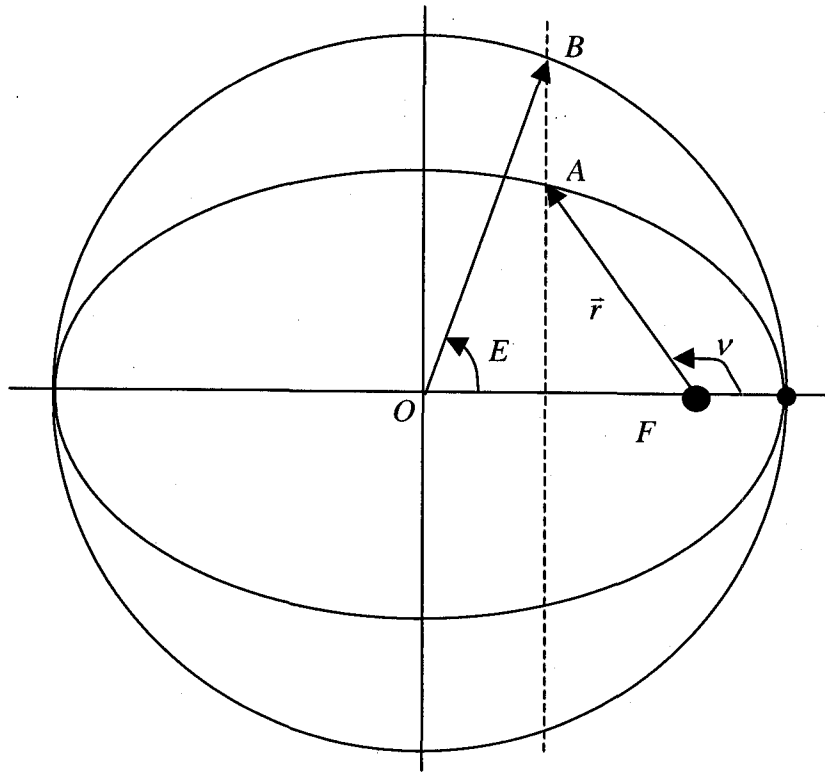
**Figure A.2**: Relationship between eccentric anomaly and true anomaly.

As stated previously, the importance of transforming from the true to the mean anomaly is that time varies linearly with the mean anomaly. That linear relationship is

$$M - M_0 = \sqrt{\frac{\mu}{a^3}}(t - t_0) \tag{A.6}$$

where $M_0$ is the mean anomaly at epoch $t_0$, and $M$ is the mean anomaly at time $t$. from Figures A.1 and A.2 and (A.4) and (A.5), it can be verified that $M = E = v = 0$ at the time of the perigee passage. Therefore, if we let $t = \tau$ the transformation between the mean anomaly and time of perigee passage would be

$$M_0 = -\sqrt{\frac{\mu}{a^3}}(\tau - t_0). \tag{A.7}$$

From (A.7), it is possible to characterize the two-body orbit in terms of the mean anomaly at epoch $M_0$ instead of the time of the perigee passage $\tau$. GPS makes use of the mean anomaly at epoch in characterizing orbits.

GPS also makes use of a parameter known as mean motion, which is given the symbol $n$ and is defined to be the time derivative of the mean anomaly. Since the mean anomaly was constructed to be linear in time for two-body orbits, mean motion is constant. From (A.6), we find the mean motion as follow

$$n = \frac{dM}{dt} = \sqrt{\frac{\mu}{a^3}}. \tag{A.8}$$

Then, (A.6) can be written as $M - M_0 = n(t - t_0)$.

Figure A.3 illustrates the three additional Keplerian orbital elements that define the orientation of the orbit. The coordinates in Figure A.3 refers to the ECEF coordinate system. The following three Keplerian elements define the orientation of the orbit in the ECEF coordinate system: $i$ = inclination of orbit, $\Omega$ = longitude of ascending node, and $\omega$ = argument of perigee.

Inclination $i$ is the angle between the Earth's equatorial plane and the satellite's orbital plane. The other two Keplerian elements in figure A.3 are defined in relation to the ascending node, which is the point in the satellite's orbit where it crosses the equatorial plane with a $+Z$ component of velocity (i.e. going from southern to northern hemisphere). The orbital element that defines the angle between the $X$-axis and the direction of the ascending node is called the right ascension of the ascending node. Because the $X$-axis is fixed in the direction of the prime meridian ($0^\circ$ longitude) in the

ECEF coordinate system, the right ascension of the ascending node is actually the longitude of the ascending node, $\Omega$. The final orbital element, known as the argument of perigee, $\omega$, measures the angle from the ascending node to the direction of perigee in the orbit. Notice that $\Omega$ is measured in the equatorial plane, whereas $\omega$ is measured in the orbital plane.

It is insufficient to use only the Keplerian orbital elements for computing the position of a GPS satellite, except very near the epoch of those elements. One solution to this problem would be to update the GPS ephemeris messages very frequently. Another solution would be for the GPS receiver to integrate the fully perturbed equation of motion, which would include a detailed force model, from epoch to the desired time. Because both of these solutions are computationally intensive, they are impractical for real-time operations. Therefore the Keplerian orbital elements in the GPS ephemeris message are augmented by "correction" parameters that allow the user to estimate the Keplerian elements fairly accurately during the periods of time between updates of the satellite's ephemeris message. Any time after the epoch of a particular ephemeris message, the GPS receiver uses the correction parameters to estimate the true orbital elements at the desired time.
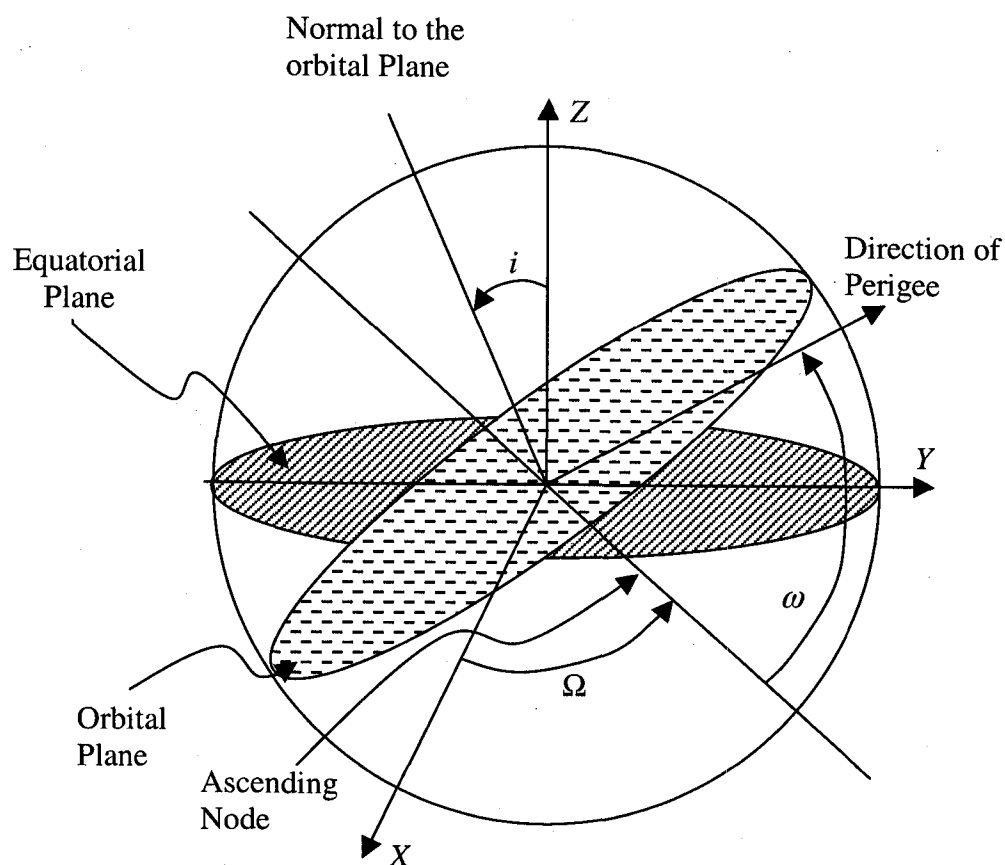
**Figure A.3**: The three Keplerian orbital elements defining the orientation of the orbit.

Table A.1 summarizes the parameters contained in the GPS ephemeris message. The first seven parameters are the osculating Keplerian orbital elements at the time of epoch. The next nine parameters allow for corrections to the Keplerian elements as functions of time after epoch.

Table A.2 provides the algorithm by which a GPS receiver computes the position vector of a satellite $(X_s, Y_s, Z_s)$ in the ECEF coordinate system from the orbital elements of Table A.1. For computation (3) in Table A.2, $t$ represents the GPS system time at

which the GPS signal was transmitted. The notation According to WGS-84, the rotation rate of the Earth is $\dot{\Omega}_e = 7.2921151467 \times 10^{-5}$ rad/sec.

You can find this algorithm, as a Matlab program *"satpos"*, in [Strang and Borre '97]'s accompanying software disk. This function calculates the position of any GPS satellite at any time. It is fundamental to every position calculation.

## Table A.1: GPS ephemeris data definitions

| | |
|---|---|
| $t_{0e}$ | Reference time of ephemeris |
| $\sqrt{a}$ | Square root of Semimajor axis |
| $e$ | Eccentricity |
| $i_0$ | Inclination angle |
| $\Omega_0$ | Longitude of the ascending node |
| $\omega$ | Argument of perigee (at time $t_{0e}$) |
| $M_0$ | Mean anomaly |
| $di/dt$ | Rate of change of inclination angle |
| $\dot{\Omega}$ | Rate of change of longitude of the ascending node |
| $\Delta n$ | Mean motion correction |
| $C_{uc}$ | Amplitude of cosine correction to argument of latitude |
| $C_{us}$ | Amplitude of sine correction to argument of latitude |
| $C_{rc}$ | Amplitude of cosine correction to orbital radius |
| $C_{rs}$ | Amplitude of sine correction to orbital radius |
| $C_{ic}$ | Amplitude of cosine correction to inclination angle |
| $C_{is}$ | Amplitude of sine correction to inclination angle |

**Table A.2**: Computation of a satellite's ECEF position vector

| | | |
|---|---|---|
| (1) | $a = \left(\sqrt{a}\right)^2$ | Semimajor axis |
| (2) | $n = \sqrt{\dfrac{\mu}{a^3}} + \Delta n$ | Corrected mean motion |
| (3) | $t_k = t - t_{0e}$ | Time from ephemeris epoch |
| (4) | $M_k = M_0 + n(t_k)$ | Mean anomaly |
| (5) | $M_k = E_k - e \sin E_k$ | Eccentric anomaly (must be solved iteratively for $E_k$) |
| (6) | $\sin v_k = \dfrac{\sqrt{1 - e^2}\,\sin E_k}{1 - e \cos E_k}$  $\cos v_k = \dfrac{\cos E_k - e}{1 - e \cos E_k}$ | True anomaly |
| (7) | $\phi_k = v_k + \omega$ | Argument for latitude |
| (8) | $\delta\phi_k = C_{us} \sin(2\phi_k) + C_{uc} \cos(2\phi_k)$ | Argument for latitude correction |
| (9) | $\delta r_k = C_{rs} \sin(2\phi_k) + C_{rc} \cos(2\phi_k)$ | Radius correction |
| (10) | $\delta i_k = C_{is} \sin(2\phi_k) + C_{ic} \cos(2\phi_k)$ | Inclination correction |
| (11) | $u_k = \phi_k + \delta\phi_k$ | Corrected argument for latitude |
| (12) | $r_k = a(1 - e \cos E_k) + \delta r_k$ | Corrected radius |
| (13) | $i_k = i_0 + (di/dt)t_k + \delta i_k$ | Corrected inclination |
| (14) | $\Omega_k = \Omega_0 + (\dot{\Omega} - \dot{\Omega}_e)t_k - \dot{\Omega}_e t_{0e}$ | Corrected longitude of node |
| (15) | $x_p = r_k \cos u_k$ | In-plane x position |
| (16) | $y_p = r_k \sin u_k$ | In-plane y position |
| (17) | $X_s = x_p \cos\Omega_k - y_p \cos i_k \sin\Omega_k$ | ECEF x-coordinate |
| (18) | $Y_s = x_p \sin\Omega_k - y_p \cos i_k \cos\Omega_k$ | ECEF y-coordinate |
| (19) | $Z_s = y_p \sin i_k$ | ECEF z-coordinate |

# REFERENCES

[1]    R. Bodor, M. Donath, V. Morellas and D. Johnson, "In-Vehicle GPS-Based Lane Sensing to Prevent Road Departure" Third Annual World Congress on Intelligent Transportation Systems, Orlando FL., 1996.

[2]    R. Bowen, P. Swanson, F. Winn, N. Rhodus and W. Feess , "GPS Operational Control System Accuracies", The ION Global Positioning System. vol. 3, 1996.

[3]    California Land Surveyors Association, "Projection Tables-California Coordinate Systems", Special Publication No. 55/88, 1988.

[4]    D. Chen and G. Lachapelle, "A Comparison of the FASF and Least-Squares Search Algorithms for Ambiguity Resolution on the Fly", KIS94, Banff, Alberta, Canada, 1994.

[5]    C. Cohen, "Attitude Determination", Global Positioning System: Theory and Applications – vol. II, Chapter 19, Progress in Astronautics and Aeronautics, vol. 164. AIAA, 1996.

[6]    C. Counselman and S. Gourevitch, "Miniature Interferometer Terminals For Earth Surveying: Ambiguity And Multipath With Global Positioning System", IEEE Transactions On Geoscience And Remote Sensing vol. GE-19, No.4 1981.

[7]    J. Crisman and C. Thorpe, "Color Vision for Road Following" Vision and Navigation, The CMU Navlab Kluwer Academic Publishing, Boston, 1990.

[8]    A. El-Mowafy and K. Schwartz, "Epoch-by-Epoch Ambiguity Resolution for Real-Time Attitude Determination Using a GPS Multiantenna System", Journal of the Institute of Navigation, vol. 42 No. 2, Summer 1995.

[9]    H J. Euler and C. Hill, "Attitude Determination: Exploiting All Information for Optimal Ambiguity Resolution", ION GPS '95 Proceedings, 1995.

[10]    E. Frei and G. Beutler, "Rapid Static Positioning Based on the Fast Ambiguity Resolution Approach: The Alternative to Kinematic Positioning" Proceedings of 2nd International Symposium on Precise Positioning with GPS, Ottawa, Canada, 1990.

[11]    S. Han, K. Wong and C. Rizos, "Instantaneous Ambiguity Resolution for Real-time GPS Attitude Determination", Proceedings of KIS97, 1997.

[12]   R. Harvey, "Development of a Precision Pointing System Using an Integrated Multi-Sensor Approach", University of Calgary, Department of Geomatics Engineering, UCGE Report No. 20117, 1998.

[13]   R. Hatch, "Instantaneous Ambiguity Resolution" Proceedings of KIS90, Banff, Canada, 1990.

[14]   B. Hofmann-Wellenhof, and H. Lichtenegger, and J. Collins, "GPS Theory and Practice", Springer WienNewYork 1997.

[15]   GPSOFT LLC, Satellite Navigation toolbox for Matlab by GPSOFT LLC, 1998.

[16]   E. Kaplan, "Understanding GPS Principles and Applications" Artech House Publisher, Boston, London, 1996.

[17]   A. Kleusberg and P. Teunissen, "GPS for Geodesy", Chapter 5, Springer-Verlag Berlin Heidelberg, 1996.

[18]   D. Lapucha, R. Barker, and Z. Liu, "High-Rate Precise Real-Time Positioning Using Differential Carrier Phase" ION GPS '95 Proceedings, 1995.

[19]   A. Leick, "GPS Satellite Surveying", John Wiley & Sons, Inc., 1995.

[20]   H. Lim, B. Newstrom, C. Shankwitz and M. Donath, "A Head Up Display Based on a DGPS and Real Time Accessible Geospatial Database for Low Visibility Driving", ION GPS '99 Proceedings, 1999.

[21]   G. Lu, "Development of GPS Multi-Antenna System for Attitude Determination" PhD Dissertation UCGE Report # 20073 University of Calgary, 1995.

[22]   B. W. Parkinson, "GPS Error Analysis" Global Positioning System: Theory and Applications – vol. I, Chapter 11, Progress in Astronautics and Aeronautics vol. 163, AIAA, 1996.

[23]   B. W. Parkinson, and P. K. Enge, "Differential GPS" Global Positioning System: Theory and Applications – Volume II, Chapter 1, Progress in Astronautics and Aeronautics vol. 164, AIAA, 1996.

[24]   D. Pomerleau, "Neural Network Perception for Mobile Robot Guide", PhD Dissertation, Carnegie Mellon University, 1992.

[25]   S. Shladover, "Review of the State of Development of Advanced Vehicle Control Systems", Vehicle System Dynamics, vol. 24, 1995.

[26]    S. Shladover, C. Desoer, J. Hedrick, M. Tomizuka, J. Walrand, W. Zhang, D. McMahon, H. Peng and S. Sheikholeslam, "Automatic Vehicle Control Developments in the PATH Program" IEEE Trans. on Vehicular Technology, vol. 40, No. 1, February 1991.

[27]    J. Sinko and R. Galijan, "An Evolutionary Automated Highway System Concept based on GPS" ION GPS '96 Proceedings, 1996.

[28]    J.J. Spilker Jr., "GPS Navigation Data", Global Positioning System: Theory and Applications – vol. I, Chapter 11, Progress in Astronautics and Aeronautics vol. 163, AIAA 1996.

[29]    G. Strang and K. Borre, "Linear Algebra, Geodesy and GPS" Wellesley-Cambridge Press, 1996.

[30]    F. Van Graas, and M.S. Braasch, "Selective Availability" Global Positioning System: Theory and Applications – vol. I, Chapter 17, Progress in Astronautics and Aeronautics vol. 163, AIAA, 1996.

[31]    J. Van Sickle, "GPS for Land Surveyors", Ann Arbor Press, 1997.

[32]    W. Zhang and R. Parsons, "An Intelligent Roadway Reference System For Vehicle Lateral Guidance/Control" Proceedings of The American Control Conference, San Diego, 1990.